Key to Author Responses to Reviews of “Sequential changes in ocean circulation and biological export productivity during the last glacial cycle: a model-data study”

CP reviewer comments #1 and author responses

AC: We thank the reviewer for their comments and the opportunity to explore some important issues in greater detail. We feel the review comments make a strong contribution to improving the quality of our work. We have followed up on the reviewer comments in detail and have attempted to address them.

We have made reference to changes to the manuscript, which are included as a supplement to the author comments, in track changes. Page and line references below refer to locations in the revised document with track changes.

We have addressed the minor comments first, and then provided a longer discussion on the major comments.

Please note that we have changed our treatment of ocean $\delta^{13}C$ proxy data, stemming from one of the other reviewer comments, to only include $\delta^{13}C$ from *Cibicides* species of benthic foraminifera. We have also made some small changes to the parameterisation of the volcanic and weathering isotopic signatures in the model, from reviewer comments. These changes required the re-calibration of our model and re-running of the model-data experiments. The model-data results changed modestly. We have updated the figures and text (tracked in the attachment) in the manuscript, accordingly.

Minor comments

RC: "Figure 1: It is not clear, how GOC (red arrows) is split up in the part upwelling in Atlantic and Indo-Pacific Ocean."

AC: In the SCP-M simple carbon cycle box model GOC is split between a part that upwells into the subpolar Southern Ocean, and a part which transports directly into the polar Southern Ocean. This is an attempt to represent the GOC model of Talley (2013). This split is arbitrarily set at 50%. We have added this information to the caption for Figure 1 "GOC upwelling in both basins is set by default to 50% split between upwelling into the subpolar and polar Southern Ocean."

RC: "Figure 1: Does your approach focusing on changes in GOC, AMOC and export production inply, all other proceses (fluxes) stay constant in time?"

AC: In the model-data experiments we allow GOC, AMOC and biological export production parameter values to vary, and we solve for them in the optimisation. The experiments include specified forcings of SST, salinity, ocean volume, polar Southern Ocean air-sea gas exchange, coral reef carbonate accumulation and cosmogenic 14C production, guided by proxy observations. Other input parameter values are held constant in the experiments.

RC: Figure 12: x-axis is wrong, eg. MIS5e is between ~114-122 ka, while it has been between ~118-128 ka in other figures.

AC: Thank you. We have fixed the chart.

RC: With respect to iron fertilisation you might check on Shaffer and Lambert (2018)

AC: Thank you, we have added it to the references throughout the document (P11, L22; P26, L7) and an additional sentence at P26, L8 (note the LaTeXdiff/track changes program struggles to fit reference changes onto the page):

"According to Shaffer and Lambert (2018), fertilisation of the surface ocean, and dust scattering effects on solar radiation, helped to push atmospheric CO_2 into and out of their glacial minima, for example at the LGM and last glacial termination."

RC: The fact that not one single process is needed to explain LGM-Holocene carbon cycle changes is long known, and has been called "the carbon stew" by some authors. You might want to check and discuss in more detail earlier modelling approaches on one glacial cycle (or longer), for example in Ganopolski and Brovkin (2017).

AC: Thanks. We have added to the introduction (P2, L23):

"Several studies have attempted to solve the problem of glacial-interglacial CO_2 by modelling either the last glacial-interglacial cycle in its entirety, or multiple glacial-interglacial cycles (e.g. Ganopolski et al., 2010; Menviel et al., 2012; Brovkin et al., 2012; Ganopolski and Brovkin, 2017). These studies highlight the roles of orbitally-forced Northern Hemisphere ice sheets in the onset of the glacial periods, and important feedbacks from ocean circulation, carbonate chemistry and marine biological productivity throughout the glacial cycle (Ganopolski et al., 2010; Brovkin et al., 2012; Ganopolski and Brovkin, 2017). Menviel et al. (2012) modelled a range of physical and biogechemical mechanisms to deliver the full amplitude of atmospheric CO_2 variation in the last glacial-interglacial cycle, using transient simulations with the Bern3D model. According to Brovkin et al. (2012), a ~50 ppm drop in atmospheric CO_2 early in the last glacial cycle was caused by cooling sea surface temperatures (SST), increased Northern hemisphere ice sheet cover, and expansion of southern-sourced abyssal waters in place of North Atlantic Deep Water (NADW) formation. Ganopolski and Brovkin (2017) modelled the last four glacial cycles with orbital forcing as the singular driver of carbon cycle feedbacks. They described the "carbon stew", a feedback of combined physical and biogeochemical changes in the carbon cycle, to drive the last four glacial-interglacial cycles of atmospheric CO_2."

We have also added the following to our discussion (P28, L10):

"Ganopolski et al. (2010) and Brovkin et al. (2012) modelled cooling SST and substitution of North Atlantic Deep Water by denser waters of Antarctic origin, in the abyssal ocean, as the main drivers of falling atmospheric CO_2 at the last glacial inception. Menviel et al. (2012) modelled a transient slowdown in the rate of overturning circulation in the North Atlantic across MIS 5d-5e."

RC: Section 5.3. You might want to check on recent finding of terrestrial carbon storage from δ13C in Jeltsch-Thömmes et al. (2019).

AC: Thanks, we have added this to our discussion of the terrestrial biosphere (P33, L24):

Jeltsch-Thommes et al. (2019) estimated a glacial-interglacial change in terrestrial biosphere of 850 Pg C (median estimate; range 450 to 1250 Pg C). Jeltsch-Thommes et al. (2019) demonstrated the importance of including ocean-sediment and weathering fluxes in their modelling estimates, and suggested other studies may underestimate the full deglacial change in the terrestrial biosphere carbon stock.

RC: Figure 14: Changes in CO2 caused by changes in terrestrial NPP and carbon stocks are missing in this figure. Please add.

AC: We have incorporated the contribution of the terrestrial biosphere to the glacial CO_2 drawdown in Figure 14. We have shown the effect of the model run with- and without the terrestrial biosphere to estimate its effects, as per Ganopolski and Brovkin (2017) Figure 9b, and we have compared with their model output.

Major comments

RC: Overall recommendation

My recommendation therefore is, that the model in its present form might be a useful tool for evaluating marine processes, and might be well used together with the available marine data (apart from δ13C), but fails to give meaningfull results for the δ13C cycle. This includes atmospheric and marine δ13C. I urge the authors to get those parts out of the manuscript. If they wish to further analyse the δ13C-cycle I believe fundamental model improvements are necessary, that can not be obtained by a major revision, but by a revised model version. Besides this, shortcomings of the steady-state approach should be discussed in more detail and the unclear (wrong?) aspects of carbonate weathering and annual fluxes in/out of the simulated system (atmosphere/ocean) need to be clarified for each MIS, maybe in a table or a new figure.

AC: We've discussed the comments of the reviewer, and clarified various parts of the modelling referred to by the reviewer, in quite some detail below. We've also made some small adjustments to $\delta^{13}C$ parameters for volcanic source carbon and silicate weathering, in the model, and incorporated those in the revised modelling results in the updated manuscript. We've clarified what our model-data results are saying about $\delta^{13}C$ in MIS 3-5, and clarified how our model deals with carbonate weathering, with specific reference to the literature and the model code (annotations provided in the Attachments to our responses). We've also discussed features of the terrestrial biosphere in more detail. We've discussed the issues associated with MIS-averaging, revised our wording in the manuscript, and also provided a better description of the model-data results. There is an updated model code to upload with the finalised manuscript.

As a more general comment on $\delta^{13}C$, we demonstrated in O'Neill et al. (2019) that the model we have used, replicates the modern atmosphere and ocean $\delta^{13}C$ data time series, and replicates the effects of anthropogenic emissions on ocean and atmospheric δ13C, including matching atmospheric data time series for the last 250 years, and GLODAPv2 data for the present, and matches Holocene data, and successfully matched LGM proxy data.

We argue that the model-data results and manuscript are best left with the $\delta^{13}C$ material retained, however with appropriate caveats to describe the shortcomings, as laid out below.

RC: "The chosen approach of steady-state analysis combined with optimization is a way, which certainly has benefits, but also shortcomings. I believe the benefits lie in the possibility to test a great number of parameter values, and this is certainly analysed with great effort and detail and worth publishing (but see my recommendation on shortenings of certain parts below). However, there is little learned on the potential short- comings and pitfalls, which in my view need to be discussed more deeply. I believe where this approach is falling to short is the following: By analysing only steady-state the authors miss out the opportunities to judge the results based on the timing (when do processes change leading to what results). I provide one example where the article nicely fails, producing a potenially right answer for very likely the wrong reason: One of the dominant features of atmospheric δ13C during the last glacial cycle is a drop by about 0.5‰ during MIS4. The steady-state approach now leads to the evalution of a mean value of atmospheric δ13C which does not really cover this decrease at all, it shows about a decline by about 0.2‰ from MIS5a to MIS4 (Fig 4). So, any explanation for this drop would be falling too short in the observed amplitude by 0.3‰."

RC: This is an interesting debate, and we thank the reviewer for the opportunity to explore this.

The aim of our study is to help diagnose the causes of the major changes in atmospheric CO_2 during the last glacial cycle. As we identify in our manuscript, there are three particularly large, sustained falls in atmospheric CO_2 between the penultimate interglacial (~125 ka) and the LGM (18-24 ka). These three major changes in atmospheric CO_2 are summarised well in the literature, for example, in Kohfeld and Chase (2017). Our aim, with our model-data study, is to understand if plausible changes in ocean circulation (GOC and AMOC) and marine biological productivity can explain the major falls in atmospheric CO_2. Other proxy data (e.g. δ13C) provide useful data constraints for a model-data study to help solve this problem. Our approach is to apply a model-data optimisation with a simple carbon cycle box model, to solve for major ocean carbon cycle parameter values during the last glacial-interglacial cycle, and to explain the major, non-transient, falls in atmospheric CO_2. To our knowledge, this is the first time that someone has attempted a multiple proxy model-data optimisation, that is optimised against atmospheric CO_2, $\delta^{13}C$, $\Delta^{14}C$, ocean $\delta^{13}C$, ocean $\Delta^{14}C$, and carbonate ion proxy data, and hard-constrained by many observational data (SST, salinity, ocean volume, sea-ice cover proxy, coral reef carbonates, atmospheric ^{14}C production rate) for the last glacial-interglacial cycle of 130 kyr. This study is quite different and unique in this regard.

This is done in an average sense across each MIS (nine of them over the last 130 kyr), using average proxy data values for each MIS and solving for the average parameter values at each MIS over the last 130 kyr. The MIS timeframes were chosen as an accessible reference point to the scientific community and because they are also simple reference points for the major atmospheric CO_2 declines in the last glacial cycle. In this way, we may not solve for maximum or minimum values in the parameters, "overshoots" and "undershoots", within each MIS, but the changes in the average values across the last glacial-interglacial cycle. We think the article has been successful in achieving what it set out to do.

The aim of our study is not to disentangle the transient or shorter-term changes in the carbon cycle within MIS stages. Other studies (e.g. Eggleston et al., 2016) have done that excellently for their area of focus (e.g. MIS 3-4 atmospheric $\delta^{13}C$), and other modelling studies have attacked this using transient simulations (e.g. Ganopolski, 2010; Menviel et al., 2012). Our study does successfully diagnose the timing of changes in major oceanic processes that drive major changes in atmospheric CO_2 during the last glacial-interglacial cycle, that are hard-constrained/brutally optimised by a host of data and observations.

With regard to your comments about MIS 3-5 and our manuscript and modelling, below, we address that in more detail to clarify what it is (and isn't) that our model-data results are telling us, and what we should have said about transient changes in our original manuscript. We clarify things quite substantially, but we are still very happy to explore the shortcomings of the approach and we have amended the manuscript with additional caveats, as explained below.

RC: Note that this δ13C feature is not rapid, it is an anomaly that has been detected from raw data by spline smoothing and is alltogether nearly 20 kyr long, however the decreasing flank falls in MIS4, the increasing flank in MIS3, thus the signal is largely smoothed out in the chosen MIS-centric analysis. The analysis of the results now comes to the conclusion that very likely changes in terrestrial carbon storage was responsible for a change in atmospheric δ13Ca of -0.2‰ (as said explaining a too little amplitude), it is furthermore said that the drop is accompanied by a 30 ppm fall in CO2 (page 12, lines 1-5), citing Hoogakker et al., 2016. I believe this is entirely wrong: The drop in CO2 happens clearly a few kyr before the drop in atmospheric δ13C, as seen in Fig. 4. Furthermore, since both CO2 and δ13C are meassured at the same samples and are both derived from gases in ice cores, this temporal offset between CO2 and atmospheric δ13C can not be explained by chronological issues. The anomalies in biosphere as documented by Hoogakker et al., 2016 all fall in line with the CO2 changes, but not with the δ13C changes, also note that Hoogakker et al., 2016 was published before the atmospheric δ13C data set of Eggleston et al. (2016). In that respect citations from Hoogakker on page 19 are also missing the correct timing: In Hoogakker NPP drops between around 70 ka (parallel to the drop in CO2), while the δ13C drop occurs 5 ka later. Also note, that in Eggleston et al. (2016) the authors of this atmospheric δ13C record tried to make sense of it by focusing on the part in which δ13C falls, but CO2 rises again (Fig 2 in that paper) focusing on an opposite behaviour than described here.""

AC: There is a major confusion here, that we will spend some time below to help with.

There are two minor comments in our original manuscript about the terrestrial biosphere and atmospheric $\delta^{13}C$ at MIS4. They are not conclusions of our work, nor are they a result of our model-data experiments, and thus don't reflect any obvious or glaring deficiency in our modelling or model-data analysis that we are aware of. The two comments are just peripheral statements we made about the terrestrial biosphere in MIS 4, with a very quick look at the atmospheric $\delta^{13}C$ data, without looking in any detail, as this excursion in the $\delta^{13}C$ pattern is not the focus of our work. In the two short sentences in our manuscript, we made casual reference of the transient, reversing change in atmospheric $\delta^{13}C$ across MIS 4 and MIS 3 (termed an "excursion" by Eggleston et al., 2016). We stated that the transient drop in $\delta^{13}C$ probably reflects a weaker terrestrial biosphere, based on reconstruction of the terrestrial biosphere for the same period, by Hoogakker et al. (2016). The first of these comment is in the "Data Analysis" section, and was just the result of a quick eyeballing of the atmospheric $\delta^{13}C$ data and another study on the terrestrial biosphere covering approximately the same time period (Hoogakker et al., 2016). You correctly point out our oversimplification of the true complexity of MIS 3-5, in our short statements.

This is simply an oversight on our part, in drafting the text and not joining the dots between the various data sources we have gathered, and our model-data results. If we look at this in a little more detail, with reference to the figures and tables in our manuscript (drawing the reviewer's attention to them here), we can provide the following (below).

If we look at Figure 2 in the manuscript, we can see that there are dramatic changes in SST (top panel), and less dramatic changes in salinity, sea-ice proxy, sea level/ocean volume, and reef C carbon between MIS 3-5. These data are well incorporated in our model-data experiments as forcings – or constraints, or, another way of saying it - values fed into the model - they hard hard-baked into our model-data results and are influencing the results. With those forcings included, our model-data experiments solve for changes in GOC, AMOC and SO Bio across MIS 3-5, and we find important changes in these parameters across MIS 3-5 (see Figure 8 where GOC, AMOC drop and Southern Ocean biological productivity increases). Therefore, our model-data experiments, and what we should say in our manuscript, is that there are large changes in SST and other observations in the ocean during MIS 4 and MIS 3 (Figure 2 top panel), as well as the changes we estimate for GOC, AMOC and Southern Ocean biological export productivity. It is likely that the combination of these features, led to the $\delta^{13}C$ pattern during MIS 3 and 4. We also note that Eggleston et al. (2016) posited changes in SST, ocean biological productivity, AMOC and Southern Ocean upwelling to explain the $\delta^{13}C$ "excursion" at MIS 3-4. There are also changes in the terrestrial biosphere, but as per the reviewer comments about timing with regards of changes in the terrestrial biosphere, atmospheric CO_2 and $\delta^{13}C$, and on closer inspection we can see that this is perhaps not a dominant driver but some background factor or simply a part of the MIS 3-4 $\delta^{13}C$ pattern.

However, it is clear, as you point out, that our MIS-averaging approach does not capture the full extent, the overshoots and undershoots, of the changes in atmospheric $\delta^{13}C$ across this period of MIS 3-5.

To address the reviewer comments, we simply reword the sentence in "Data analysis" you refer to (i.e. before the model results section), to better reflect the data we have used and

how that data is described (e.g. Eggleston et al., 2016) and also the literature that has focussed in detail on atmospheric $\delta^{13}C$ at MIS 3-4.

Original text: "*The large drop in $\delta^{13}C$ in MIS 4 accompanies a ~30 ppm fall in CO_2. The drop in $\delta^{13}C$ is likely caused by a reduction in the terrestrial biosphere, itself driven by the fall in CO_2 (Hoogakker et al., 2016)*."

We reword this and include the caveat about how our MIS-averaging does not include the full amplitude of changes within MIS 4 and 3, at P15 L23:

"The large drop in $\delta^{13}C$ in MIS4, reverses in MIS 3 (Fig. 4(B)). This excursion in the $\delta^{13}C$ pattern likely resulted from sequential changes in SST (cooling), AMOC, Southern Ocean upwelling and marine biological productivity (Eggleston et al., 2016). Eggleston et al. (2016) parsed the atmospheric $\delta^{13}C$ signal into its component drivers across MIS 3-5, using a stack of proxy indicators, and highlighted the sequence of events between the end of MIS 5 and beginning of MIS 3, and their cumulative effects to deliver the full change in atmospheric $\delta^{13}C$. Our MIS-averaging approach fails to capture the full amplitude of the changes in atmospheric $\delta^{13}C$ during MIS 3-5, and only captures the changes in the mean-MIS value, serving to understate the full extent of transient changes in responsible processes. In addition, the MIS-averaging approach misses the sequential timing of changes in processes within each MIS. These are limitations of our steady-state, MIS-averaging approach. "

Then on P22 L24, in reference to the terrestrial biosphere:

Original text: "*Notably, there is a distinct drop in NPP at MIS 4, a period where atmospheric CO_2 falls by ~30 ppm (Fig. 4(A)). Falling NPP and persistent respiration of the terrestrial biosphere carbon stock during MIS 4, which releases δ13C-negative carbon to the atmosphere, can explain the steep drop in atmospheric δ13C during the same period (Fig. 4(B))*.

We simply delete the reference to the terrestrial biosphere and atmospheric δ13C (in red above).

Plus, we have added a caveat to the discussion on limitations of the work that our MIS-averaging approach misses the full amplitude of transient changes (P34, L21).

"Our MIS time-slicing obscures details in the proxy records within MIS. For example, Yu et al. (2013) observed a transient drop in carbonate ion concentrations in the deep Pacific Ocean during MIS 4, and there are large transient changes in atmospheric $\delta^{13}C$ during MIS 3-4. Ganopolski et al. (2010) and Menviel et al. (2012) modelled transient collapses and rebounds in AMOC during MIS 4 (and other short-term changes in atmospheric dust supply and depth of biological nutrient remineralisation), which could have contributed to the full observed magnitude of changes in atmospheric $\delta^{13}C$ across this period (e.g. Eggleston et al., 2016) - not captured with our MIS-averaging approach."

However, what we are getting at in our response here, is that although our MIS-averaging strategy misses the full amplitude of transient changes or "excursions" in the proxy record, this doesn't mean that we don't meaningfully capture the data signals across the glacial-interglacial cycle, in our model-data experiments, as data constraints on our model-data experiments. This is a more nuanced but very important point, that we explore in more detail in the following.

A closer look at MIS 3-5 atmospheric CO_2 and $\delta^{13}C$ and our model-data results

Our model-data experiments at MIS 3,4 and 5, contain forcings of the model with observationally-derived SST, salinity, sea-ice proxy, sea level/ocean volume, and reef carbonate carbon fluxes. In addition to the model forcings, our MIS-averaged model-data results show a fall in GOC and AMOC, and an increase in Southern Ocean biological export productivity from MIS 5 into MIS 4. This outcome is supported by many proxy observations from the ocean for this time period including ocean carbonate ion proxy, ocean δ13C and dust records for the Southern Ocean and intense cooling in the North Atlantic Ocean (e.g. Oliver et al., 2010; Yu et al., 2016; Kohfeld and Chase, 2017). In addition, our results agree with transient modelling of the last glacial-interglacial cycle, across this period MIS 3-5. Ganopolski et al. (2010), Brovkin et al. (2012) and Menviel et al. (2012) all show a slowdown in AMOC at this time. Ganopolski and Brovkin (2017), in Figure 9(c) in their paper, model a contribution to atmospheric CO_2 drawdown from dust iron-fertilisation of Southern Ocean marine biological productivity in MIS 4. Therefore, our model-data conclusions for MIS 4 are consistent with the proxy data and also transient modelling exercises for this period.

Further to the review comments, we undertook a simple reconnaissance modelling experiment to test our MIS-average model-data results, at more detailed time intervals, against the non-MIS averaged data for atmospheric CO_2 and $\delta_{13}C$ through the MIS 3-5 period, to see if they hold up.

Eggleston et al. (2016) attempted to disentangle transient changes in the atmospheric $\delta^{13}C$ pattern during MIS 4 and MIS 3 (Heading 4.2 in their paper "Transient Changes at the Onset and End of MIS 4"). The first process they identify is iron fertilisation from dust over the Southern Ocean and a possible increase in SO biological export productivity (as above, we modelled increased SO biological export in this period too) to lower atmospheric CO_2 (but this would increase atmospheric $\delta^{13}C$). Then, Eggleston et al. (2016) mention cooling SST (a key part of our model constraints), where they plot a global average (we model latitude bands), which would also lead to lower atmospheric CO_2 as well as lower $\delta^{13}C$ (colder ocean fractionates more $\delta^{13}C$). Then, they mention slowing AMOC as a minor cause of lower atmospheric CO_2 and higher $\delta^{13}C$. Then, Eggleston et al. (2016) mention the effects of carbonate compensation and ocean alkalinity in lowering atmospheric CO_2, and with minor effects on $\delta^{13}C$ (captured in our model in MIS average).

Then, Eggleston et al. (2016) mention that Nd isotope and Pa/Th ratios in proxy data support a more pronounced slowdown in AMOC, which lasted until the end of MIS 4 (also in our model-data result for MIS 4, as discussed above and in the manuscript). Eggleston et al. (2016) discuss a weakening and shoaling of AMOC and expansion of AABW at this time, and

quote the hypothesised changes to AABW and AMOC of Ferrari et al. (2014). This would have lowered atmospheric CO_2 but increased atmospheric $\delta^{13}C$.

Then, Eggleston et al. (2016) mention that iron dust fertilisation may have reduced at the end of MIS 4 (showing the dust proxy data as evidence), leading to a drop in SO biological productivity, which would increase CO_2 and lower atmospheric $\delta^{13}C$, reversing the hypothesised changes in early part of MIS 4 (note our results show SO biological export productivity drops off from MIS 4 levels at MIS 3 – Figure 8 in the manuscript). At this time, SST warmed a small amount in the SO, and cooled in the North Atlantic, with presumably offsetting effects. According to Eggleston et al. (2016), quoting opal flux data, a short-term increase in SO upwelling likely led to the final drop in atmospheric $\delta^{13}C$ to reach the trough of the $\delta^{13}C$ pattern near the boundary if MIS 3-4 (not captured in our MIS-averaged modelling).

We forced our model with the data in Figure 2 in the manuscript, without averaging for the MIS stages, over 1kyr intervals for the period 47-75 ka. We then took our model-data results for the average parameter values across MIS 3-5 as shown in the manuscript, and profiled them to vary within each MIS according to the hypothesised changes from Eggleston et al. (2016), described above, also at 1 kyr intervals. In this way, we allow the parameters to vary within the MIS stages, but constrained to meet the MIS-average values, in their average, from our model-data experiments as shown in the manuscript.

Figure 1 below (top panel) shows model-data results compared with the proxy data for atmospheric CO_2 and Figure 1 (bottom panel) shows the same for atmospheric δ13C. This shows that taking the forcings for SST, salinity, sea-ice cover proxy, sea level/volume and coral reef carbonates (as per Table 2 of the manuscript), and time-profiled average MIS values for MIS 3-4-5 from the model-data experiments (taking the averages from Figure 8), accounts for the full amplitude of changes in atmospheric CO_2 and atmospheric $\delta^{13}C$ across this period, the overshoots and undershoots. The model-data results also account for the MIS-averaged proxy data across MIS 3, MIS 4 and MIS 5, as per our manuscript. The model results oscillate relative to the δ13C data, due to the 1 kyr intervals we have applied (we understand the $\delta^{13}C$ data has been smoothed), but it is easy to make this a 1 year/1 second interval exercise and it will produce a smoother set of results, for future analysis (in another body of work).

Completing this analysis to match the transient atmospheric CO_2 and $\delta^{13}C$ data across MIS 3-5, does not change our findings as presented in the manuscript, but actually reinforces them.

Figure 1: 1kyr-interval model results for MIS 3-5 compared to proxy data for atmospheric CO_2 (top panel) and atmospheric $\delta^{13}C$ (bottom panel). These model runs take as inputs the carbon cycle forcings from Table 1 in the manuscript, and our average values for GOC, AMOC and Southern Ocean biological export profiled with the pattern described by Eggleston et al. (2016). Atmospheric CO_2 data from Bereiter et al. (2015), and $\delta^{13}C$ data from Eggleston et al. (2016)

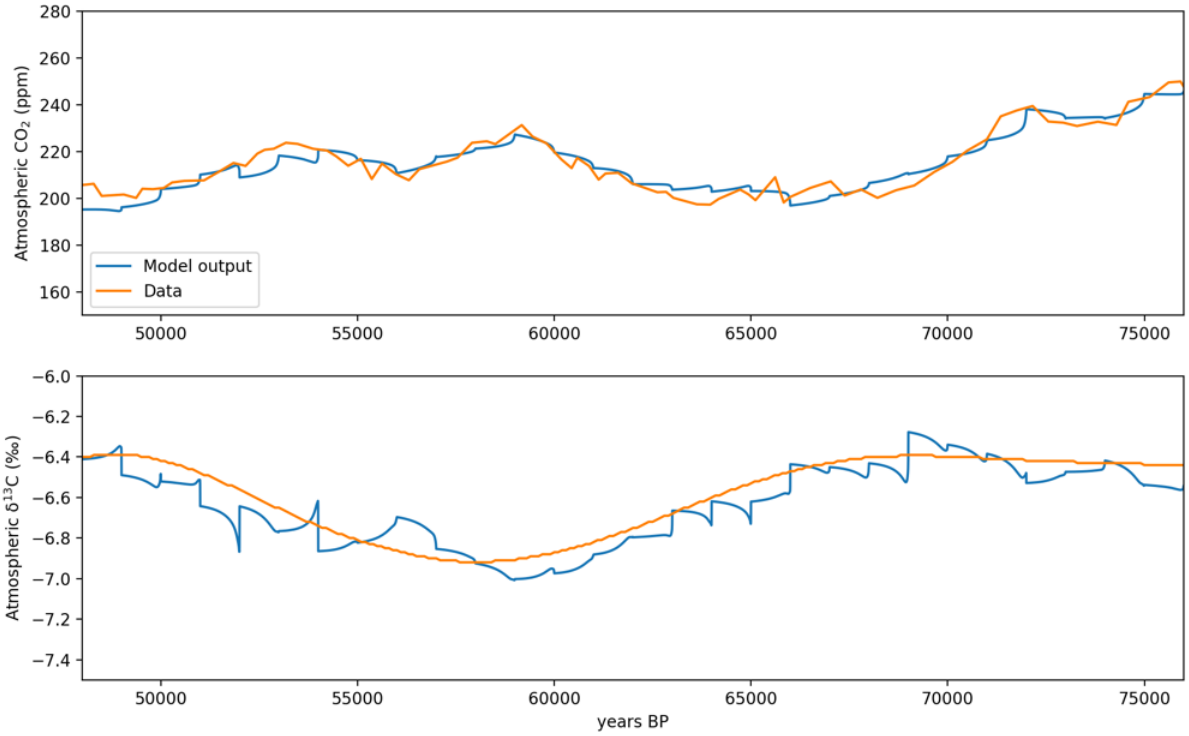

Therefore, while the model-data results we present in the manuscript do not describe fully the transient or short-term changes in the carbon cycle within each MIS, they are not inconsistent with the transient data observations – as evidenced by a 1 kyr-interval extension of our model-data results for MIS 3-5 (Figure 1), and comparison with proxy data and other modelling studies. Our model-data results show that, on average, GOC and AMOC weakened in MIS 4, and SO biology on average, was stronger, although these values fluctuated around their mean values within the MIS. We emphasise that these findings above are still peripheral to the main objective of our manuscript (major, sustained changes in atmospheric CO_2 through the last glacial-interglacial cycle), although this helps shed some more light on our model-data results in the context of the reviewer comments.

RC: "The second most dramatic change in atmospheric δ13C is a sharp drop by 0.2‰ during Termination I, a time window which has been chosen to be not be included in this steady-state analysis, again missing the opportunity to use 13C to pin down responsible processes.."

AC: We disagree. We argue that the responsible processes for the major and sustained changes in atmospheric CO_2 over the last glacial-interglacial cycle (e.g. SST, ocean circulation, biological export productivity, sea level, coral reefs, salinity, terrestrial biosphere) actually show themselves much more clearly, in sequence over the last 130 kyr, than the very short last glacial termination – whereby many processes were interacting in a relatively, very short period of time, and not easily untangled.

Our approach to attempting to solve for large changes in atmospheric CO_2, is to study the 100 kyr lead-up to the LGM, where the large changes separate out much more clearly into unique events over 100 kyr. Many studies have attempted to answer the problem of glacial-interglacial CO_2 by focussing on the LGM and Holocene periods alone (e.g. Peterson et al.,

2014; Menviel et al. 2016; Muglia et al., 2018). Others may try to get at this by looking at 10-18 ka period with transient modelling, where all the changes in the carbon cycle rapidly unwound (e.g. Menviel et al., 2012; Joos et al., 2004, Ganopolski and Brovkin (2017)), but that's not our paper. That's almost an entirely different approach to the explicit approach of our paper which was NOT to focus on the transient termination of the last glacial maximum, which has been studied in great detail elsewhere. Our paper is focussed on the major, non-transient, drops in atmospheric CO_2 in the lead-up to the last glacial maximum over 100 kyr – a much longer period that nicely shows up the sequential changes in the carbon cycle.

We have added references to the studies mentioned, to point readers in that direction if that is their area of focus, at P8 L7.

"We are interested in the LGM and Holocene as discrete periods, so our experiment time slice for MIS 2 is truncated at 18 ka, and our MIS 1 simply covers the Holocene, removing overlaps with the glacial termination. Therefore, our modelling excludes the last glacial termination (~11-18 ka). The glacial termination period was highly transient, with atmospheric CO_2 varying by ~85 ppm in <10 kyr, and large changes in carbon isotopes. Thus, it is anticipated that in a model-data reconstruction, model parameters would vary substantially for this period. Our strategy of integrating the model forward to an equilibrium state for each MIS as intervals of discrete climate and CO_2, would be unsuitable when applied to the last glacial termination. Joos et al. (2004), Ganopolski et al. (2010), Menviel et al. (2012), Menviel and Joos (2012), Brovkin et al. (2012) and Ganopolski and Brovkin (2017) provide coverage of the termination period with transient simulations of the last glacial-interglacial cycle, using intermediate complexity models (more complex than our model)."

Further, in our discussion of limitations of the study (P34 L27):

"We omitted the transient last glacial termination from our analysis, a period in which atmospheric CO_2 rose ~85 ppm in 8 kyr. Future model-data optimisation work could probe this period at 1 kyr intervals, or with transient, data-optimised simulations, to profile the unwinding of processes that led to the last glacial cycle CO_2 drawdown."

RC: Only the long-term trend in δ13C of +0.2‰ from the penultimate interglacial to the Holocene seemed to be meaningful covered by the approach

AC: The change in $\delta^{13}C$ across the last glacial-interglacial cycle is a bit larger than +0.2 per mil, as stated by the reviewer comment. The change in atmospheric $\delta^{13}C$ is quoted as +0.4 per mil in the literature (e.g. Schneider et al., 2013; Eggleston et al., 2016) and is a very important feature of the last glacial-interglacial cycle of atmospheric $\delta^{13}C$. Noted our MIS-averaging also understates this full variation, but it is a very important long-term and sustained feature of the last glacial-interglacial cycle, so it is important that our analysis meaningfully captures this feature. As per Eggleston et al. (2016):

"*Due to the lack of a complete δ13C(atm) record connecting the various data sets, unanswered questions remained.* ***Most importantly****, the penultimate glacial maximum (PGM) was found to be 0.4‰ isotopically lighter in δ13C(atm) than the Last Glacial Maximum (LGM), and the penultimate warm period (marine isotope stage (MIS) 5e) was*

also more negative in δ13C(atm) by a similar amount. This is a surprisingly large difference, on the order of the changes in δ13C(atm) observed during glacial terminations."

While we don't focus on the MIS 3-5 transient $\delta^{13}C$ excursion, with better explanation provided above we can demonstrate our approach produces results that are consistent with more detailed interpretations of the transient proxy record, such as Eggleston et al. (2016).

Reviewer comments: the δ13C cycle

AC: We address the reviewer comments individually, and then provide annotated snapshots of the model code as supporting evidence in the Attachment A to our author comments.

RC: "As already seen above the steady-state approach might not be the best way to tackle atmospheric δ13C. Furthermore, for an evaluation of δ13C in general in such steady- state experiments as performed here the fluxes (e.g. as mol C/yr) and δ13C-signatures in/out of the simulated atmosphere/ocean carbon cycle are essential: atmosphere- land carbon fluxes, volcanic CO2 outgassing, weathering, and burial of organic and inorganic carbon in the sediments. Little to non of those fluxes (and δ13C-signatures) are given in the text itself. If I dig into the python source code of the model (or the description of version 1 in O'Neill et al. (2019)) I find a few information, but the source code is difficult to interpret as a non-user and some information seemed to be either misleading or wrong. An examples: Continental weathering consists of two different processes depending on the rock type that is weathered. In carbonate weathering 1 mol of CaCO3 together with 1 mol of CO2 from the atmosphere leads to the entry of 2 mol of HCO−3 into the surface ocean. In silicate weathering 2 mol of atmospheric CO2a˘ are necessary to weather 1 mol of CaSiO3 leading again to the entry of 2 mol of HCO−3 into the surface ocean. For details see, for example Lord et al. (2016). From the description of weathering in O'Neill et al. (2019) I have the impression that the carbonate weathering is not depicted correctly (no consumption of atmospheric CO2). "

AC: Re carbon fluxes/$\delta^{13}C$. We have added the below table to the Supplementary Information to describe the various prescribed fluxes of C and $\delta^{13}C$ signatures in our (revised) modelling exercise. This includes some changes from the original model/and model-data runs, from this set of review comments, and also the other reviewer comments. These changes in the model from the revised model-data experiments, will be uploaded with the final manuscript to a new Zenodo link.

Further below, we have clarified our treatment of carbonate and silicate weathering, carbonate weathering $\delta^{13}C$ signature, and we have modified our volcanic $\delta^{13}C$ and silicate weathering $\delta^{13}C$ signatures in the model (incorporated in the revised manuscript model-data results provided in the revised manuscript), in response to the reviewer comments.

Table 1: parameterisation of various fluxes of C and δ13C in the modelling experiments (**CP_RC1_Tab1.png**)

Parameter (units)	Value
Terrestrial biosphere $\delta^{13}C$ (‰)	-23
Marine biological productivity $\delta^{13}C$ (‰)	-19
Carbonate weathering DIC flux $\delta^{13}C$ (‰)	0
Silicate weathering CO_2 flux $\delta^{13}C$ (‰)	Atmosphere $\delta^{13}C$
Volcanic CO_2 $\delta^{13}C$ (‰)	-4.5
Marine carbonate $\delta^{13}C$ (‰)	0
Air-sea $\delta^{13}C$ fractionation factors	0.9989-0.999
Air-sea D14C fractionation factors	0.98-0.998
Volcanic CO_2 emissions (mol (GtC) yr^{-1})	6 x 10^{12} (0.1)
Carbonate weathering flux of C (mol m^{-3} yr^{-1})	1.5
Silicate base weathering flux of C (mol m^{-3} yr-1)	7.5 x 10^{-3}
Silicate weathering slope with respect of atmospheric CO_2 (m^{-3} yr^{-1})	0.7
Calculated carbonate weathering flux of C at 275 ppm atmospheric CO_2 (Tmol yr^{-1})	10
Calculated carbonate weathering flux of C at 190 ppm atmospheric CO_2 (Tmol yr^{-1})	7
Calculated silicate weathering flux of C at 275 ppm atmospheric CO_2 (Tmol yr^{-1})	6
Calculated silicate weathering flux of C at 190 ppm atmospheric CO_2 (Tmol yr^{-1})	5
Terrestrial NPP interglacial base rate (PgC yr^{-1})	66

Re carbonate and silicate weathering fluxes

We consulted Lord et al. (2016), as recommended by the reviewer in the RC above, and we note that the approach to carbonate weathering of Lord et al. (2016) is identical to ours, in that the activity of carbonate rock weathering simply transfers fluxes of DIC and Alk (in ratio 1:2) to the ocean via rivers, which causes a sink of CO_2 to the ocean, and their treatment of silicate weathering is very similar to ours (see below, where we looked into more detail in the rock weathering model of Lord et al. (2016), which is described in detail in Colbourn et al. (2013)).

For example, in Lord et al. (2016):

“In all schemes, the terrestrial rock-weathering module calculates global fluxes of ALK and

DIC from carbonate and silicate rock weathering and routes them to the coastal ocean".

And importantly, as described in in Colbourn et al. (2013), the carbonate weathering model used in Lord et al. (2016):

"Note that there is only one mole of DIC for each mole of Ca^{2+}; this is a short-circuiting of the atmosphere based on the assumption that the atmosphere and surface ocean are well mixed on the timescales considered here. Instead of removing one mole of CO_2 from the atmosphere – and by implication the ocean – and adding two **moles of bicarbonate to the ocean nothing is taken from the atmosphere and one mole of bicarbonate is added to the ocean**."

In addition to Lord et al. (2016), we also found our approach for carbonate and silicate weathering to be identical to a range of other studies – they are shown and referenced below. We also found our approach to δ13C in carbonate weathering, as shown by the model code as shown in the Attachment to these comments (with line-by-line annotation) was identical to that used in Sano and Williams (1996) and Mook (1986), the references suggested by the reviewer for us to consult (see RC below).

As pointed out by the reviewer, some confusion for the reader about carbonate and silicate weathering, is perhaps contributed from our simple, high level model description paper which glosses over some details (O'Neill et al., 2019) and perhaps non-user friendliness of the model code. We will add better descriptive text in our model code for the final model upload to this manuscript upon finalisation. We've provided line-by-line references to our model code in the Attachment to these responses, to help understanding.

Further on the treatment of carbonate and silicate weathering in SCP-M

The treatment of carbonate and silicate weathering in SCP-M is described in O'Neill et al. (2019) and mainly takes into account Walker and Kasting (1992), Toggweiler (2008) and Zeebe (2012) for its basis. Walker and Kasting (1992) provides the theoretical basis for treatment of carbonate and silicate rock weathering/river fluxes in many carbon cycle models (e.g. Zeebe, 2012; Colbourn et al., 2013; Lord et al., 2016). For example, Zeebe (2012) applies to the LOSCAR carbon cycle model a simple, parameterised weathering scheme based on Walker and Kasting (1992) and the same scheme was applied in simple carbon cycle feedback modelling applied by Toggweiler (2008) and Hogg (2008). An almost identical approach, was also applied by Lenton and Britton (2006), and Colbourn et al. (2013) and Lord et al. (2016). The only difference with Lenton and Britton (2006) and Colbourn et al. (2013) from our simple model, is that they applied additional temperature and terrestrial biosphere dependencies for rock weathering.

In summary, continental silicate and carbonate rock weathering are both represented in the SCP-M model. Both supply alkalinity and carbon to the surface ocean in ratio 2:1 (e.g. more alkalinity than DIC).

The weathering equation used in the model, are as per the model documentation (O'Neill et al., 2019), and the original model code at (https://doi.org/10.5281/zenodo.1310161), and is reproduced here:

$dC/dt\_{weath} = (W_{SC} + (W_{SV} + W_{CV})AtCO_2)$

where W_{SC} is a constant silicate weathering term set at $0.75x10^{-4}$ mol m^{-3} $year^{-1}$, W_{SV} is a variable rate of silicate weathering per unit of atmosphere CO_2 (ppm), set to 0.5 mol m^{-3} atm^{-1} CO_2 $year^{-1}$ and W_{CV} is the variable rate of carbonate weathering with respect to atmosphere CO_2, set at 1.5-2.0 mol m^{-3} atm^{-1} CO_2 $year^{-1}$ (Toggweiler, 2008).

There is a slight difference between carbonate weathering versus silicate weathering, in our model, in terms of the direct consumption of CO_2 from the atmosphere when weathering takes place. This direct consumption of CO_2 is assumed to be fully reversed in the case of carbonate weathering, but is only partially reversed in the case of silicate weathering. The main CO_2 sink activity of the carbonate weathering, is therefore is in the alkalinity fluxes to the ocean and its effects on relative pCO_2 in the ocean versus the atmosphere (e.g. Colbourn et al., 2013).

Carbonate weathering

Weathering of carbonate rocks initially takes up CO_2 from the atmosphere (one mol), and supplies calcium and bicarbonate ions to the ocean (an additional mol of carbon), as per the following equation:

$CaCO3+H2O+CO2= Ca^{2+}+2HCO^{-}3$

Therefore, two moles of carbon and one mole of calcium enter the ocean for each mole of $CaCO_3$ weathered. This raises ocean carbon and alkalinity by two units each. In steady state, subsequent precipitation of $CaCO_3$ releases the same amount of CO_2 back to the atmosphere that was consumed by weathering (Zeebe, 2012) – a short-term circular loop that leads to a net zero direct consumption of CO_2 from the atmosphere from carbonate weathering (e.g. Colbourn et al., 2013; Lord et al., 2016). This is described in detail in Zeebe (2012).

Figure 2: Extract of the Zeebe (2012) schematic description of carbonate weathering (**CP_RC1_Fig2.png**)

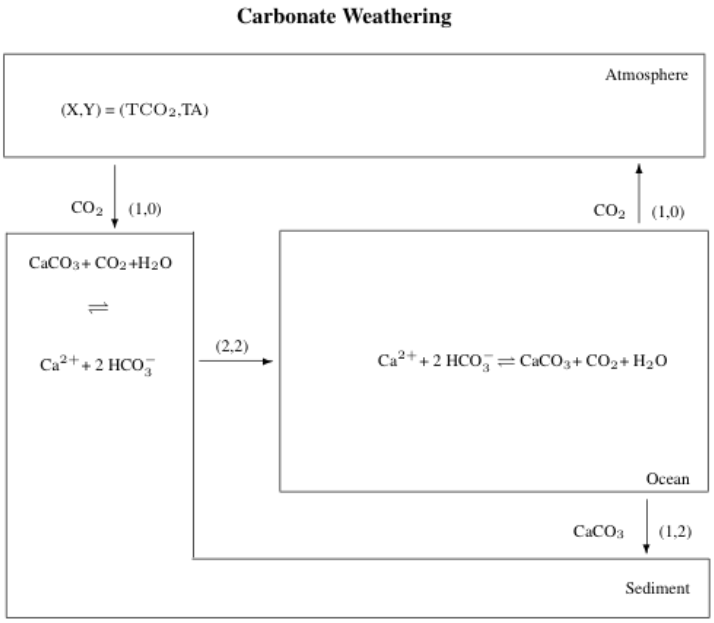

This return of CO_2 to the atmosphere (one mol of carbon) leaves a net addition to the ocean of carbon and alkalinity from carbonate weathering in 1:2 ratio (Zeebe, 2012). The ocean carbon and alkalinity balance is later restored due to subsequent burial and $CaCO_3$ and carbonate compensation (Zeebe, 2012).

According to Zeebe (2012):

"*As a result, although the addition of Ca2+ and 2 HCO 3 increases ocean TCO2 : TA in a 2:2 ratio, on a net basis CaCO3 weathering increases ocean TCO2 : TA in a 1:2 ratio because one mole of CO_2 returns to the atmosphere. If influx equals burial, carbonate weathering thus represents a zero net balance for atmospheric CO_2.*"

For our steady state modelling, we assume the CO_2 consumed directly by the carbonate weathering process is returned to the atmosphere – a net zero of **direct** consumption of CO_2 from the atmosphere. This is a short-circuiting of the process, but not incorrect (refer Colbourn et al. (2013) quote reproduced above, about "short-circuiting" direct atmospheric CO_2 effect of carbonate weathering). Therefore, the fluxes associated with carbonate weathering are those of DIC and alkalinity into the surface ocean boxes of the model. This is the same approach applied by Toggweiler (2008), and Lenton and Britton (2006), and identical to the approach of Lord et al. (2016), and Colbourn et al. (2013). For these studies, the sink of atmospheric CO_2 from carbonate weathering comes indirectly through the effects of alkalinity supplied to the surface ocean which lowers pCO_2 and draw CO_2 into the ocean. Some interesting quotes from those references below, with bolded parts for emphasis.

The approach for carbonate weathering in Lord et al. (2016) (the reference suggested by the reviewer), is referenced in that study to Colbourn et al. (2013), and is described in Colbourn et al. (2013) as:

"*Note that there is only one mole of DIC for each mole of Ca2+;* ***this is a short-circuiting of the atmosphere based on the assumption that the atmosphere and surface ocean are well mixed on the timescales considered here. Instead of removing one mol of CO2 from the atmosphere – and by implication the ocean – and adding two moles of bicarbonate to the ocean (as in Eq. 1), nothing is taken from the atmosphere and one mole of bicarbonate is added to the ocean*****."**

And "***The fluxes are then used to calculate fluxes of DIC (FDIC) and Alkalinity (FAlk)***".

We note further from Colbourn et al. (2013):

*"**In the case of carbonate weathering there is an overall null cycle for CO2, whereas silicate weathering transfers CO2 to the Earth's crust***."

In summary, our simple box modelling representation of carbonate weathering is consistent with the theory of carbonate chemistry, and the literature on modelling of carbonate weathering. Our calculated estimate of 10 Tmol C yr^{-1} from carbonate weathering supplied to the ocean at 275 ppm atmospheric CO_2, is comparable to that of 12 Tmol mol C yr^{-1} in Morse and Mackenzie (1990) and Zeebe (2012), Archer et al. (1998), but higher than that assumed by Colbourn et al. (2013) and Lord et al. (2016) of 5 Tmol C yr^{-1}. In those latter two studies, they simply assume an even, equal split of the fluxes of silicate and carbonate weathering in their model spin-up Fsil=Fcarb=5 Tmol C yr^{-1}. However, Colbourn et al. (2013) quote post-spin-up, pre-industrial total flux of weathering of 12-20 mol C C yr^{-1}, split equally between carbonate and silicate weathering (6-10 mol C yr^{-1} each).

We have supplied an annotated snapshot of our model code, in the Attachment A to these comments (below).

<u>Silicate weathering</u>

Silicate rock weathering can be described by the following chemical equation:

$$CaSiO_3 + H_2O + 2\,CO_2 = Ca^{2+} + 2HCO^-_3 + SiO_2$$

Silicate rock weathering removes 2 mols of CO_2 from the atmosphere for each mole of $CaSiO_3$ weathered. The subsequent precipitation of $CaCO_3$ in the ocean releases one mole of CO_2 back to the atmosphere, with the other mole of CO_2 consumed by the atmosphere, taken up in $CaCO_3$, which may end up buried in the marine sediments (Zeebe, 2012). In steady state, over long timeframes, the silicate weathering direct consumption of atmospheric CO_2 balances out volcanic emissions of CO_2 (*Berner et al., 1983; Zeebe and Caldeira, 2008, Zeebe, 2012).* Because the steady state in the silicate weathering is achieved over a much longer timeframe (1e5-1e6 years), it is appropriate to model a direct sink of CO_2 from the atmosphere associated with silicate weathering. The steady state atmosphere-ocean response to carbonate weathering only requires a relatively short timeframe, hence we can model the steady state assumption of carbonate weathering returning its direct consumption of CO_2 to the atmosphere (Walker and Kasting, 1992; Lenton and Britton,

2006; Toggweiler, 2008, Zeebe, 2012).

Therefore, relative to carbonate weathering, there is an additional step applied with silicate weathering. To account for the unit of CO_2 consumed directly from the atmosphere in silicate weathering that is not returned (one more unit than carbonate weathering, as per Zeebe, 2012), and using the approach of Toggweiler (2008), we also subtract an amount equal to a unit of silicate weathering directly from the atmosphere. This is the same approach of Zeebe (2012) who applies a doubling of the molar flux of silicate weathering (to replicate two mols of CO_2 initially drawn from the atmosphere), and that of Toggweiler who subtracts a flux of CO_2 directly from the atmosphere (but no direct consumption of CO_2 in the case of carbonate weathering) to account for the additional unit of CO_2 consumed by silicate weathering (when compared with carbonate weathering). This flux is subtracted directly from Atmospheric CO_2 in SCP-M as referenced in the model equation above (and described in the code in Attachment A to these comments). This flux, subtracted from the atmosphere, negates the effects on atmospheric CO_2 of the units of C added to the ocean by the silicate weathering flux of C. Volcanic CO_2 emissions are set equal to the amount of CO_2 taken directly from the atmosphere by silicate weathering, to reflect the long-term offset of volcanic emissions by silicate weathering (Walker and Kasting, 1992; Archer et al., 1998, Toggweiler, 2008; Zeebe, 2012, Colbourn et al., 2013; Brault et al., 2017).

As described in Walker and Kasting (1992), Toggweiler (2008), Zeebe (2012) Brault et al. (2017), Colbourn et al. (2013, 2015) and Lord et al. (2016), in steady state the silicate weathering flux feedback for CO_2 matches the volcanic CO_2 emissions, which we have set in SCP-M. Note, for anthropogenic scenarios we separate volcanic emissions from weathering flux, because the silicate weathering feedback under the forcing of atmospheric CO_2, is expected to increase at a greater rate than volcanic emissions (volcanic emissions do not respond to anthropogenic emissions of CO_2).

Our calculation for silicate weathering yields a flux of carbon to the oceans 6.3 T mol C yr^{-1}. At 275 ppm atmospheric CO_2. Our volcanic emissions rate is set to this figure, which is in good agreement with Lord et al. (2016) who set their volcanic C flux at 5.6 Tmol yr^{-1} to balance the silicate weathering component.

AC: Furthermore, from the python code I learned that weathering (probably meaning carbonate weathering, since in silicate weathering all CO2 comes from the atmosphere with its δ13C-signature) has a δ13C-signature of −6.9‰, similarly as volcanic CO2. While the volcanic δ13C seems to be in the expected range (although on the lower side) I believe the weathering δ13C-signature is wrong, since carbonate rocks have a typical δ13C-signature of about +1-2‰, see for example Sano and Williams (1996); Mook (1986).

AC: Re carbonate weathering. The $\delta^{13}C$ of carbonate weathering in our model is not -6.90 per mil, as stated in the reviewer comment above, but it is 0 per mil, via our application of the reference standard value for $\delta^{13}C$ (the Pee Dee Belemnite) = 0. This feature is shown clearly in the annotated excerpt of the model code in the Attachment A. 0 per mil is the identical value for carbonate weathering used in the first reference provided by the reviewer (Sano and Williams, 1986), and precisely in the middle of the range (+/- 1 per mil)

used in the second reference provided by reviewer (Mook, 1986). We have added text to our model code to make this more obvious.

With regards to silicate weathering $\delta^{13}C$. In the SCP-M model the $\delta^{13}C$ of silicate weathering CO_2 drawdown was originally set at -6.90 per mil, which is the same as the volcanic $\delta^{13}C$ we had assumed. This approach was consistent with offsetting volcanic CO_2 emissions with silicate weathering (Zeebe, 2012; Toggweiler, 2008, Lord et al., 2016; Colbourn et al., 2013, 2015; Walker and Kasting, 1991). This is a simplification with regards to the $\delta^{13}C$, and therefore we have changed this, and now applied the atmospheric $\delta^{13}C$ signature output from the model to the silicate weathering flux (this is now updated in our model results/re-runs). As per the reviewer comments we have now set the $\delta^{13}C$ of the direct consumption of CO_2 by silicate weathering, to take atmospheric $\delta^{13}C$ value. This is a modest change, however, as atmospheric $\delta^{13}C$ is in the range -6.3-7 per mil in the last glacial-interglacial cycle, and we had initially assumed a fixed value of -6.90 per mil.

We also note the reviewer comment that our assumption of -6.90 per mil for volcanic CO_2 emissions is at the low end of literature estimates. We have modified this to -4.5 (compared with -4.0 in Zeebe, 2012).

In summary, the changes we have incorporated in the final set of model runs for this manuscript, guided by the reviewer comments:

- We have changed the $\delta^{13}C$ of silicate weathering direct consumption of CO_2 from the atmosphere, to the atmospheric $\delta^{13}C$ signature outputted from model at each time step, as suggested in the reviewer comments (previously it was set as -6.90 per mil).
- We have adjusted our $\delta^{13}C$ of volcanic emissions from -6.90 to -4.50 per mil, which is more of a “middle of the range” value.
- We have tidied up the model code description of carbonate weathering and its $\delta^{13}C$ (for upload to the Zenodo repository upon finalisation of the manuscript).

RC: I also do not understand how their approach with not explicitly considering terrestrial carbon change (terrestrial carbon to my understanding is covered as externally to the atmosphere/ocean system, fluxes in/out of it prescribed by optimization) covers changes in C3 vs C4 photosynthesis (which have a significantly different isotopic frac- tionation) on glacial/interglacial timescales (Collatz et al., 1998; Köhler and Fischer, 2004) which leads to differences in the mean terrestrial δ13C and therefore also the changes in the δ13C-cycle as a whole (Kaplan et al., 2002).

AC: Thanks for the comment. Our response is broken in two parts 1) the terrestrial biosphere and 2) C3 vs C4 photosynthesis.

In summary, the terrestrial biosphere is explicitly considered in our modelling. It is two boxes within the carbon cycle box model we have used. It is not prescribed by optimisation.

We have decided not to assess C3 versus C4 photosynthesis and its effects on δ13C fractionation.

We discuss both of these points in more detail below.

Terrestrial biosphere in SCP-M

The terrestrial biosphere is treated in SCP-M as two boxes that exchange carbon with the atmosphere based on fluxes of net primary productivity (NPP) (carbon in) and respiration (carbon out). It is part of the carbon cycle that includes the terrestrial biosphere-atmosphere-ocean-sediments-volcanoes etc. Our box model applies a simple representation of the terrestrial biosphere, whereby biological productivity responds to carbon fertilisation. Therefore, CO_2 is the driver of terrestrial biosphere productivity in this model. We apply the two-box terrestrial box model scheme of Harman et al. (2011). The inputs are starting estimates of net primary productivity (NPP), the terrestrial biosphere carbon stock, plant respiration rate and atmospheric CO_2. The approach of Harman et al. (2011) is to split the terrestrial biosphere into a fast-response (grasslands and grassy components of savannah systems) and a slow-response (woody trees) component. In this model, the productivity is mostly focussed on the plants/grasses component.

The formula is shown in the model documentation paper (O'Neill et al., 2019) and Harman et al. (2011), and is reproduced here:

$$dAtCO2/dt = -N_{pre}RP[1+\beta LN(AtCO2)] + Cstock/k + D_{forest}$$

Where Npre is NPP at a reference pre-industrial level of atmospheric CO2, RP is a parameter to split NPP between short-term terrestrial biosphere carbon stock and the longer term stock (Cstock1 and Cstock2). B is a parameter with a value typically in the range 0.4-0.8 (Harman et al., 2011). Cstock is the carbon stock in each terrestrial biosphere box, k is the respiration timeframe for each box. Dforest is the prescribed rate of deforestation emissions for present day simulations and projections. A terrestrial biosphere fractionation factor is applied for the carbon isotopes.

This flux out of the atmosphere feeds into the two terrestrial biosphere stocks of carbon (Cstock1 and Cstock2), and the boxes lose carbon to the atmosphere by respiration, as per the equation above. This differential equation for NPP, respiration, and the net flux into and out of the terrestrial biosphere (increase or decrease in the terrestrial biosphere carbon stock), solves at each time step of the model, taking the model's output of CO_2 and then the NPP, respiration, Cstock1 and Cstock2 carry forward into the next simulation. The time step of the model is one year, with 10,000 years for each model-data simulation, so this is appropriate to allow the terrestrial biosphere to adjust within each simulation.

Harman et al. (2011) model the terrestrial biosphere primarily as a function of atmospheric CO_2. They also incorporate an optional temperature dependency. This is the same approach used in the simplest 4Box terrestrial biosphere module of the Bern Simple Carbon Model (Strassman and Joos, 2018; Seigenthaler and Joos, 1992; Kicklighter et al., 1999; Meyer et

al., 1999), and described by Enting (1994) – although we understand that there are various terrestrial biosphere modules applied with the Bern models, and most are more complex. As far as we can discern, the simple carbon fertilisation approach is also used in Jelstch-Thommes et al. (2019), which also applies the simplest 4Box terrestrial biosphere of the simple Bern model.

There are other possible drivers of the NPP – temperature, precipitation, soil nutrient levels. In the context of our simple carbon cycle model, we are mainly interested in CO_2. We don't model atmospheric temperature, and if we were to try to incorporate atmospheric temperature as a driver of terrestrial biosphere, we would also need to incorporate it for terrestrial weathering. There is a limit to how much detail we want to include in the model given we are conducting many simulations (~80,000) in our model-data optimisations across the MIS of the last glacial-interglacial cycle.

We do note that there are studies devoted to determining whether the CO_2 fertilisation effect or climate is the dominant control on terrestrial biosphere NPP and the size of the terrestrial biosphere carbon stock. According to Hoogakker et al. (2016), CO_2 fertilization, rather than climate, is the primary driver of lower glacial net primary productivity by the terrestrial biosphere, accounting for around 85% of the reduction in global NPP at the LGM. Kaplan et al. (2002) also concluded that over glacial-interglacial timescales, global terrestrial carbon storage is controlled primarily by atmospheric CO_2, while the climate has more influence on the isotopic composition. Otto et al. (2002) also found that the CO_2 fertilization effect is mostly responsible for the total increase in vegetation and soil carbon stocks since the last glacial maximum. Kohler et al. (2010) prioritised CO_2 fertilisation as the driver of terrestrial biosphere in their "control" main simulation scenario for glacial-interglacial cycles over the last 740 kyr, but also ran scenarios with a climatic driver for the terrestrial biosphere to estimate the effects of "fast" climate changes on atmospheric $\delta^{13}C$. Other studies arguing that atmospheric CO_2 is an important, or is the main driver of terrestrial biosphere productivity include Kicklighter et al. (1999), Joos et al. (2004), Schimel et al. (2015), Sitch et al. (2008), Arneth et al. (2017). This view has been contested by van der Sleen et al. (2015).

Given we don't model the atmospheric temperature or precipitation, we saw limited additional benefit to introduce them into our model of the terrestrial biosphere, although it would not be difficult to do this. Finally, given that CO_2 and atmospheric temperature co-vary closely, across glacial cycles, it seems of limited benefit to split these effects out in our simple carbon cycle modelling exercise. For example, Meyer et al. (1999) found similar results for modelling carbon uptake in the terrestrial biosphere whether only CO_2 fertilisation, or CO_2 fertilisation + climate, were included as drivers of NPP – but noting this was not tested for the LGM.

Our aim is not to contribute new findings on the terrestrial biosphere, but we present the behaviour of the terrestrial biosphere in our manuscript to confirm that our exhaustively multi-proxy constrained model-data output is consistent with the range of literature estimates of variations in the terrestrial biosphere in the last glacial-interglacial cycle and LGM-Holocene period, and we show this. For example, our experiment shows a change in the terrestrial biosphere carbon stock of +630 PgC between the MIS 2 (LGM) and MIS 1

(Holocene) period. This compares with other estimates of +540 PgC (Brovkin et al., 2007), +~820-850 PgC (Joos et al., 2004) – with the majority by CO_2 fertilisation, ~+500 PgC (Kohler et al., 2010), +~500 PgC (Brovkin et al., 2012), +850 PgC (Jeltsch-Thommes et al., 2019), +511 +/- 289 PgC (Peterson et al., 2014), +378 +/- 88 PgC (Menviel et al., 2016). Another estimate of the LGM-Holocene terrestrial biosphere change is 550-694 Pg C (Prentice et al., 2011), which our result of 630 Pg C sits comfortably within.

Our estimate is actually towards the upper end of the literature ranges, suggesting if anything we could exaggerate the effects of the terrestrial biosphere from the LGM to the Holocene period, with perhaps little to gain by splitting out temperature and precipitation effects. If did, we would probably also need to consider other important features such as soil nutrients and local humidity.

While we have a simple, but explicit two-box representation of the terrestrial biosphere, we don't believe that this detracts from our model-data results, as shown in Figures 9-11 and Figure 12 specifically for the terrestrial biosphere.

C3 and C4 photosynthesis.

In summary, our model exercise doesn't take account of C3 versus C4 photosynthesis in the terrestrial biosphere, or consider its effects on the $\delta^{13}C$ signature of the terrestrial biosphere. In response to the reviewer comments, we looked into this in more detail to see if we can improve our modelling – noting that it is very easy to update the model code for something like this. For example, we re-ran the model-data experiments as part of one of the other reviewer comments, so could easily incorporate more detail for the terrestrial biosphere, such as C3%/C4% variation in $\delta^{13}C$.

Our approach was to understand and quantify the references provided by the reviewer, review approaches by other modelling exercises for the glacial-interglacial cycle of last 130 kyr, and decide whether we should re-run the modelling with an alternative treatment of the terrestrial biosphere to cater for C3%/C4% and $\delta^{13}C$. As part of investigation, we also constructed the C3/C4 model of Collatz et al. (1998)/Kohler and Fischer (2004) in a python module that easily fits into the carbon cycle box model, to evaluate whether it would improve our modelling (described below and attached to these comments).

Kohler and Fischer (2004), suggested reading by the reviewer, in their excellent paper do make a very good point about C3/C4 photosynthesis in the context of glacial-interglacial $\delta^{13}C$, that is worth reproducing here as a summary:

"*Oceanic inorganic carbon is becoming 0.4 heavier during the G/IG transition, which is in good agreement with both modelling studies and data constraints (Curry et al., 1988; Duplessy et al., 1988; Michel et al., 1995).* ***It should be noted that 85% of this calculated oceanic change in $\delta^{13}C$ can be explained by the increase in the terrestrial carbon stock and only the missing fraction of 15% by changes in the abundance of the two photosynthetic pathways. Thus, uncertainties in the current knowledge on C_3/C_4 plant distribution during the LGM are of minor importance for the overall simulation results.*** "

Collatz et al. (1998)/Kohler and Fischer (2004) modelling approach

The Collatz et al. (1998) approach to modelling C3 vs C4 %, is based on the estimation of a "cross-over temperature" for dominance of C4 or C3 plants. Above the cross-over temperature, C4 plants are favoured. Below the cross-over temperature, C3 plants are favoured. Collatz et al. (1998) derived a simple equation for the cross-over temperature of C3 vs C4. The cross-over temperature exhibits a positive relationship with atmospheric CO_2. Therefore, as CO_2 goes up, the cross-over "hurdle" temperature for C4 dominance also increases, so C4% has a negative relationship with CO_2. While increasing temperatures may favour C4 plants, if CO_2 was also increasing, this would tip the advantage back towards C3 plants. The cross-over temperature calculation of Collatz et al. (1998) is shown as (**CP_RC1_T50.png**):

$$T_{50}(^{\circ}\mathrm{C}) = \frac{10}{\ln Q_{10}} \ln\left(\frac{p\mathrm{O}_2(1+0.5\frac{\alpha_{C3}}{\alpha_{C4}})}{0.8 \cdot p\mathrm{CO}_2 \cdot s_{25}(\frac{\alpha_{C3}}{\alpha_{C4}}-1)}\right) + 25.$$

Where T_{50} is the crossover temperature for C4 and C3 dominance, where a_{C3} is the "intrinsic quantum yield for C3 photosynthesis" and p_i is the leaf internal pCO_2, assumed to be equal to 0.8 x atmospheric pCO_2. s_{25} is the value of s at 25°C and Q_{10} is the relative change in s for a change in temperature.

s is defined as (**CP_RC1_s.png**):

$$s = 2,600\ Q_{10}^{\frac{T_X-25}{10}}$$

To analyse C4%, Kohler and Fisher (2004) extended the Collatz et al. (1998) equation and provide a simple set of equations to estimate C4% and C3% between the glacial and interglacial periods, using the change in temperature relative to changes in the cross-over temperature between the two periods (**CP_RC1_C3C4.png**):

$$\widetilde{C^*_{\mathrm{C4}}} = C^*_{\mathrm{C4}} \cdot (1 - a_{\mathrm{C3/C4}} \cdot (\Delta T - \Delta T_{50})),$$
$$\widetilde{C^*_{\mathrm{C3}}} = C^*_{\mathrm{C3}} \cdot (1 + a_{\mathrm{C3/C4}} \cdot (\Delta T - \Delta T_{50})).$$

We reconstructed this model of Collatz et al. (1998)/Kohler and Fischer (2004) in the attached python script (python cannot be uploaded, so we have attached a pdf of the model code, the data dependencies of atmospheric CO_2 and temperature for the last glacial-interglacial cycle (.txt data files), can also be provided). We use the cross-over temperature

calculation of Collatz et al. (1998), the C4% model of Kohler and Fischer (2004), and estimate an average terrestrial biosphere $\delta^{13}C$ using the C4% and C3% output from this model and estimates of $\delta^{13}C$ for C4 and C3 plants.

https://zenodo.org/record/3889704#.XuH3Ji1L0_U

To test our simple model works, we satisfy the estimate of T_{50} of 22 deg C at atmospheric pCO_2 of 350 ppm from Collatz et al. (1998), and, as per Kohler and Fischer (2004) Figure 4, ~18 deg C at atmospheric pCO_2 of ~280 ppm, and ~11 deg C for atmospheric pCO_2 of ~190 ppm.

We forced our version of the C4% model of Kohler and Fischer (2004)/Collatz et al. (1998) with atmospheric temperature and CO_2 through the last glacial-interglacial cycle (Figure 3 below). The atmospheric temperature data of Jouzel et al. (2007) is derived from Antarctic ice cores, so it likely overstates the amplitude global average temperature cooling during the glacial period. Jouzel et al. (2007) show peak cooling of ~11 degrees C, which is greater than global estimates in the range 3-6 deg C (Schneider von Deimling et al., 2006a; Holden et al., 2009; Schmittner et al., 2011; Annan and Hargreaves, 2013). We take an intermediate average global LGM cooling of 4.5 degrees, and scale the profile of Jouzel et al. (2007) to the average global amplitude of cooling of 4.5 deg C for the LGM, which is the middle of the range of global estimates. This is a simplification, but appropriate for our reconnaissance exercise. We also apply the last glacial-interglacial cycle atmospheric CO_2 data of Bereiter et al. (2015) – Figure 3 below.

In terms of what starting values to use for $\delta^{13}C$ for the C3 and C4 plants, we note a huge variation in the possible values to use for $\delta^{13}C$ of C3 plants, and also note a large variation in the estimates for average $\delta^{13}C$ of the terrestrial biosphere applied in terrestrial biosphere and carbon cycle modelling exercises for the last glacial-interglacial cycle. We discuss in more detail below, but flag that natural variation in the average values assumed for $\delta^{13}C$ fractionation of the terrestrial biosphere, and variation in $\delta^{13}C$ values assumed between modelling studies, greatly outweigh the posited variation in $\delta^{13}C$ fractionation from C4% vs C3%.

Carbon cycle modelling exercises show a large range (e.g. Brovkin et al., 2002 (-16 per mil), Menviel et al. (2016) (-23.3 per mil), Jelstch-Thommes et al. (-24 per mil), and the study of Kohler and Fisher applied an average of -16 per mil (C3 -19 per mil, C4 -5 per mil). For this simple exercise, we take the starting average δ13C for terrestrial biosphere taken from Jeltsch-Thommes et al. (2019) (this text was a suggested reference by the reviewer) of -24 per mil, and back out the average starting C3 and C4 $\delta^{13}C$ assuming the PI value of C4% of 20% applied in Kohler and Fischer (2004) (the reference suggested by the reviewer). This yields a starting $\delta^{13}C$ for C3 plants of -27 per mil, and -14 per mil for C4 plants. For comparison, Kohn et al. (2010) provided a range of $\delta^{13}C$ estimates for C3 plants of -20 to -37 per mil, with a global average of -27 per mil. O'Leary et al. (1988) provided a synthesis of global data of -27.1 per mil for C3 plants and -13 per mil for C4 plants.

We model C4% to vary from the preindustrial starting estimate of 20% (Kohler and Fischer, 2004), up to an average of 25% during the LGM (Figure 3). We model average $\delta^{13}C$ for the terrestrial biosphere to vary between the range -24.2-23.6 per mil during the last glacial-interglacial cycle, a variation of 0.6 per mil (Figure 3 below).

Figure 3: Modelling of the share of C4 photosynthetic plants (C4%) (bottom panel) and average terrestrial biosphere $\delta^{13}C$ fractionation factor (middle panel) as a function of atmospheric CO_2 and temperature for the last glacial-interglacial cycle (**CP_RC1_Fig3.png**).

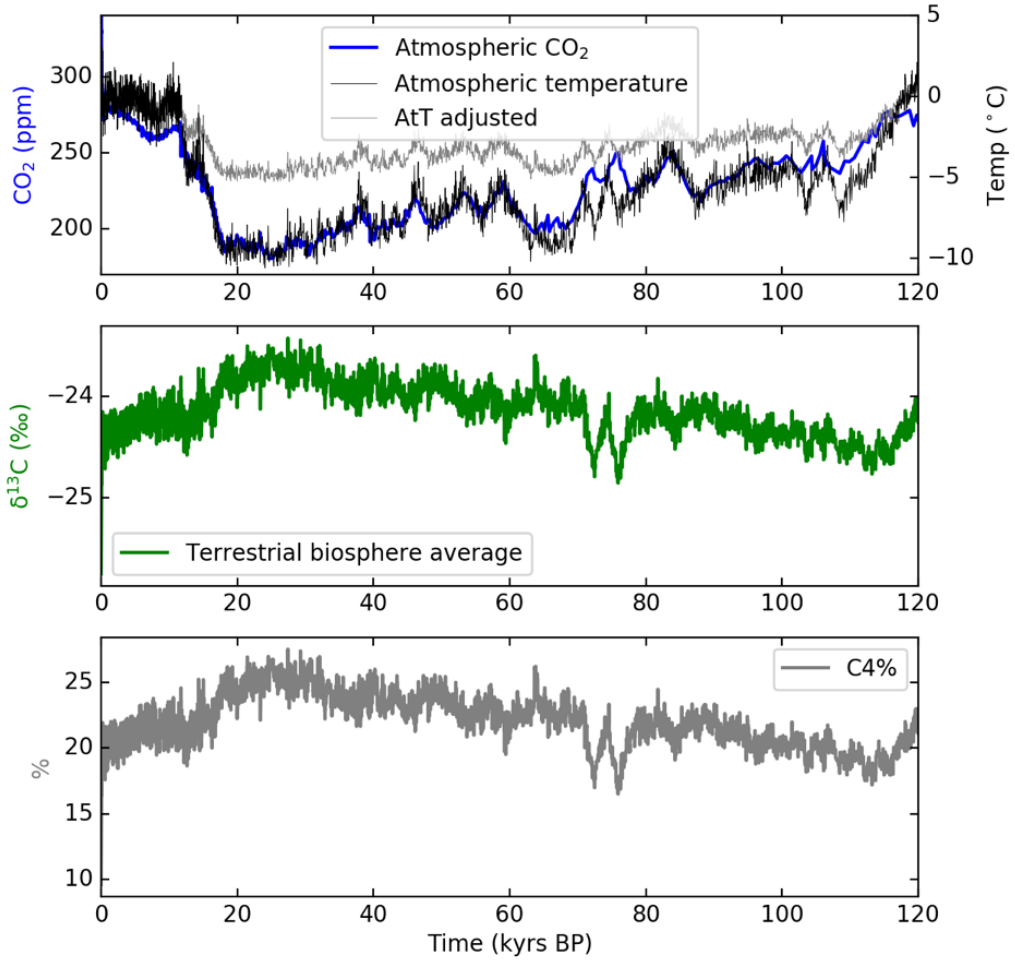

Our estimated C4% from using the Collatz et al. (1998) equation (25%) is a little higher than Kohler and Fischer (2004) (24%) and this likely reflects differing atmospheric CO_2 and temperature assumptions. For example, Kohler and Fischer (2004) take average northern hemisphere average temp change of -5 degrees, and southern of -8 degrees. We have inputted a global average change of -4.5 degrees C as per the literature range of 3-6 degrees C cooling. However, there must be something else being applied by Kohler and Fischer (2004) to achieve their LGM "target" C4% of 30-33%.

The approach of Kohler and Fischer (2004) was to establish a target variation of C4% between the LGM and the PI and then to see what parameterisations of their model runs could reach that target. Our estimate of LGM C4% is of 25% is far below the "targeted" C4% of 30-33% from Kohler and Fischer (2004). Their study found that varying the C4% amplitude

in the Collatz et al. (1998) C3/C4% share model could increase C4% from 20% to 24%, but increasing the grassland succession amplitude increased the C4% up to 42%, a much bigger change than the C3/C4% share model alone. Furthermore, according to Huang et al. (2001), local moisture conditions might be even more important than any temperature or CO_2 effects on C3/C4%.

The grassland succession factor is an equation contributed by Kohler and Fischer (2004) to estimate the effects of changes in the tree-line (the divide between where trees and grasses grow) as a function of changes in temperature, between the LGM and PI. According to Kohler and Fisher (2004), this is the main driver for the C4% change and change in the terrestrial biosphere $\delta^{13}C$ fractionation, perhaps not the temperature and CO2-dependant equation of Collatz et al. (1998).

Kaplan et al. (2002) posit something different again, that the major driver of changed terrestrial biosphere $\delta^{13}C$ discrimination since the LGM is retreating ice sheets, with an additional or ancillary role for C3/C4 plant substitution.

Our estimated change in terrestrial biosphere $\delta^{13}C$ fractionation of ~+0.6 per mil, is below the estimate from Kohler and Fischer of 1.3 per mil, and that reflects that they include the grassland succession factors in their LGM-PI analysis. The offset in assumed $\delta^{13}C$ fractionation between C3 and C4 of -13 per mil (-27 per mil less -14 per mil) is very similar to their chosen -14 per mil (-19 per mil less -5 per mil), suggesting that the differences reflect the use of another factor outside C3/C4%, the grassland succession factors, to drive their results.

Beyond the simple exploratory attempt above, modelling highly uncertain grassland succession factors, or ice sheet retreat/advance, or localised moisture and temperature changes, to try and explain uncertain changes in C3% vs C4%, for which the starting values themselves could fall within huge ranges of uncertainty, looks beyond the scope of our study.

We note that, with regard to the estimates of C4% used by Kohler and Fisher to create "targets" for pre-industrial and LGM periods, Kohler and Fisher (2004) say the following:

"NPP and f_{C4} for the LGM are based on modelling studies only and, thus, represent only weak indicators which were only used for uncertainty estimates." And furthermore, on P16:

"However, because the constraints on NPP and the **fraction of C_4 plants were based on only a few mostly modelling studies, we merely interpret those as a model evaluation**."

These findings underscore the uncertainty of estimates for quantifying C4/C3 and therefore $\delta^{13}C$ of the terrestrial biosphere. This uncertainty is amplified in the actual estimates of $\delta^{13}C$ for C3 and C4 plants, as we discuss below.

The Figure below is reproduced from Kohn (2010), and shows the range in $\delta^{13}C$ fractionation for C3 plants alone, which spans -20 to -37 per mil, and is impacted by many factors including temperature, precipitation, and effects of canopies and new growth (**CP_RC1_Kohn1_extract.png**).

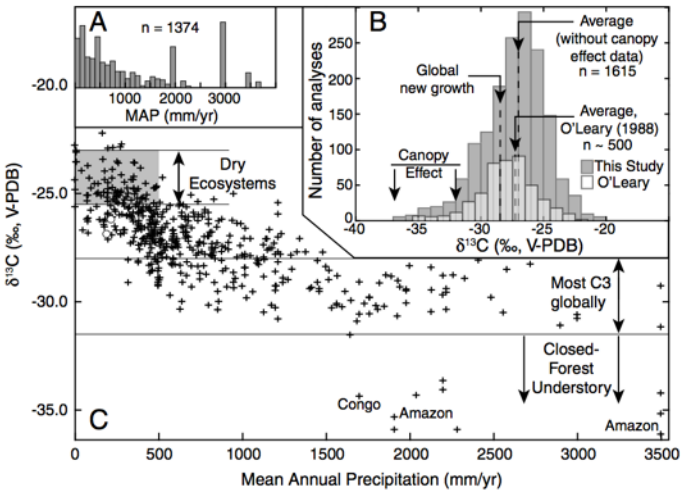

Fig. 1. (*A*) Histogram of MAP values for isotopically charact.erized C3 plants, showing emphasis on relatively arid ecosystems (MAP ≤ 500 mm/yr) and tropical rainforests (spikes at MAP ~ 2,000, 3,000 mm/yr). (*B*) Histogram of $\delta^{13}C$ values of modern C3 plants. Data compiled in this study average −27.0‰, excluding analyses from the understory of closed-canopy forests. Estimated global average composition, based on global trends in precipitation and vegetation, is approximately −28.5‰, significantly lower than typically assumed. An accurate average $\delta^{13}C$ value for C3 plants is needed for accurate models of carbon fluxes, atmospheric CO_2 compositions, and soil organic matter. (*C*) $\delta^{13}C$ values vs. MAP showing increasing $\delta^{13}C$ with aridity. Data sources are listed in *SI Text*. White dots are average compositions of data from a large collection made in a single month during a wet year (35).

Furthermore, more recently, Kohn (2016) attempted to estimate the change in $\delta^{13}C$ for C3 plants from the LGM to modern day, based on atmospheric CO2, and also to quantify the effects of precipitation on C3 plant $\delta^{13}C$. This Figure shows the variation in C3 $\delta^{13}C$ discrimination itself, is even bigger than the posited effect of C3/C4% (see Figure below from Kohn (2016) - **CP_RC1_Kohn2_extract.png**).

To model C3 and C4 $\delta^{13}C$ properly, there are other important effects in C3 plants (on their own), that would need to be taken into account. For example, Francois et al. (1999) point out that changes in the $\delta^{13}C$ fractionation from a changing C4% were partially offset by changes in the opposite sign in the fractionation of C3 plants due to the modification of the intercellular CO_2 pressure within their leaves.

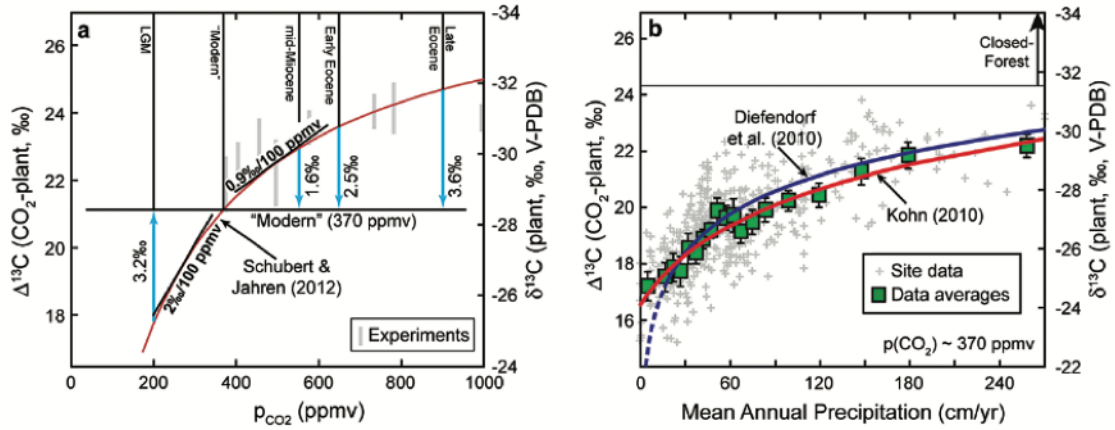

Figure 1 Proposed models for factors that influence $\delta^{13}C$ of C3 plants. **(a)** p_{CO2}. Differences are illustrated between geological conditions vs. AD 2000 (p_{CO2} = 370 ppmv, average $\delta^{13}C$ = -28.5 for C3 biomass). LGM = Last Glacial Maximum. Note inverse relationship between $\delta^{13}C$ and $\Delta^{13}C$. Experiments are for above-ground biomass (Schubert and Jahren, 2012), shifted to fit preferred curve. **(b)** Mean annual precipitation (data and data averages from Kohn, 2010).

Peer group/modelling approaches

In exploring this issue of C3 vs C4% and $\delta^{13}C$ further, and to benchmark our work against the peers who are modelling and analysing the last glacial-interglacial cycle (0-130 ka), we investigated the literature. C3 versus C4 fraction in photosynthesising plants is not discussed much in the literature of modelling of the last 130 kyr glacial-interglacial cycle of carbon. We couldn't find any reference to C3/C4 photosynthesis and $\delta^{13}C$ in Eggleston et al. (2016), who contributed the atmospheric $\delta^{13}C$ data we used in our model-data analysis. We don't find any mention of C3/C4 photosynthesis and its effects on $\delta^{13}C$ in any of Ganopolski et al. 2010, Brovkin et al. 2012, Eggleston et al., 2016; Ganopolski and Brovkin, 2017; Kohfeld and Chase, 2017.

Brovkin et al. (2002) simply state, with reference to their CLIMBER-2 model of the last glacial-interglacial cycle:

"*Most of the carbon (ca. 85%) is allocated to the C3 photosynthesis pathway and the remaining carbon (15%) to the C4 pathway. The globally averaged $\delta^{13}C$ fractionation factor for terrestrial biosphere is 0.984.*" (-16 per mil).

We find no reference to any changes for glacial interglacial C3 and C4 and terrestrial biosphere $\delta^{13}C$ modelled in Brovkin et al. (2007, 2012), or Ganopolski (2010, 2017).

The transient modelling of the last glacial-interglacial cycle, undertaken by Menviel et al. (2012b), does not mention C3 and C4 photosynthesis, or its effects on δ13C fractionation.

We note that Kohler et al. (2010), mention the parameterisation of C4% in the terrestrial biosphere in their 740 kyr transient simulations with the BICYCLE model. In their control simulation (CTRL) they had a representation of the terrestrial biosphere that emphasised CO_2 fertilisation as the dominant control on terrestrial biosphere NPP, and limited or no change (hard to tell from reading) in C4% on the glacial-interglacial $\delta^{13}C$ of the terrestrial

biosphere. There is an extended scenario TB+ which emphasises climate as the driver of the terrestrial biosphere, faster response of NPP/terrestrial biosphere and parameterises higher C4% in the LGM (and associated change in the $\delta^{13}C$ of the terrestrial biosphere), leading to a combined small effect on deep Pacific $\delta^{13}C$ of 0.1 per mil.

However, in discussing the all-important drivers of the changes in atmospheric pCO2, $\delta^{13}C$ and deep Indo-Pacific $\delta^{13}C$, and mean ocean δ13C, for termination I, as listed in Kohler et al. (2010) Table 3, C4% and terrestrial $\delta^{13}C$ changes are not mentioned. The features listed by Kohler et al. (2010) as the drivers are: lower ocean temperatures, smaller terrestrial carbon storage, lower sea level, weaker NADW formation, enhanced marine export production, larger sea ice cover (gas exchange), higher Southern Ocean stratification.

There is a little more discussion of the C4% and terrestrial biosphere in terms of the LGM and Holocene, which unfortunately is only a small fraction of our 130 kyr period of interest.

For example, Joos et al. (2004) modelled a change in terrestrial biosphere $\delta^{13}C$ between the LGM and Holocene of 0.5 per mil. However, they observed the following:

"Changes in the mean terrestrial isotopic signature have a minor impact on the modeled changes in $\delta^{13}C$ of DIC…….The estimated oceanic $\delta^{13}C$ shift is 0.05% smaller than in the standard case, if the land biosphere-atmosphere $\delta^{13}C$ difference is kept at the Holocene value of -17 per mil."

Menviel et al. (2012a) provided an interesting quote and the following caveat with their modelling of the last glacial termination and Holocene:

"A caveat is that a constant atmosphere-land isotopic fractionation factor is applied in the inverse approach by Elsig et al. [2009] and in this study, therefore not taking into account any relative changes in the occurrence of C3/C4 plants and other influences on fractionation. However, using the LPJ-DGVM vegetation model, Joos et al. [2004] found that changes in fractionation and C3/C4 plant abundance due to climate and CO2 changes lead to a decrease in $\delta^{13}C$ signature of the terrestrial biosphere of about 0.5 per mil from the early Holocene (10 ka B.P.) to pre-industrial times. **A 0.5 permil decrease in biosphere $\delta^{13}C$ translates into an atmospheric δ13C decrease of about 0.02 permil. This suggests that changes in the atmosphere-land isotopic fractionation have a small influence on the results presented above**. "

We note another paper relevant to our manuscript, by Menviel et al. (2016) and focussed on the LGM (18-24 ka), made brief mention of C3/C4, and described that they undertook a sensitivity of -0.7 per mil and +0.5 mil around their average estimate of -23.3 per mil $\delta^{13}C$ for the terrestrial biosphere, but the modelling results of that sensitivity are not discussed further in the paper. That type of sensitivity is pretty easy to undertake for analysing only the LGM and the Holocene, as any studies on C3 vs C4 (Kohler and Fisher, 2004; Kaplan et al. 2002, Francois et al., 1999; Joos et al., 2004) have looked at this time period – even though they produce uncertain estimates for the % C3 vs C4 and therefore $\delta^{13}C$ fractionation factor. It is a much more difficult proposition to come up with values for a sensitivity for the last

glacial-interglacial cycle in its entirety (130,000 years), but that may be an interesting piece of work on its own – future work.

Studies focussed on the terrestrial biosphere

We note the references that focussed specifically on the terrestrial biosphere in detail as the major focus of their work, in the early 2000's, or example those provided by the reviewer (e.g. Collatz et al., 1998; Kaplan et al., 2002, Kohler and Fisher, 2004), and another (e.g. Francois et al., 1999), focused only for the Last Glacial Maximum and PI/modern periods None of them examined the last glacial-interglacial cycle which was ~130 kyrs in duration. All of these studies above, to our understanding, produced uncertain results.

A recent study devoted to analysing the terrestrial biosphere in detail/major focus (Jeltsche-Thommes et al. (2019) - suggested by the reviewer), does not mention this feature C3 vs C4%. Jeltsche-Thommes (2019), in their study focussed on the terrestrial biosphere from the last glacial maximum to the Holocene, simply state:

"The $\delta^{13}C$ signature of terrestrial carbon is set to −24 ‰." (at the top of page 856).

We wondered whether we can contribute something important here with regard to C3/%/C4% and the terrestrial biosphere $\delta^{13}C$ that has not been considered by any of our peer group of model-data analysis of the last glacial-interglacial cycle.

In summary, there are studies that focussed specifically on the terrestrial biosphere, using dedicated vegetation models. We see that these studies had great detail for the terrestrial biosphere, but were very light on detail for other features of the carbon cycle (ocean circulation and biology, volcanism, weathering, the effects of calcium carbonate compensation). In reviewing these papers, and consistent with our prior understanding, there is not great confidence on quantifying the change in C3 and C4 proportions during the LGM and Holocene, and this is particularly worse during the time period we have analysed up to 130 ka. The papers of Collatz et al. (1998), Kaplan et al. (2002), Kohler and Fisher (2002), all focus on the period LGM-present. There is no coverage of the last glacial cycle 130-20 ka, which is the focus of our study. Furthermore, studies that do focus on the last glacial-interglacial cycle of atmospheric CO_2, eg Brovkin, Ganopoloski, do not mention C3 versus C4 fractionation in their papers – making difficult any comparison. We even note that a paper we have referenced in our manuscript, Hoogakker et al. (2016), a paper devoted entirely to the terrestrial biosphere in the last glacial-interglacial cycle, does not address C3 versus C4 plant composition.

As shown above, it is actually an easy process to add the C3 and C4 equations of Collatz et al. (1999) and Kohler and Fischer (2004), and also a temperature dependency for NPP, as we have shown above and with the attached code (Attachment B). We could do this and then re-do the simulations as an appendix or addendum (or a sensitivity).

We could even just apply a sensitivity on the $\delta^{13}C$ of terrestrial biosphere of +1/-1 per mil change between LGM and Holocene. However, that's a straightforward exercise for the

LGM and Holocene comparison, but it would involve us trying to fit the uncertain LGM-Holocene changes back for the entire last glacial cycle, which is another highly uncertain exercise. We note all of the studies referenced in the reviewer comments and described here, considered C3 vs C4 only for the LGM to Holocene-modern period, but we've explicitly looked at the lead-up to the LGM over the period from 130 ka. We would not like to try to extrapolate changes in C3 v C4 for the LGM over the entire last glacial-interglacial cycle, and implementing the Collatz et al. (1998)/Kohler and Fischer (2004) module would not help us much in that regard as it only explains less than half of the change $\delta^{13}C$ of terrestrial biosphere from the LGM (the rest explained by changes in grassland vs forest succession).

There is huge uncertainty around average $\delta^{13}C$ factors for plants, and that extends even further to C3 and C4 $\delta^{13}C$, and their possible respective shares and variations. The indicated changes of 0.3-1.8 per mil terrestrial biosphere $\delta^{13}C$ between the Holocene and LGM, from the literature described above, are very minor compared to the absolute uncertainties and range in $\delta^{13}C$ of the terrestrial biosphere itself.

Summary on terrestrial biosphere and C3 vs C4 photosynthesis

We investigated these topics enthusiastically, based on the reviewer's comments. We're very confident, based on our assessment of the papers above, that our model results will not change by much at all, and the paper conclusions by nothing at all, by varying our approach to the terrestrial biosphere (equally for rock weathering as discussed above). If the CP Journal Editors and the reviewer feel greatly compelled that we need to modify our modelling approach, we certainly can (these would not be major model revisions, only minor adjustments). Our preferred approach, is to simply add a caveat that our model-data experiments don't consider the effects of C3/C4 photosynthesis on $\delta^{13}C$ fractionation of the terrestrial biosphere.

Amendments to the manuscript

We have added the following text to the model description (P5 L24):

"The terrestrial biosphere is represented in SCP-M as a stock of carbon that fluxes with the atmosphere, governed by parameters for net primary productivity (NPP) and respiration. In SCP-M, NPP is calculated as a function of carbon fertilisation, which increases NPP as atmospheric CO_2 rises via a simple logarithmic relationship, using the model of Harman et al. (2011). This is a simplified approach, which omits the contribution of temperature and precipitation on NPP. Other, more complex models of the carbon cycle applied to glacial-interglacial cycles have a more detailed treatment of the terrestrial biosphere, including climate dependencies (e.g. Brovkin et al., 2002; Menviel et al., 2012). A number of studies emphasise the role of atmospheric CO_2 as the driver of terrestrial biosphere NPP on glacial-interglacial cycles (Kaplan et al., 2002; Otto et al., 2002; Joos et al., 2004; Hoogakker et al., 2016), although other studies cast doubt on the relative importance of atmospheric CO_2 versus temperature and precipitation (Francois et al., 1999; van de Sleen et al., 2015).

The isotopic fractionation behaviour of the terrestrial biosphere may also vary on glacial-interglacial timeframes. This has been studied for the LGM, Holocene and the present day

(e.g. Collatz et al., 1998; Francois et al., 1999; Kaplan et al., 2002; Kohler and Fischer, 2004; Joos et al., 2004; Kohn, 2016). The variation in isotopic fractionation within the terrestrial biosphere reflects changes in the relative proportions of plants with the C3 and C4 photosynthetic pathways, but also strong variations within the same photosynthetic pathways themselves (Francois et al., 1999; Kohn, 2010; Schubert and Jahren, 2012; Kohn, 2016). The drivers for these changes include relative sea level and exposed land surface area (Francois et al., 1999), global tree-line extent (Kohler and Fischer, 2004), atmospheric temperature and CO_2 (Collatz et al., 1998; Francois et al., 1999; Kohler and Fischer, 2004; Kohn, 2010; Schubert and Jahren, 2012), global and localised precipitation and humidity (Huang et al., 2001; Kohn, 2010; Schubert and Jahren, 2012; Kohn, 2016), and also changes in the intercellular CO_2 pressure in the leaves of C3 plants (Francois et al., 1999).

Estimated changes in average terrestrial biosphere $\delta^{13}C$ signature between the LGM and the Holocene fall in the range -0.3-1.8‰ (less negative $\delta^{13}C$ signature in the LGM), with further changes estimated from the onset of the Holocene to the pre-industrial, and even greater changes to the present day (due to rising atmospheric CO_2). This feature has been covered in detail within studies that focussed on the terrestrial biosphere between the LGM and Holocene, but less so in modelling and model-data studies of the last glacial-interglacial cycle. Menviel et al. (2016) provided a sensitivity of -0.7+0.5‰ around an average LGM value of -23.3‰ for the LGM, based on previous modelling of the LGM-Holocene timeframe by Joos et al. (2004). Another modelling study (Menviel and Joos, 2012), assessed the variation in LGM-Holocene $\delta^{13}C$ of the terrestrial biosphere to be a minor factor and it was omitted. Kohler and Fischer (2004) assessed the changing $\delta^{13}C$ signature of plants between the LGM and Holocene to be a minor factor in setting $\delta^{13}C$ of marine DIC, compared to the change in the absolute size of the terrestrial biosphere across this period.

Given the uncertainty around the starting estimates of $\delta^{13}C$, the uncertain LGM-Holocene changes, the large number of potential drivers, and the further uncertainty in extrapolating the posited LGM-Holocene changes back for the preceding 100 kyr, and the modest changes relative to the average $\delta^{13}C$ signature (and the very large range in, for example, present day estimates of C3 plant $\delta^{13}C$ (Kohn, 2010, 2016), we omit this feature with the caveat that there is added uncertainty in our terrestrial biosphere results with respect of the $\delta^{13}C$ signature applied. We apply an average $\delta^{13}C$ signature of -23‰, similar to values assumed by Menviel et al. (2016) and Jeltsch-Thommes et al. (2019) (23.3‰, -24‰ respectively), but more negative than assumed in Brovkin et al. (2002), Kohler and Fischer (2004) and Joos et al. (2004) (-16-(-17)‰).

Our aim is not to contribute new findings of the terrestrial biosphere, but to ensure that the simple representation of the terrestrial biosphere in SCP-M provides the appropriate feedbacks to our (exhaustive) glacial-interglacial cycle model-data optimisation experiments, that are in line with published estimates."

We have also updated the discussion of our model results for the terrestrial biosphere, to provide a bit more detail and some additional references (Section 5.3), plus an additional

caveat in the “advantages and limitations section” (P34, L18).

“Furthermore, we apply a simple representation of the terrestrial biosphere in our model-data experiments, relying primarily on atmospheric CO_2 as the driver for NPP. This approach provided reasonable results for the terrestrial biosphere carbon stock and NPP, on the whole, but may miss some detail in the terrestrial biosphere during the last glacial-interglacial cycle.”

Future work could enhance this set of modelling results with more detail in the terrestrial biosphere. For example, the modelling values for ocean circulation and biology derived here, could be used to solve for the optimal data-matching values for C3 and C4 plant productivity, with separate $\delta^{13}C$-fractionation factors, to help inform that area of study.

Attachment A

Carbonate rock weathering in SCP-M

The reviewer mentioned the model code. In terms of the model equations and model code, the flux of carbon to the ocean from carbonate weathering is set in our model by the following equation (please see O'Neill et al. (2019) and the annotated model code snapshot below):

RVCARB=WCARB*AtCO2 (1)

Where WCARB is a weathering parameter with respect of atmospheric CO_2 and is set at 1.5-2.0 mol C/m3/atmosphere. At 275 ppm atmospheric CO2, this is a flux of 10 x1012 mol C annum. (for comparison, this flux is 12 x 1012 mol C annum in Morse and Mackenzie (1990), Zeebe (2012) and Archer et al. (1998), and 14.9 Tmol C annum in Toggweiler (2008). This flux of carbon is added to the low latitude surface box of the model (as per Toggweiler (2008), Zeebe (2012), Hogg (2008)), and alkalinity is added in the ratio ALK:DIC 2:1 (as per Toggweiler (2008), Zeebe (2012), Colbourn et al.,2013) by multiplying RVCARB by 2.0 to create the river flux of alkalinity to the ocean surface boxes. This 2:1 flux of alkalinity:carbon reflects that the initial one mol of CO2 consumed by the carbonate weathering equation, has been returned to the atmosphere (the DIC proportion of 1 is 2 mols less one mol returned to the atmosphere) as per Zeebe (2012) and Lenton and Britton (2006).

The fluxes of DIC and Alk from carbonate weathering are added to the ocean via the river fluxes of C and Alk (see below). This lowers pCO2 in the ocean surface box and therefore draws CO2 from the atmosphere into the ocean, a net sink of CO2 from carbonate rock weathering. We do not subtract a mol of CO2 directly from the atmosphere in our equation for atmospheric CO2, as for the time scale modelled ~10 kyr, we are taking the short-cut of assuming the CO2 taken up directly from the atmosphere from carbonate weathering, is released back to the atmosphere upon precipitation of CaCO3 into the ocean (Zeebe (2012), Toggweiler (2008)). Carbonate weathering is therefore a flux of carbon and alkalinity to the surface ocean via a river flux, leading to lowering of pCO2 in the surface ocean box and subsequent drawdown of CO2 from the atmosphere. An almost identical approach to ours, was applied by Lenton and Britton (2006), a paper devoted to the study of rock weathering as a sink of atmospheric CO2. The only difference is that Lenton and Britton (2006) applied an additional temperature and terrestrial biosphere dependency on weathering.

We consulted Lord et al. (2016) as suggested in the reviewer comments. Lord et al. (2016) use the cGenie model to estimate weathering feedbacks from atmospheric CO2 emissions. Lord et al. (2016) is a paper that is devoted to the feedback of rock weathering on atmospheric CO2. The treatment of carbonate weathering, in terms of setting this simply as fluxes of DIC and Alk in the ratio of 1:2 to the surface ocean box, is identical to ours. Where they differ, is because they are looking in much more detail at the effects of terrestrial rock weathering, they also explore other dependencies for rock weathering, such as temperature, terrestrial biosphere productivity and run-off rates. Ours has an atmospheric CO2 dependency, as per Zeebe (2012), Toggweiler (2008), Walker and Kasting (1992).

Silicate rock weathering in SCP-M

The treatment of silicate weathering in the SCP-M model is:

RVSIL=(BSIL+WSIL*AtCO2) (2)

Where BSIL is a constant weathering rate of 0.75 e-4 mol/m3/yr (Toggweiler, 2008), and WSIL is a rate varying with atmospheric CO2, set at 0.5 mol/m3/atmosphere as per Toggweiler (2008). For atmospheric CO2 of 275 ppm, this is a weathering flux of 5.7 x 1012 mol C annum (5 x 1012 mol in Zeebe (2012) and 5.63 x 1012 mol annum in Toggweiler (2008)).

The silicate and carbonate weathering fluxes of carbon, are added to the surface ocean boxes of the box model. Alkalinity is also added, in a ratio of 2:1 to the carbon fluxes (Sarmiento and Gruber (2006), Toggweiler (2008), Zeebe (2012)).

However, there is an additional step applied with silicate weathering. To account for the unit of CO2 consumed directly from the atmosphere in silicate weathering (one more unit than carbonate weathering, as per Zeebe, 2012), and using the approach of Toggweiler (2008), we also subtract an amount equal to a unit of silicate weathering directly from the atmosphere. This is the same approach of Zeebe (2012) who applies a doubling of the flux of silicate weathering, and that of Toggweiler who subtracts a flux of CO2 directly from the atmosphere to account for the additional unit of CO2 consumed by silicate weathering (when compared with carbonate weathering). This flux is subtracted directly from Atmospheric CO2 in SCP-M. This flux subtracted from the atmosphere negates the effects on atmospheric CO2 of the units of C added to the ocean by the silicate weathering flux of C. The effect of the more alkaline ocean (alk:C is 2:1 in the silicate weathering flux) is to draw down the volcanic emissions of CO2. Volcanic CO2 emissions are set equal to the amount of CO2 taken directly from the atmosphere by silicate weathering, to reflect the long-term offset of volcanic emissions by silicate weathering (Walker and Kasting, 1992; Archer et al., 1998, Toggweiler, 2008; Zeebe, 2012, Brault et al., 2017). In Walker and Kasting, 1992; Toggweiler, 2008; Zeebe, 2012; Brault et al., 2007, volcanic emissions are also set to the silicate weathering drawdown of CO2.

As described in Walker and Kasting, 1992; Toggweiler, 2008; Zeebe, 2012; Brault et al., 2007, Colbourn et al. (2013, 2015); Lord et al. (2016), in steady state the silicate weathering flux feedback for CO2 matches the volcanic CO2 emissions, which we have set in SCP-M. Note, for anthropogenic scenarios we separate weathering flux from volcanic emissions, as it is clearly a non-steady state simulation, and the silicate weathering feedback, under the forcing of atmospheric CO2, is expected to increase at a greater rate than volcanic emissions.

We note that Zeebe (2012) implements the scheme slightly differently to ours, by subtracting fluxes of carbonate and silicate weathering from the atmosphere, but by doubling the silicate flux to account for the net removal of CO2 from the atmosphere (balanced by volcanic emissions). In Zeebe (2012) when CO2 is returned to the atmosphere from precipitation of CaCO3 in the ocean surface boxes, there is a net zero direct flux of CO2

from the atmosphere from carbonate weathering and a direct flux of CO2 from the atmosphere of 1 mol from silicate weathering.

The SCP-M model code for carbonate and silicate weathering

Below is the description and extract of the original model code presented in O'Neill et al. (2019) as referenced by the reviewer. A revised model code, incorporating the changes described in this response, will be uploaded with the final manuscript.

Line 418 shows the equation (1) above, where the carbonate rock weathering (RVCARB) is calculated from atmospheric CO2 with the WCARB parameter.
Line 419 shows the equation (X) above where the silicate rock weathering (RVSIL) is calculated from atmospheric CO2 and a constant.
Line 420 the silicate weathering amount to be directly subtracted from the atmosphere, as described above, "weaths", is identified.
Line 423 Volcanic emissions is set to equal "weaths", the direct (net) amount of CO2 taken from the atmosphere by silicate weathering, as described above.
In line 425-428 there is the option to apply an input value for volcanic emissions instead of setting it to equal silicate weathering. This is for the model runs with analysis of anthropogenic emissions/short time frames and is switched off for our experiments.
In Line 431 the net effect of volcanic emissions and silicate weathering on atmospheric CO2 is calculated
In Line 432 the above terrestrial fluxes of carbon can be disabled by a switch (for sensitivities and model testing) via "TerrestrialGeo" (1 is on, 0 = off).
In line 435 the δ13C of silicate weathering drawdown of CO2 from the atmosphere is set to the hardwired value of -6.90. In the revised model code it is now set to atmospheric δ13C within each model time step.
In line 436 the δ13C for silicate weathering direct atmospheric CO2 flux and volcanic emissions of CO2 are applied to their fluxes of carbon and converted to molar concentrations in the atmosphere. (we have now amended the volcanic emissions δ13C to a value of -4.5 per mil).
In line 437 the terrestrial δ13C fluxes can be switched on or off (for model testing or sensitivity) via "TerrestrialGeo" (1 is on, 0 = off).
In line 438 the radiocarbon content (zero, dead) of volcanic emissions and weathering fluxes is applied.
In line 442 both RVCARB and RVSIL fluxes of carbon are added to the surface ocean box via river flux.
In line 443 alkalinity flux is added to the surface box in ration 2:1, leading to a lowering in pCO2 in the surface box and a drop in atmospheric CO2.
In line 475 ocean δ13C is calculated. **The river flux of C (derived from weathering) is introduced to the surface ocean box with a δ13C of the standard value "Sstand" (δ13C=0) as discussed above. The dissolution of marine carbonates also introduces carbon with the standard value for δ13C (δ13C = 0) to the ocean boxes**.
In line 481 the net fluxes of volcanic emissions and silicate weathering drawdown of CO2 are added to the equation for atmospheric CO2.

In line 484 the δ13C of net fluxes of volcanic emissions and silicate weathering drawdown of CO2 are added to the equation for atmospheric δ13C.

The confusion with the reviewer likely comes from our comment in the model code in line 416 "# As per Toggweiler (2008) only silicate weathering is a sink of CO2 from the atmosphere". We will delete this statement as it is a poor descriptor.

In addition, we should modify the following comment
"# Weathering of carbonate rocks is a source of carbon to the low latitude surface ocean via rivers" with "…source of carbon **and alkalinity**"
Therefore, it is indeed the case in SCP-M that both carbonate and silicate weathering ultimately work as sinks of atmospheric CO2 by altering the surface boxes' alkalinity.

Figure 1: Original model documentation paper (O'Neill et al., 2019) model code extract from https://zenodo.org/record/1310161#.Xm7Mby17E_U (**CP_RC1_code1.png**)

```
414 ## Weathering, river fluxes and volcanic emissions-------------------------
415
416     # As per Toggweiler (2008) only silicate weathering is a sink of CO2 from the atmosphere
417     # Weathering of carbonate rocks is a source of carbon to the low latitude surface ocean via riv
418     RVCARB=WCARBs*AtCO2
419     RVSIL=(BSILs+WSILs*AtCO2)
420     weaths=RVSIL*Varr[0,0] #silicate rock weathering sink of CO2, carbonate weathering is a source
421
422     # Volcanic carbon emissions
423     volcs=weaths # volcanic emissions in step with silicate weathering as per Toggweiler (2008)
424     # unless anthropocene scenario, hardwired estimate
425     if AnthEmits==1:
426         volcs=volcs1
427     else:
428         volcs=weaths
429
430     # net source/sink of terrestrial carbon
431     TerrC=(volcs-weaths)/Varrat
432     TCflux=TerrC*TerrestrialGeo
433
434     # weathering and volcanism 13C and 14C fluxes
435     weathd13C=weathd13C
436     TerrSC=(-weaths*weathd13C+volcs*volcd13C)/Varrat
437     TSCflux=TerrSC*TerrestrialGeo
438     TRCflux=TerrC*TerrRC*TerrestrialGeo
439
440     # River fluxes
441     RiverCflux=np.zeros([7,1])
442     RiverCflux[0,0]=(RVCARB+RVSIL) # mol/m3 Incorporates source of carbonate weathering
443     RiverAlkflux=RiverCflux*2.0 #Alk:C ratio 2:1 as per Toggweiler (2008)
444     RiverPflux=np.zeros([7,1])
445     RiverPflux[0,0]=RiverP_mols/Varr[0,0]
446     PSedflux=np.zeros([7,1])
447     PSedflux[5,0]=RiverP_mols/Varr[5,0]
448
```

(CP_RC1_code2.png)

```
464    ## Step forward model calculations----------------------------------------
465
466        # Model equations
467
468        # Ocean boxes
469        Parr = Parr +dt*secsyr*(np.dot(PhysMat, Parr)+BioP+RiverPflux*Rivers-PSedflux*Rivers)
470        Carr = Carr + dt*secsyr*(np.dot(PhysMat, Carr)+BioC+cflux+NetCflux+RiverCflux*Rivers)
471        Alkarr = Alkarr + dt*secsyr*(np.dot(PhysMat, Alkarr)+NetAlkflux+RiverAlkflux*Rivers)
472        Fearr = Fearr + dt*secsyr*(np.dot(PhysMat, Fearr)+BioFe)
473        Siarr = Siarr + dt*secsyr*(np.dot(PhysMat, Siarr)+BioSi)
474        Oarr = Oarr + dt*secsyr*(np.dot(PhysMat, Oarr)+BioO)
475        SCarr = SCarr+ dt*secsyr*(np.dot(PhysMat, SCarr)+BioSC+Scflux+NetCflux*Sstand+
476                                  RiverCflux*Sstand*Rivers)
477        SCratio=SCarr/Carr
478        RCarr = RCarr + dt*secsyr*(np.dot(PhysMat, RCarr)+BioRC+Rcflux+NetCflux*(RCarr/Carr)-(RCD1*R
479
480        # Atmosphere
481        AtCO2 = AtCO2 + dt*secsyr*(Atcflux+TCflux-((CFert-Respire)/Varrat)+
482                                   ((AnthEmit+DeforestC)/Varrat)*AnthEmits)
483        pCO2a=np.append(pCO2,AtCO2) # create an array of all pCO2
484        SCAt = SCAt+dt*secsyr*(AtSCflux+TSCflux-((CFert-Respire)/Varrat)*TerrBioSC*
485                               TerrestrialBios+(AnthSC1+DeforestSC)/Varrat
486                               *AnthEmits)
487        RCAt = RCAt+dt*secsyr*(AtRCflux+RCS1At/Varrat-RCD1At*RCAt*Varrat/Varrat-TRCflux-((CFert-Resp
488                               *TerrestrialBios+((AnthRC1+DeforestRC)/Varrat)*AnthEmits+(Bomb14C/Var
```

Reference standard for d13C=0per mil

The code extract below shows the values chosen for weathering input parameters, as described in the text above. At line 321, weathδ13C is the value that was applied to silicate weathering, NOT carbonate weathering as assumed by the reviewer.
(**CP_RC1_code3.png**)

```
310 # Continental weathering atmospheric CO2 sink and flux into oceans
311 # Generally following Toggweiler (2008)
312 WCARB=2.0 # mol/m3/atm/yr as per Toggweiler (2008)
313 WCARBs=WCARB/secsyr
314 BSIL=0.75e-4 # mol/m3/yr as per Toggweiler (2008)
315 BSILs=BSIL/secsyr
316 WSIL=0.5 #mol/m3/atm/yr as per Toggweiler (2008)
317 WSILs=WSIL/secsyr
318
319 # Carbon isotops for volanic emissions and weathering
320 volcd13C=-6.90 #per mil
321 weathd13C=-6.90 #per mil
322 volcd13C=(volcd13C/1000+1)*Sstand
323 weathd13C=(weathd13C/1000+1)*Sstand
324 TerrRC=0.0 # 14C dead
```

If you look above you will see this was applied to silicate weathering direct consumption of atmospheric CO2, not carbonate weathering. We have amended silicate weathering direct CO2 consumption to take atmospheric d13C

References

Annan, J. D. and Hargreaves, J. C.: A new global reconstruction of temperature changes at the Last Glacial Maximum, Clim. Past, 9, 367–376, https://doi.org/10.5194/cp-9-367-2013, 2013.

Archer, D. E., Kheshgi, H., and Maier-Reimer, E.: Dynamics of fossil fuel CO2 neutralization by marine CaCO3, Global Bio- geochem. Cy., 12, 259–276, 1998.

Arneth, A., Sitch, S., and J. Pongratz, e. a.: Historical carbon dioxide emissions caused by land-use changes are possibly larger than assumed, Nature Geoscience, 10„ 79–84, 2017.

Bereiter, B., Eggleston, S., Schmitt, J., Nehrbass-Ahles, C., Stocker, T., Fischer, H., Kipfstuhl, S., and Chappellaz, J.: Revision of the EPICA Dome C CO2 record from 800 to 600kyr before

present, Geophys. Res. Lett, 2015.

Berner, R. A., Lasaga, A. C., and Garrels, R. M.: The carbonate- silicate geochemical cycle and its effect on atmospheric carbon dioxide over the past 100 million years, Am. J. Sci., 283, 641– 683, 1983.

Brault M-O, Mysak LA, and Matthews HD. 2017. Carbon cycle implications of terrestrial weathering changes since the last glacial maximum. FACETS 2: 267–285. doi:10.1139/ facets-2016-0040

Brovkin, V., Claussen, J. B. M., Ganopolski, A., Kubatzki, C., Petoukhov, V., and Andreev, A.: Carbon cycle, vegetation, and climate dynamics in the Holocene: Experiments with the CLIMBER-2 model, Global Biogeochemical Cycles, 16, 1139, doi:10.1029/2001GB001 662, 2002.

Brovkin, V., Ganopolski, A., Archer, D., and Munhoven, G.: Glacial CO2 cycle as a succession of key physical and biogeochemical processes, Climate of the Past, 8, 251–264, 2012.

Ciais, P., Tagliabue, A., Cuntz, M., Bopp, L., Scholze, M., Hoffmann, G., Lourantou, A., Harrison, S. P., Prentice, I. C., Kelley, D. I., Koven, C., and Piao, S. L.: Large inert carbon pool in the terrestrial biosphere during the Last Glacial Maximum, Nature Geoscience, 5, 74–79, 2012.

Colbourn, G., A. Ridgwell, and T. Lenton (2013), The Rock Geochemical Model (RokGeM) v0.9, Geosci. Model Dev., 6, 1543– 1573, doi: 10.5194/gmd-6-1543-2013.
Collatz, G., Berry, J., and Clark, J.: Effects of climate and atmospheric CO2 partial pressure on the global distribution of C4 grasses: present, past, and future, Oecologia, 114, 441–454, 1998.

Eggleston, S., Schmitt, J., Bereiter, B., Schneider, R., and Fischer, H.: Evolution of the stable carbon isotope composition of atmospheric CO2 over the last glacial cycle, Paleoceanography, 31, 434–452, 2016.

Enting, I. G., Wigley, T. M. L. and Heimann, M. 1994. Future emissions and concentrations of carbon dioxide: Key ocean/atmosphere/land analyses. CSIRO Division of Atmospheric Research Technical Paper No. 31.

Ferrari, R., Jansen, M., Adkins, J., Burke, A., Stewart, A. L., and Thompson, A.: Antarctic sea ice control on ocean circulation in present and glacial climates, PNAS, 111, 8753–8758, 2014.

Francois, L., Godderis, Y., Warnant, P., Ramstein, G., de Noblet, N., and Lorenz, S.: Carbon stocks and isotopic budgets of the terrestrial biosphere at mid-Holocene and last glacial maximum times, Chemical Geology, 159, 163–199, 1999.

Ganopolski, A. and Brovkin, V.: Simulation of climate, ice sheets and CO2 evolution during the last four glacial cycles with an Earth system model of intermediate complexity, Climate of the Past, 13, 1695–1716, 2017.

Ganopolski, A., Calov, R., and Claussen, M.: Simulation of the last glacial cycle with a coupled climate ice-sheet model of intermediate complexity, Climate of the Past, 6, 229–244, 2010.

Harman, I., Trudinger, C., and Raupach, M.: SCCM – the Simple Carbon-Climate Model: Technical Documentation, CAWCR Technical Report 047, CSIRO Centre for Australian Weather and Climate Research, CSIRO Marine and Atmospheric Research, FC Pye Laboratory, GPO Box 3023, Canberra, ACT, 2601, Australia, 2011.

Hogg, A. M.: Glacial cycles and carbon dioxide: A conceptual model, Geophys. Res. Lett., 35, L01 701, doi:10.1029/2007GL032 071, 2008.

Holden, P. B., Edwards, N. R., Oliver, K. I. C., Lenton, T. M., and Wilkinson, R. D.: A probabilistic calibration of climate sensitiv- ity and terrestrial carbon change in GENIE-1, Clim. Dynam., 35, 1–22, doi:10.1007/s00382-009-0630-8, 2009.

Hoogakker, B. et al.: Terrestrial biosphere changes over the last 120 kyr, Climate of the Past, 12, 51–73, 2016.

Huang, Y., Street-Perrott, F., Metcalfe, S., Brenner, M., Moreland, M., and Freeman, K.: Climate change as the dominant control on glacial-interglacial variations in C3 and C4 plant abundance, Science, 293, 1647–1651, 2001.

Jeltsch-Thommes, A., Battaglia, G., Cartapanis, O., Jaccard, S., and Joos, F. J.: Low terrestrial carbon storage at the Last Glacial Maximum: constraints from multi-proxy data, Climate of the Past, 15, 849–879, 2019.

Joos, F., Gerber, S., Prentice, I. C., Otto-Bliesner, B., and Valdes, P.: Transient simulations of Holocene atmospheric carbon dioxide and terrestrial carbon since the Last Glacial Maximum, Global Biogeochemical Cycles, 18, GB2002, doi:10.1029/2003GB002 156, 2004.

Jouzel, J., Masson-Delmotte, V., Cattani, O., Dreyfus, G., Falourd, S., Hoffmann, G., Nouet, J., Barnola, J.M., Chappellaz, J., Fischer, H., Gallet, J.C., Johnsen, S., Leuenberger, M., Loulergue, L., Luethi, D., Oerter, H., Parrenin, F., Raisbeck, G., Raynaud, D., Schwander, J., Spahni, R., Souchez, R., Selmo, E., Schilt, A., Steffensen, J.P., Stenni, B., Stauffer, B., Stocker, T., Tison, J.-L., Werner, M., Wolff, E.W., 2007. Orbital and millennial Antarctic climate variability over the last 800,000 years. Science 317, 793–796.

Kaplan, J., Prentice, I., Knorr, W., and Valdes, P.: Modeling the dynamics of terrestrial carbon storage since the Last Glacial Maximum, Geophysical Research Letters, 22, 2074, doi:10.1029/2002GL015 230, 2002.

Kicklighter, D. W. et al., A first order analysis of the potential role of CO2 fertilization to affect the global carbon budget: A comparison study of four terrestrial biosphere models, Tellus, Set. B, 51, 343-366, 1999.

Kohfeld, K. and Chase, Z.: Temporal evolution of mechanisms controlling ocean carbon uptake during the last glacial cycle, Earth and Planetary Science Letters, 472, 206–215, 2017.

Kohler, P. and Fischer, H.: Simulating changes in the terrestrial biosphere during the last glacial/interglacial transition, Global and Planetary Change, 43, 33–55, 2004.

Köhler, P., Fischer, H., and Schmitt, J.: Atmospheric δ13CO2 and its relation to pCO2 and deep ocean δ13C during the late Pleistocene, Paleoceanography, 25, doi:10.1029/2008PA001 703, 2010.

Kohn, M.: Carbon isotope compositions of terrestrial C3 plants as indicators of (paleo)ecology and (paleo)climate, PNAS, 107, 19 691– 19 695, 2010.

Kohn, M.: Carbon isotope discrimination in C3 land plants is independent of natural variations in pCO2, Geochemical Perspectives Letters, 2, 35–43, 2016.

Lenton, T. M., and C. Britton (2006), Enhanced carbonate and silicate weathering accelerates recovery from fossil fuel CO2 perturbations, Global Biogeochem. Cycles, 20, GB3009, doi:10.1029/2005GB002678.

Lindgren, A., Hugelius, G., and Kuhry, P.: Extensive loss of past permafrost carbon but a net accumulation into present-day soils, Letters to Nature, 560, 219–222, 2018.

Lord, N. S., A. Ridgwell, M. C. Thorne, and D. J. Lunt (2016), An impulse response function for the “long tail” of excess atmospheric CO2 in an Earth system model, Global Biogeochem. Cycles, 30, 2–17, doi:10.1002/2014GB005074.

Lueker, T. J., Dickson, A. G., and Keeling, C. D.: Ocean pCO2 calculated from dissolved inorganic carbon, alkalinity, and equations for K-1 and K-2: validation based on laboratory measurements of CO2 in gas and seawater at equilibrium, Marine Chemistry, 70, 105–119, 2000.

Menviel, L. and Joos, F.: Toward explaining the Holocene carbon dioxide and carbon isotope records: Results from transient ocean carbon cycle-climate simulations, Paleoceanography, 27, PA1207, doi:10.1029/2011PA002 224, 2012.

Menviel, L., Joos, J., and Ritz, S.: Simulating atmospheric CO2, 13C and the marine carbon cycle during the Last Glacial-Interglacial cycle: possible role for a deepening of the mean remineralization depth and an increase in the oceanic nutrient inventory, Quaternary Science Reviews, 56, 46–68, 2012.

Menviel, L., Mouchet, A., Meissner, K. J., Joos, F., and England, M. H.: Impact of oceanic circulation changes on atmospheric δ13CO2, Global Biogeochemical Cycles, 29, 1944–1961, 2015.

Menviel, L., Yu, J., Joos, F., Mouchet, A., Meissner, K. J., and England, M. H.: Poorly ventilated deep ocean at the Last Glacial Maximum inferred from carbon isotopes: A data-model comparison study, Paleoceanography, 31, 2–17, 2016.

Meyer, R., F. Joos, G. Esser, M. Heimann, G. Hooss, G. Kohlmaier, W. Sauf, R. Voss, and U. Wittenberg. The substitution of high-resolu- tion terrestrial biosphere models and carbon sequestration in response to changing CO2 and climate, Global Biogeochem. Cycles, 13, 785-802, 1999.

Mook, W. G.: 13C in atmospheric CO2, Netherlands Journal of Sea Research, 20, 211–223, 1986.

Morse, J. W. and Mackenzie, F. T.: Geochemistry of Sedimentary Carbonates, Developments in sedimentology, 48, Elsevier, Ams- terdam, 707 pp., 1990.
Muglia, J., Skinner, L., and Schmittner, A.: Weak overturning circulation and high Southern Ocean nutrient utilization maximized glacial ocean carbon, Earth and Planetary Science Letters, 496, 47–56, 2018.

O'Neill, C., A. Mc. Hogg, M.J. Ellwood, S. E., and Opdyke, B.: The [simple carbon project] model v1.0, Geosci. Model Dev., 12, 1541–1572, https://doi.org/10.5194/gmd–12–1541–2019, 2019.

Otto, D., Rasse, D., Kaplan, J., Warnant, P., and Francois, L.: Biospheric carbon stocks reconstructed at the Last Glacial Maximum: com- parison between general circulation models using prescribed and computed sea surface temperatures, Global and Planetary Change, 33, 117–138, 2002.

Peterson, C. D., Lisiecki, L. E., and Stern, J. V.: Deglacial whole-ocean δ13C change estimated from 480 benthic foraminiferal records, Paleoceanography, 29, 549–563, 2014.

Prentice, I. C., Harrison, S. P. & Bartlein, P. J. Global vegetation and terrestrial carbon cycle changes after the last ice age. New Phytologist (2011) 189: 988–998 doi: 10.1111/j.1469-8137.2010.03620.x

Sano, Y., and S. N. Williams (1996), Fluxes of mantle and subducted carbon along convergent plate boundaries, Geophys. Res. Lett., 23(20), 2749–2752, doi:10.1029/96GL02260.

Schimel, D., B. B. Stephens, and J. B. Fisher (2015), Effect of increasing CO2 on the terrestrial carbon cycle, Proc. Natl. Acad. Sci. U.S.A., 112(2), 436–441, doi:10.1073/pnas.1407302112.
Schmitt, J., Schneider, R., Elsig, J., Leuenberger, D., Lourantou, A., Chappellaz, J., Köhler, P., Joos, F., Stocker, T., Leuenberger, M., and Fischer, H.: Carbon Isotope Constraints on the Deglacial CO2 Rise from Ice Cores, Science, 336, 711–714, 2012.

Schmittner, A., Urban, N., Shakun, J., Mahowald, N., Clark, P., Bartlein, P., Mix, A., and Rosell-Mele´, A.: Climate Sensitivity Estimated from Temperature Reconstructions of the Last Glacial Maximum, Science, 334, 1385–1388, 2011.

Schneider von Deimling, T., Ganopolski, A., Held, H., and Rahmstorf, S.: How cold was the Last Glacial Maximum?, Geophys. Res. Lett., 33, L14709, doi:10.1029/2006GL026484, 2006a.

Schneider, R., Schmitt, J., Kohler, P., Joos, F., and Fischer, H.: A reconstruction of atmospheric carbon dioxide and its stable carbon isotopic composition from the penultimate glacial maximum to the last glacial inception, Climate of the Past, 9, 2507–2523, 2013.

Schubert, B. and Jahren, A.: The effect of atmospheric CO2 concentration on carbon isotope fractionation in C3 land plants, Geochimica et Cosmochimica Acta, 96, 29–43, 2012.

Shaffer, G. and Lambert, F.: In and out of glacial extremes by way of dust-climate feedbacks, PNAS, 115, 2026–2031, 2018.

Siegenthaler, U. & F. Joos (1992) Use of a simple model for studying oceanic tracer distributions and the global carbon cycle, Tellus B: Chemical and Physical Meteorology, 44:3, 186-207, DOI: 10.3402/tellusb.v44i3.15441

Sitch, S., et al. (2008), Evaluation of the terrestrial carbon cycle, future plant geography and climate-carbon cycle feedbacks using five Dynamic Global Vegetation Models (DGVMs), Global Change Biol., 14(9), 2015–2039, doi:10.1111/j.1365-2486.2008.01626.x

Strassmann, K. M. and Joos, F.: The Bern Simple Climate Model (BernSCM) v1.0: an extensible and fully documented open-source re-implementation of the Bern reduced-form model for global carbon cycle–climate simulations, Geosci. Model Dev., 11, 1887–1908, https://doi.org/10.5194/gmd-11-1887-2018, 2018.

Talley, L.: Closure of the global overturning circulation through the Indian, Pacific, and Southern Oceans: Schematics and transports, Oceanography, 78, 257–303, 2013.

Tarnocai, C., Canadell, J., Schuur, E., Kuhry, P., Mazhitova, G., and Zimov, S.: Soil organic carbon pools in the northern circumpolar permafrost region, Global Biogeochemical Cycles, 23, GB2023, doi:10.1029/2008GB003 327, 2009.

Toggweiler, J. R.: Origin of the 100,000-yr time scale in Antarc- tic temperatures and atmospheric CO2, Paleoceanography, 23, PA2211, https://doi.org/10.1029/2006PA001405, 2008.

Treat, C., Kleinen, T., Broothaerts, N., Dalton, A., Dommain, R., Douglas, T., Drexler, J., Finkelstein, S., Grosse, G., Hope, G., Hutchings, J., Jones, M., Kuhry, P., Lacourse, T., Lähteenoja, O., Loisel, J., Notebaert, B., Payne, R., Peteet, D., Sannel, A., Stelling, J., Strauss, J., Swindles, G., Talbot, J., Tarnocai, C., Verstraeten, G., C.J. Williams, Z. X., Yu, Z., Väliranta, M., Hättestrand, M., Alexanderson, H., and Brovkin, V.: Widespread global peatland establishment and persistence over the last 130,000 y, PNAS, 116, 4822–4827, 2019.

van der Sleen, P., P. Groenendijk, M. Vlam, N. P. R. Anten, A. Boom, F. Bongers, T. L. Pons, G. Terburg, and P. A. Zuidema (2015), No growth stimulation of tropical trees by 150 years of CO2 fertilization but water-use efficiency increased, Nat. Geosci., 8(1), 24–28, doi:10.1038/Ngeo2313.

Walker, J.C.G. and Kasting, J.F., 1991. Effects of fuel and forest conservatkm on future levels of atmospheric carbon dioxide. Palaeogeogr., Palaeoclimatol., Pa[acoecol. (Global Planet. Change Sect.), 97: 151-189.

Yu, J., Menviel, L., Jin, Z. D., Thornalley, D., Barker, S., Marino, G., Rohling, E. J., Cai, Y., Zhang, F., Wang, X., Dai, Y., Chen, P., and Broecker, W. S.: Sequestration of carbon in the

deep Atlantic during the last glaciation, Nature Geoscience, 9, 319–325, 2016.

Zeebe, R. E. and Caldeira, K.: Close mass balance of long-term carbon fluxes from ice-core CO2 and ocean chemistry records, Nat. Geosci., 1, 312–315, doi:10.1038/ngeo185, 2008.

Zeebe, R. E.: LOSCAR: Long-term Ocean-atmosphere-Sediment CArbon cycle Reservoir Model v2.0.4, Geosci. Model Dev., 5, 149–166, https://doi.org/10.5194/gmd-5-149-2012, 2012.

CP reviewer comments #2 and author responses

AC: We thank the reviewer for their comments, suggestions and input into this manuscript. These comments make a substantial contribution to improving the quality of our work, particularly with reference to our treatment of the oceanic δ13C data. Please see below our responses to the individual comments.

We have made reference to changes to the manuscript, which are included as a supplement to the author comments, in track changes. Page and line references below refer to locations in the revised document with track changes.

RC 1. The authors base their paper on a recently published carbon cycle box model (O'Neill et al. 2019). They provide a brief description of the model but I found that this manuscript would benefit better description of some of the key parameters that are quite important to this paper, such as the controls on Z (biological productivity). It was very unclear to me on first reading how values of Z were ascertained.

AC: To address this comment we have added the following text to (P3, L30). In addition to the biological productivity, it includes a bit more detail on some other processes, stemming from the other reviewer comments:

"We used the SCP-M carbon cycle box model in our model-data experiment (O'Neill et al., 2019). In summary, SCP-M contains simple parameterisations of the major fluxes in the Earth's surface carbon cycle (Fig. 1). SCP-M incorporates the ocean, atmosphere, terrestrial biosphere and marine/continental sediment carbon reservoirs, weathering and river fluxes, and a number of variables including atmospheric CO_2, DIC, phosphorus, alkalinity, carbon isotopes (^{13}C and ^{14}C) and the carbonate ion.

SCP-M calculates ocean pCO_2 using the equations of Follows et al. (2006), and applies the first and second "dissociation constants" of carbonic acid estimated by Lueker et al. (2000), to calculate $HCO-$ and CO^{2-}_3 concentrations, respectively, in units of µmol kg^{-1}, in each ocean box. The model employs partial differential equations for determining the concentration of elements in each box, with each box represented as a row and column in a matrix. In this paper, we extend SCP-M by incorporating a separate basin for the combined Pacific and Indian Oceans (Fig. 1), following the conceptual model of Talley (2013), to incorporate modelling and proxy data for those regions of the ocean. This version of SCP-M consists of 12 ocean boxes plus the atmosphere and terrestrial biosphere. SCP-M splits out depth regions of the ocean between surface boxes (100-250m average depth), intermediate (1,000m average depth), deep (2,500m average depth) and abyssal depth boxes (3,700 (Atlantic) - 4,000m (Pacific-Indian) average depth). The Southern Ocean is split into two boxes, including a polar box which covers latitude range 60-80 degrees South (box 12 in Fig. 1) and sub polar boxes in the Atlantic (box 7) and Pacific-Indian (box 12) basins, which cover latitude range 40-60 degrees South. See O'Neill et al. (2019) for a discussion of the choice of box depth and latitude dimensions.

The major ocean carbon flux parameters of interest in this model-data study, are global ocean circulation (GOC), Ψ_1, Atlantic meridional overturning circulation (AMOC), Ψ_2, and ocean biological export productivity, Z. The ocean circulation parameters Ψ_1 and Ψ_2 are simply prescribed in units of Sverdrups (Sv, 10^6 m^3 s^{-1}). Ocean biological export productivity Z is calculated using the method of Martin et al. (1987). The biological productivity flux, at 100m depth, is attenuated with depth for each box according to the decay rule of Martin et al. (1987). Each sub surface box receives a biological flux of an element at its ceiling depth, and loses a flux at its floor depth (lost to the boxes below it). The difference is the amount of element that is remineralised into each box. The input parameter is the value of export production at 100m depth, in units of mol C m^{-2} yr^{-1} as per Martin et al. (1987). Equation (1) shows the general form of the Martin et al. (1987) equation:

$$F=F_{100}(d/100)^b \quad (1)$$

Where F is a flux of carbon in mol C m^{-2} yr^{-1}, F_{100} is an estimate of carbon flux at 100m depth, d is depth in metres and 20 b is a depth scalar. In SCP-M, the Z parameter implements the Martin et al. (1987) equation. Z is an estimate of biological productivity at 100m depth (in mol C m^{-2} yr^{-1}), and coupled with the Martin et al. (1987) depth scalar, controls the amount of organic carbon that sinks from each model surface box to the boxes below. Each subsurface ocean box receives a flux of carbon from the box above it, at its ceiling depth (also the floor of the overlying box), and loses carbon as a function of the depth of the bottom of the box. Remineralisation in each box is accounted for as the difference between the influx and out-flux of organic carbon.

The terrestrial biosphere is represented in SCP-M as a stock of carbon (a box) that fluxes with the atmosphere, governed by parameters for net primary productivity (NPP) and respiration. In SCP-M, NPP is calculated as a function of carbon fertilisation, 25 which increases NPP as atmospheric CO_2 rises via a simple logarithmic relationship, using the model of Harman et al. (2011). This is a simplified approach, which omits the contribution of temperature and precipitation on NPP. Other, more complex models of the carbon cycle applied to glacial-interglacial cycles have a more detailed treatment of the terrestrial biosphere, including climate dependencies (e.g. Brovkin et al., 2002; Menviel et al., 2012). A number of studies emphasise the role of atmospheric CO_2 as the driver of terrestrial biosphere NPP on glacial-interglacial cycles (Kaplan et al., 2002; Otto et al., 2002; 30 Joos et al., 2004; Hoogakker et al., 2016), although other studies cast doubt on the relative importance of atmospheric CO_2 versus temperature and precipitation (Francois et al., 1999; van der Sleen, 2015).

The isotopic fractionation behaviour of the terrestrial biosphere may also vary on glacial-interglacial timeframes. This has been studied for the LGM, Holocene and the present day (e.g. Collatz et al., 1998; Francois et al., 1999; Kaplan et al., 2002; Kohler and Fischer, 2004; Joos et al., 2004; Kohn, 2016). The variation in isotopic fractionation within the terrestrial biosphere reflects changes in the relative proportions of plants with the C3 and C4 photosynthetic pathways, but also strong variations within the same photosynthetic

pathways themselves (Francois et al., 1999; Kohn, 2010; Schubert and Jahren, 2012; Kohn, 2016). The drivers for these changes include relative sea level and exposed land surface area (Francois et al., 1999), global tree-line extent (Kohler and Fischer, 2004), atmospheric temperature and CO_2 (Collatz et al., 1998; Francois et al., 1999; Kohler and Fischer, 2004; Kohn, 2010; Schubert and Jahren, 2012), global and localised precipitation and humidity (Huang et al., 2001; Kohn, 2010; Schubert and Jahren, 2012; Kohn, 2016), and also changes in the intercellular CO_2 pressure in the leaves of C3 plants (Francois et al., 1999). Estimated changes in average terrestrial biosphere $\delta^{13}C$ signature between the LGM and the Holocene fall in the range -0.3-1.8‰ (less negative $\delta^{13}C$ signature in the LGM), with further changes estimated from the onset of the Holocene to the pre-industrial, and even greater changes to the present day (due to rising atmospheric CO_2). This feature has been covered in detail within studies that focussed on the terrestrial biosphere between the LGM and Holocene, but less so in modelling and model-data studies of the last glacial-interglacial cycle. Menviel et al. (2016) provided a sensitivity of -0.7+0.5‰ around an average LGM terrestrial biosphere value $\delta^{13}C$ of -23.3‰, based on previous modelling of the LGM-Holocene timeframe by Joos et al. (2004). Another modelling study (Menviel and Joos, 2012), assessed the variation in LGM-Holocene $\delta^{13}C$ of the terrestrial biosphere to be a minor factor and it was omitted. Kohler and Fischer (2004) assessed the changing $\delta^{13}C$ signature of plants between the LGM and Holocene to be a minor factor in setting $\delta^{13}C$ of marine DIC, compared to changes in the absolute size of the terrestrial biosphere across this period. Given the uncertainty and ranges of starting estimates of terrestrial biosphere $\delta^{13}C$, the uncertain LGM-Holocene changes, the large number of potential drivers, and the further uncertainty in extrapolating the posited LGM-Holocene changes back for the preceding 100 kyr, and the modest changes relative to the average $\delta^{13}C$ signature (and the very large range in, for example, present day estimates of C3 plant $\delta^{13}C$ (Kohn, 2010, 2016), we omit this feature with the caveat that there is added uncertainty in our terrestrial biosphere results with respect of the $\delta^{13}C$ signature applied. We apply an average $\delta^{13}C$ signature of -23‰, similar to values assumed by Menviel et al. (2016) and Jeltsch-Thommes et al. (2019) (23.3‰, -24‰ respectively), but more negative than assumed in Brovkin et al. (2002), Kohler and Fischer (2004) and Joos et al. (2004) (-16-(-17)‰). Our aim is not to contribute new findings of the terrestrial biosphere, but to ensure that the simple representation of the terrestrial biosphere in SCP-M provides the appropriate feedbacks to our (exhaustive) glacial-interglacial cycle model-data optimisation experiments, that are in line with published estimates.

Air-sea gas exchange is based on the relative pCO_2 in the surface ocean boxes and the atmosphere, and a parameter that 30 sets its rate in m day^{-1}, P (Fig. 1). pCO_2 is calculated using the method of Follows et al. (2006). SCP-M represents ocean carbonate chemistry with a parameterisation of shallow water carbonate production, linked to the Z parameter by an assumption for the relative proportion of carbonate vs organic matter, known as "the rain ratio" (e.g. Archer and Maier-Reimer, 1994; Ridgwell, 2003). Carbonate dissolution is calculated based on the ocean box or marine surface sediment calcium carbonate

concentration versus a depth-dependant saturation concentration (Morse and Berner, 1972; Millero, 1983). Most other carbon 35 cycle processes are parameterised simply, such as volcanic emissions, continental weathering, anthropogenic emissions and cosmic ^{14}C fluxes. The isotopes of carbon are calculated applying various fractionation factors associated with the biological, physical and chemical fluxes of carbon (O'Neill et al., 2019).

We have added a simple representation of shallow water carbonate fluxes of carbon and alkalinity in SCP-M's low latitude surface boxes, to cater for this feature in theories for glacial cycle CO_2 (e.g. Berger, 1982; Opdyke and Walker, 1992; Ridgwell et al., 2003; Vecsei and Berger, 2004; Menviel and Joos, 2012), using:

$$dC_i/dt\ reef = C_{reef}/V_i \quad (2)$$

Where C_{reef} is the prescribed flux of carbon out of/into the low latitude surface ocean boxes during net reef accumula- tion/dissolution, in mol C yr^{-1}, and V_i is the volume of the low latitude surface box i. The alkalinity flux associated with reef production/dissolution is simply Eq. 2 multiplied by two (e.g. Sarmiento and Gruber, 2006).

The major fluxes of carbon are parameterised simply in SCP-M to allow them to be solved by model-data optimisation with respect of atmospheric and ocean proxy data. In this study, the values for GOC, AMOC and biological export productivity at 100m depth, are outputs of the model-data experiments, as they are deduced from a data optimisation routine. Their input values for the experiments are ranges, as described in 2.2.1. SCP-M's fast run time and flexibility renders it useful for long term paleo-reconstructions involving large numbers of quantitative experiments and data integration (O'Neill et al., 2019). SCP-M is a simple box model, which incorporates large regions of the ocean as averaged boxes and parameterised fluxes. It is an appropriate tool for this study, in which we evaluate many tens of thousands of simulations to explore possible parameter combinations, in conjunction with proxy data. The model used for this paper is located at https://doi.org/10.5281/zenodo.3559339.

RC: Figure 1 – this graphic, while nice and colourful, is challenging for reading the actual numbers and symbols (especially the white ones which do not show up at all on my colour print). Readability is more important than colour! I suggest making box numbers, symbols all BLACK using larger fonts so that they are readable.

AC: Thanks. To address this comment, for Figure 1 we have upgraded the box number font size, in bold and black, and we increased font sizes for text elsewhere in the diagram. We would like to retain the colour coding of parameter symbols with their associated flux arrows. To address the RC, we have expanded the font size of these to help with readability (please see attached revised manuscript at Figure 1).

RC: Pg 5 lines 15-17. This sentence seems out of place: "Therefore, our modelling excludes the last glacial termination (~11-18 ka)." Should it occur before the previous sentence?

AC: Thanks, we have relocated the misplaced sentence (P8, L14).

RC: Section 2.2.1 Model forcings: Although the authors ultimately conclude that sea ice cover – as a barrier mechanism constraining air-sea CO2 exchange – is not that important, the authors should emphasize limitations of their use of the ice core sea ice proxy. First, this proxy is non-linear, so their simulations probably over estimate early (MIS5d) sea ice cover and underestimate later (MIS4-2) sea ice cover. This point is made very clearly by Wolff et al. 2010 (and supports) the authors' assertion that the barrier effect of sea ice early in the glaciation is probably small.

Text added in the methodology section (P8, L28).

"Our treatment of sea-ice cover is simply as a regulator of air-sea gas exchange in the polar ocean surface boxes. This treatment misses important linkages that likely exist between sea-ice cover and Southern Ocean upwelling, wind-sea surface interactions, NADW formation, deep ocean stratification, nutrient distributions and biological productivity (Morrison and Hogg, 2013; Ferrari et al., 2014; Jansen, 2017; Kohfeld and Chase, 2017; Marzocchi and Jansen, 2017). Furthermore, our linear application of the sea-ice proxy data of Wolff et al. (2010) to our air-sea gas exchange parameter may serve to overestimate its effect on the model results early in the glacial period (MIS 5d), and underestimate it during MIS 2-4 (Wolff et al., 2010). "

RC: Furthermore, it is worth pointing out somewhere in the discussion that this modelling exercise only examines the potential role of sea ice as a barrier to CO2 exchange, and not its synergistic (and likely more important) roles in influencing nutrient distributions, marine productivity, and a trigger for deep ocean circulation changes. The authors state this somewhat in their "Advantages and limitations" section, but I think that this point could be made more explicitly.

AC: To address this comment, we have added the following (P27, L23):

"This finding may reflect our approach to treat polar sea-ice cover simply as a regulator of the rate of air-sea gas exchange in the polar oceans. This approach may neglect other effects of sea-ice cover including as a trigger for changes in Southern Ocean upwelling, NADW formation rates, deep ocean stratification, nutrient distributions and biological productivity (Morrison et al., 2011; Brovkin et al., 2012; Ferrari et al., 2014; Kohfeld and Chase, 2017; Jansen, 2017; Marzocchi and Jansen, 2017). For example, Brovkin et al. (2012) found that in the CLIMBER-2 model, atmospheric CO2 was more sensitive to sea ice cover when it was linked to weakened vertical diffusivity in the Southern Ocean of tracers such as DIC, thereby reducing outgassing of CO_2."

RC: Another larger issue that the sea ice proxy highlights is the spatial heterogeneity of the Southern Ocean and how the model results are linked with reality: the sea ice proxy likely represents changes very close to the continent and early glacial changes in sea ice are not well reproduced in the few long sea ice records that are found near the APF. This not only suggests that a barrier effect of sea ice would be limited to only part of the Southern Ocean, it points to larger issues with treating the Southern Ocean as one box, with an unclear delineation of how much of the S. Oc. this box is presumed to cover. If the

box is supposed to ONLY cover those areas close to the continent where AABW and Circumpolar Deepwater processes that influence GOC are most important, then the authors' main conclusion of increases in S. Oc. export production aren't well supported by paleoceanographic data which show reductions in export South of the APF for the majority of the glacial cycle between MIS5d and MIS2. Some discussion of what the Southern Ocean box actually represents - and this potential disconnect with paleoceanographic data - is warranted.

AC: SCP-M has two Southern Ocean boxes in each basin: a polar and sub polar Southern Ocean box. These are: polar Southern Ocean box for both basins (box 12 in Figure 1) which covers 60-80 deg S, sub polar Atlantic box (box 7 in Figure 1, 40-60 deg S) and sub polar Pacific-Indian box (box 11, 40-60 deg S). The sea ice forcing/air-sea gas exchange is undertaken for the polar Southern Ocean box. The biological export productivity experiment is undertaken for the sub polar Southern Ocean boxes in each basin, as per the regions highlighted for increased glacial period biological activity by Martinez-Garcia (2014) and Lambert et al. (2015), Shoenfelt et al. (2018). Put another way, our Southern Ocean biological flux experiments are not concerned with the APF, but with the open Southern Ocean box.

We have added the following text in the model description in Section 2.1 (P5, L6):

"The Southern Ocean is split into two boxes, including a polar box which covers latitude range 60-80 degrees South (box 12 in Fig. 1) and sub polar boxes in the Atlantic (box 7) and Pacific-Indian (box 12) basins, which cover latitude range 40-60 degrees South. See O'Neill et al. (2019) for a discussion of the choice of box depth and latitude dimensions."

We have also added the following text in the first paragraph of Section 2.2.1 Model parameters and forcing (P8, L26):

"Note the polar Southern Ocean box which is forced with reduced air-sea exchange, is separate from the sub polar Southern Box in which the biological export productivity parameter is varied in the model-data experiment."

RC: Throughout the paper the authors refer to "abyssal" and "deep" water masses for all basins, but I was never able to find the depth cut-offs that were used to distinguish these depths in the different basins. Please put them in the figure captions and text (not just supplemental information, if it is there.)

AC: We have added the following text in the model description in Section 2.1 (P5, L4):

"SCP-M splits out depth regions of the ocean between surface boxes (100-250m average depth), intermediate (1,000m average depth), deep (2,500m average depth) and abyssal depth boxes (3,700-4,000m average depth). The Southern Ocean is split into two boxes, including a polar box which covers latitude range 60-80 degrees South (box 12 in Fig. 1) and sub polar boxes in the Atlantic (box 7) and Pacific-Indian (box 12) basins, which cover latitude range 40-60 degrees South. See O'Neill et al. (2019) for a discussion of the choice of box depth and latitude dimensions."

We have also added depth references to the Caption on Figure 1, Figures 5-7, Figures 9-11

RC: The authors discuss briefly that previous studies have only used the C. wuellerstorfi data to reconstruct deep ocean δ13C (Peterson et al. study; Kohfeld and Chase study). Which data did these authors select from Oliver et al. (2010)? They mention only using "deep" and "abyssal" sites (again, depths undefined) on page 11, but they do not indicate whether they have filtered the data to only include C. wuellerstorfi (or even Cibicidoides spp), which they SHOULD be doing if they haven't. Otherwise, the changes in δ13C described on page 12 are invalid as descriptions of deep ocean circulation changes in δ13C.

AC: The work of Oliver et al. (2010) was to aggregate ocean δ13C data, estimate and correct for species-related problems or errors, and thereby provide a dataset to be used for assessing ocean circulation changes. The Oliver et al. (2010) dataset is split into Planktonic and Benthic species data. We had used the benthic datasets. We had given Oliver et al. (2010) the benefit of the doubt, in our first manuscript, as they had gone to substantial effort to produce a δ13C dataset for paleooceanographic purposes.

However, on the suggestion of the reviewer, we have revisited the data and filtered the Cibicides species for the δ13C dataset, which also includes Cibicides data contributed by Govin et al. (2009) and Piotrowski et al. (2009).

We have re-constructed our ocean δ13C database using only the Cibicides species δ13C data, re-calibrated the model for a new set of (penultimate) interglacial starting data, and re-run all of our model-data experiments. The revised manuscript (attached) incorporates these changes in the text, charts and tables.

The data section is updated as follows (P13, L4):

"Oliver et al. (2010) compiled a global dataset of 240 cores of marine $\delta^{13}C$ data encompassing benthic and planktonic species over the last ~150 kyrs. Oliver et al. (2010) observed considerable uncertainties associated with the broad range of species included, particularly for the planktonic foraminifera. By comparison, Peterson et al. (2014) aggregated marine $\delta^{13}C$ for the LGM and late Holocene periods, as time period averages, exclusively sampling benthic *C. wuellerstorfi* data, which is a more reliable indicator of marine $\delta^{13}C$ (Oliver et al., 2010; Peterson et al., 2014). To narrow the range of uncertainty, we constrain our use of marine $\delta^{13}C$ data to the deep and abyssal benthic *Cibicides* species foraminifera samples in the Oliver et al. (2010) dataset, supplemented with *Cibicides* species $\delta^{13}C$ proxy data from Govin et al. (2009) and Piotrowski et al. (2009) (Table 2). Figure 3 shows the $\delta^{13}C$ data locations from Oliver et al. (2010), which are concentrated in the Atlantic Ocean. We mapped and averaged the carbon isotope data into SCP-M's boxes on depth and latitude coordinates (Fig. 1), and averaged for each MIS time slice."

RC: On Page 12, the authors qualitatively describe the differences between "deep" and "abyssal" changes in δ13C. Why leave this discussion qualitative, when the data are available and quantification would be hugely useful. These data in the Pacific that are described are the data that pin the authors' entire argument surrounding early changes in GOC. I think that this warrants a bit more quantification of these data (once species other than Cibicidoides are filtered out of the dataset). I would be interested to know if the differences between deep and abyssal δ13C in the Indo-pacific are statistically significant, and I think plots of the probability distribution functions of these data would be very useful.

AC: Thanks. Following from this comment we've investigated a number of ways to analyse the data. We have focussed on the $\delta^{13}C$ data (*Cibicides*, as above) only, for this analysis, as there is continuous coverage for deep and abyssal boxes for the Atlantic and Pacific-Indian oceans across all of the MIS stages we are interested in.

We applied some tests for statistical significance of the various boxes throughout the MIS stages. We used a Welch's paired unequal variance t-test for statistically different mean $\delta^{13}C$ between deep and abyssal boxes, and also for differences in the offsets in mean $\delta^{13}C$ between deep and abyssal boxes, between MIS stages. We have added this to the supplementary information file and referenced its location from the main document (P17 L13).

As per the reviewer comment, we first plot the distribution of mean $\delta^{13}C$ values for each of the deep and abyssal boxes across the MIS stages.

Figure 1: Distribution histograms of $\delta^{13}C$ data for the Pacific-Indian (left column) and Atlantic Ocean (right column) deep (100/1,000-2,500m) and abyssal (>2,500m) boxes. Plots also show the mean $\delta^{13}C$ for each box (vertical dashed lines), and the calculated offset between the deep and abyssal mean $\delta^{13}C$ values (**CP_RC2_Fig1.png**).

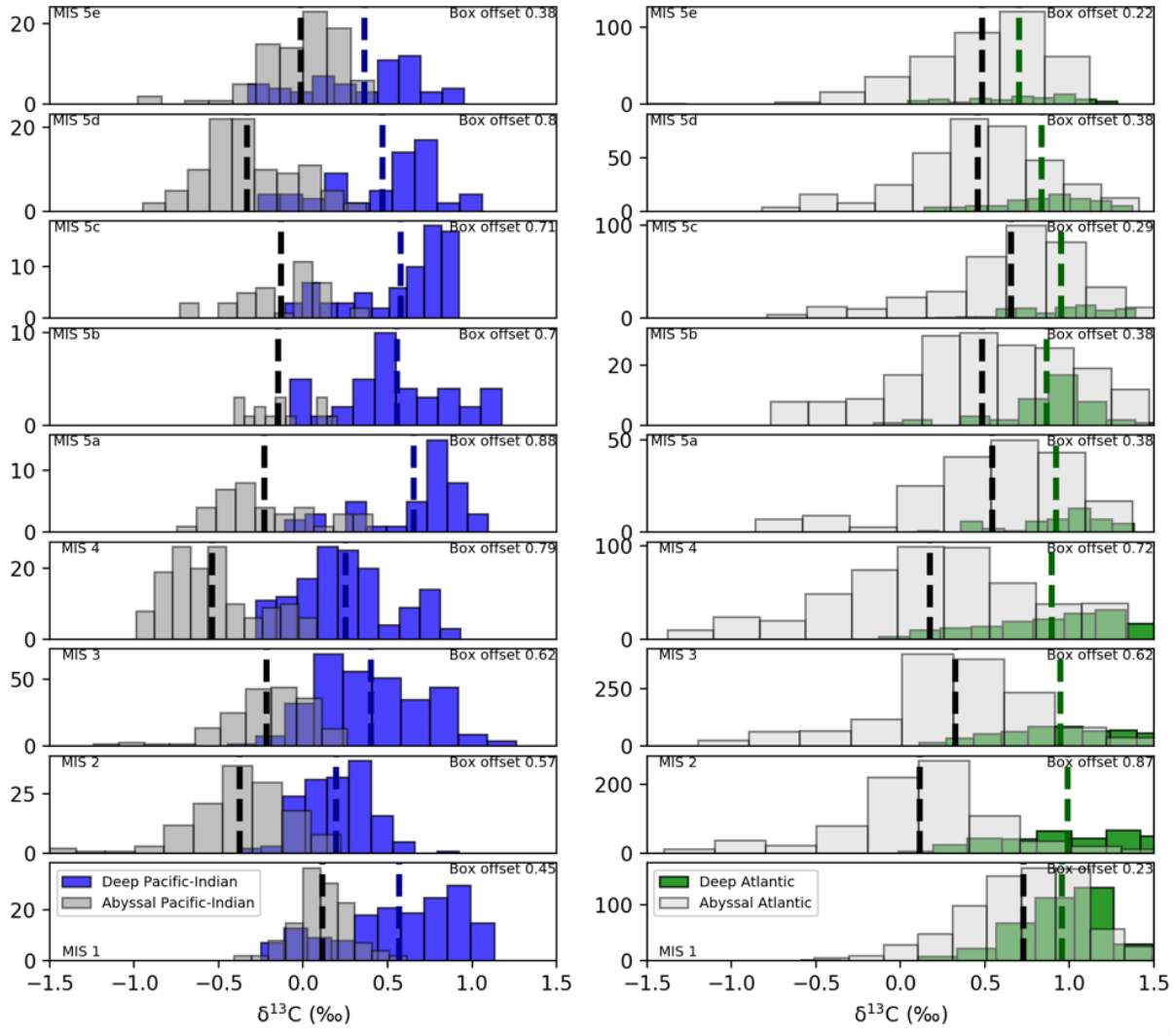

We applied a Welch's paired t-test to test for statistical independence of the means of $\delta^{13}C$ in the deep and abyssal ocean boxes for Atlantic and Pacific-Indian, within each MIS. This returns p-values very close to zero for every box pair and every MIS. A p-value <0.05 means that we reject the null hypothesis that the abyssal and deep ocean boxes are statistically the same. That is, our deep and abyssal boxes in the model are statistically independent of each other, in terms of mean $\delta^{13}C$. This simply confirms that our abyssal and deep ocean boxes are not the same in terms of mean $\delta^{13}C$ in each MIS.

Table 1: Tests for statistical independence of the mean $\delta^{13}C$ between deep and abyssal boxes (**CP_RC2_Tab1.png**)

	Abyssal-deep Pacific-Indian		Abyssal-deep Atlantic	
MIS	t-statistic	p-value	t-statistic	p-value
MIS5e	-7.0	0	5.1	0
MIS5d	16.1	0	9.8	0
MIS5c	13.0	0	7.8	0
MIS5b	9.5	0	6.3	0
MIS5a	13.2	0	6.9	0
MIS4	24.0	0	17.6	0
MIS3	23.3	0	21.6	0
MIS2	18.8	0	31.6	0
MIS1	14.2	0	11.9	0

Given we discuss in the manuscript (qualitatively) the changes in the offset between deep and abyssal ocean δ13C through the MIS, we can test to see if the changes in deep-abyssal offset from the penultimate interglacial (MIS 5e) to the glacial periods are statistically significant. The chart below shows the deep-abyssal offsets in δ13C for the Pacific-Indian and Atlantic Ocean boxes through each MIS of the last glacial-interglacial cycle. We show the absolute deep-abyssal δ13C offsets for Pacific-Indian and Atlantic Ocean boxes, for each MIS (columns). We also show the deep-abyssal δ13C offsets relative to the penultimate interglacial in MIS 5e (lines).

The Pacific-Indian δ13C offset shows a widening in MIS 5d, relative to MIS 5e, which is maintained until MIS 5a, and then begins a slow decline. The offset declines to a similar value to MIS 5e, by MIS 1 (the Holocene). The Atlantic deep-abyssal δ13C offset does not increase meaningfully until MIS 4, and then peaks at MIS 2 (the LGM), before contracting at MIS 1 to a value almost the same as MIS 5e.

Figure 2: Offsets between mean deep and abyssal box δ13C for each MIS in the last glacial-interglacial cycle for the Pacific-Indian (blue columns) and Atlantic Ocean (grey columns). Changes in the offsets from the penultimate interglacial (MIS 5e) are shown by the blue (Pacific-Indian) and grey (Atlantic) lines (**CP_RC2_Fig2.png**).

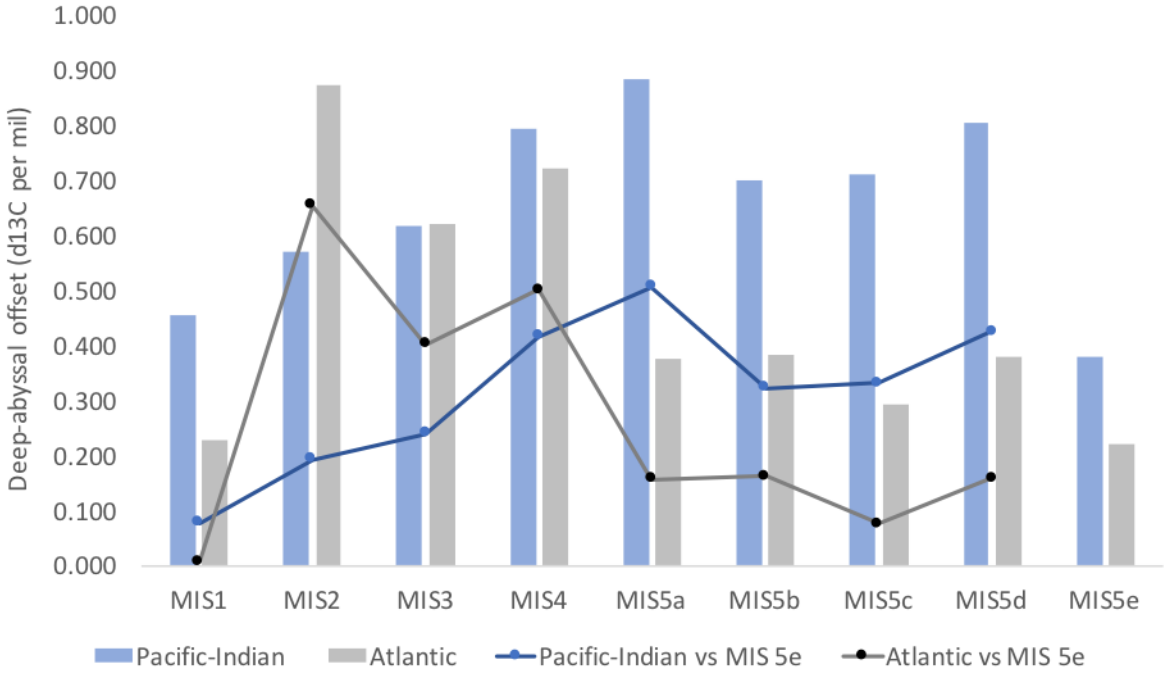

We further undertook Welch's paired T-tests for the independence of deep-abyssal offsets in mean δ13C with respect of the penultimate interglacial period (MIS 5e), for the periods MIS 1-5e. The null hypothesis is that the deep-abyssal offset in mean δ13C in each MIS is not statistically independent of MIS 5e (i.e. statistically the same and not supportive of a change in deep-abyssal δ13C distribution that may be delivered by a changed ocean process). p-values>0.05 lead to the null hypothesis being accepted, whereas p-values <0.05 lead to the null hypothesis being rejected and confirm statistical independence of the deep-abyssal offsets relative to MIS 5e (perhaps supportive of a changed ocean distributive process in the glacial period). Deep-abyssal offsets for the Pacific-Indian during MIS 2-MIS5d are statistically independent of MIS 5e, supportive of a changed oceanic distribution of δ13C throughout the glacial period. The MIS 1 Pacific-Indian deep-abyssal δ13C offset is not statistically independent of MIS 5e, indicating a similar deep-abyssal δ13C distribution between the last and penultimate interglacial periods. For the Atlantic Ocean, deep-abyssal mean δ13C offsets are not statistically independent with respect to MIS 5e (p-value >0.05, accept null hypothesis), until the period MIS 2-4. Atlantic deep-abyssal mean δ13C offset in MIS 1 is not statistically different from MIS 5e.

Table 2: Statistical tests for significance of difference in deep-abyssal δ13C offsets versus penultimate interglacial (MIS 5e). 'Accept'/red is to accept the null hypothesis - no statistically significant difference, 'Reject'/green is to reject the null hypothesis – statistically significant difference with respect of MIS 5e (**CP_RC2_Tab2.png**).

	Pacific-Indian (vs MIS 5e)			Atlantic (vs MIS 5e)		
MIS	t-statistic	p-value	Accept/ reject null	t-statistic	p-value	Accept/ reject null
MIS 5e	0.0	0.500	Accept	0.0	0.500	Accept
MIS5d	3.8	0.000	Reject	1.4	0.079	Accept
MIS5c	3.0	0.002	Reject	0.7	0.253	Accept
MIS5b	2.9	0.002	Reject	1.5	0.074	Accept
MIS5a	4.5	0.000	Reject	1.4	0.082	Accept
MIS4	3.7	0.000	Reject	4.5	0.000	Reject
MIS3	2.1	0.017	Reject	3.6	0.000	Reject
MIS2	1.7	0.044	Reject	5.9	0.000	Reject
MIS1	0.7	0.246	Accept	0.1	0.478	Accept

The statistical analysis above is helpful and provides support for our model-data experiment results – that GOC slowed in MIS 5d and AMOC slowed in MIS 4. However, we do want to make the point that our model-data results don't hang on one particular data point to deliver these findings, in any MIS. They are constrained and optimised with many observations. The model-data results in the first instance are telling us that, the many observational forcings we have imposed in each MIS (SST, salinity, sea-ice cover proxy, coral reef carbonates) are not enough to deliver the change in atmospheric CO2, atmospheric and ocean δ13C, D14C and CO23 proxy data. Changes from within the set of ocean circulation, mixing and/or biology parameters are needed. Note the result for GOC that is hinted at by the δ13C data, that we model in our experiments, is sustained throughout the last glacial cycle, not just at MIS 5d.

The main point of our work, and what has taken substantial effort, is to undertake an exhaustive model-data optimisation using a carbon cycle box model and multiple atmospheric and ocean proxy data. The model-data results don't just rely on one data point, the results need to be the best fit for all the data used, in each MIS. This is where this model-data experiment differentiates itself from many others.

We have included the distribution plot and T-test table above, in the manuscript's Supporting Information. We make reference to this material in the manuscript when discussing the data charts in the "Data Analysis" section. This chart/table provide supplemental support to the model-data analysis, the latter being the focus of our manuscript. We feel that the manuscript is becoming very voluminous and we also think that this analysis would require its own section in the manuscript (However, it is presented in this response to the discussion (preserved online) and in the SI).

RC: Some type of quantification would also be very useful for the authors' description of the "transient drop in abyssal Atlantic ocean CO3= at MIS5b" on page 14. I was not convinced that this transient drop exists from the figure presented.

AC: Yes, the axes on these charts are a little difficult to decipher small changes in the data. We wish to show the range of shallow-deep CO23 data (not just deep-abyssal), as the pattern is quite interesting at the LGM-Holocene. Our suggestion is to add the changes in units for the pattern that we wish to describe (P17, L35):

"There is a modest drop in abyssal Atlantic Ocean CO^{2-}_3 at MIS 5b (-13 µmol kg^{-1} relative to MIS 5c), which coincides with a minor drop in abyssal Atlantic Ocean $\delta^{13}C$ (-0.19‰) and atmospheric CO_2 (-14 ppm), suggesting a possible common link."

RC: Please note on the bottom of page 13 and top of page 14 that the authors mean to refer to Figure 7 (not 6) to describe carbonate ion concentration data.

AC: Thank you, we have corrected these references in the manuscript.

RC: Last sentence before Results section: Please cite the figures you are using to make these observations about changes in δ13C and DD14C

AC: We have added the figure references

RC: Similar quantification would be useful in the comparison between the carbonate ion concentration model output and data in Figure 9 and in the discussion on page 16-17.

AC: Figure references for Figure 9 added to the text here

References

Govin, A., Michel, E., Labeyrie, L., Waelbroeck, C., Dewilde, F., and Jansen, E.: Evidence for northward expansion of Antarctic Bottom Water mass in the Southern Ocean during the last glacial inception, Paleoceanography, 24, doi:10.1029/2008PA001 603, 2009.

Lambert, F., Tagliabue, A., Shaffer, G., Lamy, F., Winckler, G., Farias, L., Gallardo, L., and Pol-Holz, D.: Dust fluxes and iron fertilization in Holocene and Last Glacial Maximum climates, Geophysical Research Letters, 42, 6014–6023, 2015.

Martinez-Garcia, A., Sigman, D., H.Ren, Anderson, R., Straub, M., Hodell, D., Jaccard, S., Eglinton, T., and Haug, G.: Iron Fertilization of the Subantarctic Ocean During the Last Ice Age, Science, 343, 1347–1350, 2014.

Oliver, K., Hoogakker, B., Crowhurst, S., Henderson, G., Rickaby, R., Edwards, N., and Elderfield, H.: A synthesis of marine sediment core d13C data over the last 150 000 years, Climate of the Past, 6, 645–673, 2010.

Piotrowski, A., Banakar, V., Scrivner, A., Elderfield, H., Galy, A., and Dennis, A.: Indian Ocean circulation and productivity during the last glacial cycle, Earth and Planetary Science Letters, 285, 179–189, 2009.

Shoenfelt, E.M., Winckler, G., Lamy, F., Anderson, R.F., and Bostick, B.C. Highly bioavailable dust-borne iron delivered to the Southern Ocean during glacial periods. PNAS 115 (44) 11180-11185, 2018. https://doi.org/10.1073/pnas.1809755115.

CP reviewer comments #3 and author responses

AC: We thank the reviewer for their comments, suggestions and input into this manuscript. These comments make a strong contribution to improving the quality of our work. Please see below our responses to the individual comments.

We have made reference to changes to the manuscript, which are included as a supplement to the author comments, in track changes. Page and line references below refer to locations in the revised document with track changes.

Please note that we have changed our treatment of ocean $\delta^{13}C$ proxy data, stemming from one of the other reviewer comments, to only include $\delta^{13}C$ from *Cibicides* species of benthic foraminifera. We have also made some small changes to the parameterisation of the volcanic and weathering isotopic signatures in the model, from reviewer comments. These changes required the re-calibration of our model and re-running of the model-data experiments. The model-data results changed modestly. We have updated the figures and text (tracked in the attachment) in the manuscript, accordingly.

Major comments:

RC 1) The "data analysis" section 3 presents the changes in atm. CO2, d13CO2, oceanic d13C, D14C and CO3(2-) as inferred from proxy records from the LIG to the LGM. This is obviously a huge task, but which I am afraid can give rise to approximations and simplifications. I would consider seriously amending this section. How can the "increase in d13C across the glacial cycle be attributed to the growth of tundra at high latitudes"? (p12, L. 2-3).

AC: Thanks for the comment. In this instance (P12, L2-3 in the original manuscript) and throughout our manuscript, we have been a bit loose with our references to tundra, permafrost and peat, as you point out in this comment and a few below.

What we mean to refer to here is the storage of carbon by the accumulation and freezing, or burial, of peat and other soil organic matter under soil overburden, and growth of cold-climate vegetation, throughout the glacial cycle (e.g. Tarnocai et al., 2009; Ciais et al., 2012; Schneider et al., 2013; Eggleston et al., 2016; Treat et al., 2019).

We have corrected the statement on P12 L2-3, and expanded a bit, including a few more references and other possible causes of the atmospheric $\delta^{13}C$ pattern, now at P15 L10:

"Atmospheric $\delta^{13}C$ (Fig. 4(B)) increased by ~0.4‰ between the penultimate interglacial (MIS 5e) and the Holocene (MIS 1), with temporary falls at MIS 5d, MIS 4 and in the last glacial termination (between MIS 1 and 2). The cause of the observed increase in atmospheric $\delta^{13}C$ across the last glacial-interglacial cycle may be the effect of accumulation and freezing, or burial in glacial sediments, of peat and other soil organic matter at the high latitudes (e.g. Tarnocai et al., 2009; Ciais et al., 2012; Schneider et al., 2013; Eggleston et al., 2016; Ganopolski and Brovkin, 2017; Treat et al., 2019). According to Treat et al. (2019),

peatlands and other vegetation accumulated carbon in the relatively warm periods, and these carbon stocks were then frozen and/or buried in glacial and other sediments during the cooler periods, throughout the last glacial cycle. This buried or frozen stock of carbon persists to the present day (Tarnocai et al., 2009), although according to Ciais et al. (2012) it may be smaller now than in the LGM. Schneider et al. (2013) evaluated several possible candidates for the rising atmospheric $\delta^{13}C$ pattern across the last glacial-interglacial cycle and could not discount any of (1) changes in the carbon isotope fluxes of carbonate weathering and sedimentation on the seafloor, (2) variations in volcanic outgassing or (3) peat and permafrost build-up throughout the last glacial-interglacial cycle.

The large drop in $\delta^{13}C$ in MIS4, reverses in MIS 3 (Fig. 4(B)). This excursion in the $\delta^{13}C$ pattern likely resulted from sequential changes in SST (cooling), AMOC, Southern Ocean upwelling and marine biological productivity (Eggleston et al., 2016). Eggleston et al. (2016) parsed the atmospheric $\delta^{13}C$ signal into its component drivers across MIS 3-5, using a stack of proxy indicators, and highlighted the sequence of events between the end of MIS 5 and beginning of MIS 3, and their cumulative effects to deliver the full change in atmospheric $\delta^{13}C$. Our MIS-averaging approach fails to capture the full amplitude of the changes in atmospheric $\delta^{13}C$ during MIS 3-5, and only captures the changes in the mean-MIS value, serving to understate the full amount of transient changes in responsible processes. In addition, the MIS-averaging approach misses the sequential timing of changes in processes within each MIS. These are limitations of our steady-state, MIS-averaging approach. The reduction in atmospheric $\delta^{13}C$ at the last glacial termination, between MIS 1 and MIS 2, coincident with a large atmospheric CO_2 increase, is attributed to the release of deep-ocean carbon to the atmosphere resulting from increased ocean circulation and Southern Ocean upwelling (Schmitt et al., 2012). The subsequent rebound of $\delta^{13}C$ in the termination period and the Holocene is believed to result from terrestrial biosphere regrowth, in response to increased CO_2 and carbon fertilisation (Schmitt et al., 2012; Hoogakker et al., 2016). "

Other amendments to this section are shown in track changes.

RC: p12, L. 11-14: How were the values for MIS3 DD14C in the Atlantic derived? From Fig. 6a, it looks like there is no data across MIS3.

AC: Thanks, this was a charting error and now the chart has been corrected to show the data for MIS 3.

RC: This is quite a shortcut to explain the deglacial D14C decrease, and maybe you want to check the references and include " increase in Southern Ocean ventilation" above anything else.

AC: P16, L4 modified to "….an acceleration in atmospheric $\Delta^{14}C$ decline at the last glacial termination is attributed to the release of old, ^{14}C -depleted waters from the deep ocean, **due mainly to increased Southern Ocean upwelling** (e.g. Sikes et al., 2000; Marchitto et al., 2007; Skinner et al., 2010; Burke and Robinson, 2012; Siani et al., 2013; Skinner et al., 2017)."

RC: P14, L. 5-6: This reads like speculation.

AC: This sentence re-worded as:
(P17, L35) "There is a modest drop in abyssal Atlantic Ocean CO^{2-}_3 at MIS 5b (-13 µmol kg^{-1} relative to MIS 5c), which coincides with a minor drop in abyssal Atlantic Ocean $\delta^{13}C$ (-0.19‰) and atmospheric CO_2 (-14 ppm), indicating a common link. Menviel et al. (2012) modelled a transient slowdown in North Atlantic overturning circulation for this period, which could explain these features. "

RC: 2) Fit with the data: 50 umol/L as an "arbitrary standard deviation' for [CO3] is huge and represents more than the [CO3] changes (0-30 umol/L) recorded across the G-IG cycles. How much was taken for the standard deviation for d13C and D14C? It looks quite large. Figures 9-11 would gain in having a more appropriate range in the y axis. At the moment the ranges and std are large, so that it almost looks like there are no changes from MIS5 to MIS 2.

AC: Re CO^{2-}_3. In response to this reviewer's comments, and a change to our data approach from the other reviewer comments (using only *Cibicides* species for $\delta^{13}C$), we have been able to reduce our default standard deviation for ocean CO^{2-}_3 from 50 umol kg^{-1} to 15 umol kg^{-1}, a substantial improvement. The rationale for setting the CO^{2-}_3 SD at an artificial level for the weighting in our model-data optimisation is dealt with in Section 2.3.2. This is an unfortunate feature of using a box model with large boxes and applying sparse proxy data. The relatively small number of CO^{2-}_3 data points in clustered locations leaves relatively small standard deviations, giving CO^{2-}_3 a disproportionate weighting in the model-data optimisation versus the other proxies. Therefore, we overcome the issue by scaling up the CO^{2-}_3 standard deviations and applying as default across all boxes and MIS time slices.

Re $\delta^{13}C$ and $\Delta^{14}C$. The standard deviations are calculated from box-averaged published proxy data and shown in the supporting information. The standard deviations look large for these box-averaged and MIS-averaged values, because the boxes in the box model are large. The ocean box $\delta^{13}C$ standard deviation is now lower in the revised manuscript due to filtering out only *Cibicides* species, from the other reviewer comments.

The issue of box size and standard deviation is addressed again in the discussion of limitations of the study (P34 L7):

"However, given the large spatial coverage of the SCP-M boxes, data for large areas of the ocean are averaged, and some detail is lost. For example, in the case of the carbonate ion proxy, we apply a default estimate of standard deviation to account for the large volume of ocean covered by SCP-M's boxes relative to the proxy data locations, and to enable the normalisation of the carbonate ion proxy data in a procedure that uses the data standard deviation as a weighting. Despite this caveat, we argue that the model-data experiment results provide a good match to the data across the various atmospheric and ocean proxies as shown in Figs 9-11."

Re Figs 9-11. The standard deviation ranges for CO^{2-}_3 and $\delta^{13}C$ are now narrower following the improvements we have made, which improves the resolution of Figs 9-11. In addition,

we have expanded y-axes where we can to help with reading the figures.

RC: 3) References: In general I find that only a few references are used over and over and sometimes not appropriately. A few additional references are included in this review. Please note the typo throughout the document in "Ridgwell".

AC: Thanks, we've now added the references suggested by the reviewer, throughout the manuscript, and we corrected the typo for Ridgwell throughout.

References added following this reviewers' comments:

Watson et al., 2000
Joos et al., 2004
Tarnocai et al., 2009
Ganopolski et al., 2010
Menviel et al., 2012
Menviel and Joos, 2012
Brovkin et al., 2012
Jaccard et al., 2013
Schneider et al., 2013
Menviel et al., 2015
Yu et al., 2016
Ganopolski and Brovkin, 2017
Lindgren et al., 2018
Mauritz et al., 2018
Yamamoto et al., 2019
Treat et al., 2019

Specific comments:

RC: 1) Abstract: The first line does not make sense. Please reformulate. L. 3 Please add "SO" in front of "biological productivity"

AC: Re-formulated as: "We conduct a model-data analysis of the marine carbon cycle to understand and quantify the drivers of atmospheric CO_2 during the last glacial cycle".

Southern Ocean added to the sentence P1 L3.

RC: 2) Introduction: - L.15-19: please be more specific. Instead of "Ocean biology" you might want to refer to "iron fertilisation and its impact on nutrient utilisation", or changes in remineralisation depth (e.g. Kwon et al. 2009).

AC: text modified to (P2 L18):

"Hypotheses for an ocean biological role include the effects of iron fertilisation on biological export productivity (e.g. Martin, 1990; Watson et al., 2000; Martinez-Garcia et al., 2014),

the depth of remineralisation of particulate organic carbon (POC) (e.g. Matsumoto, 2007; Kwon et al., 2009; Menviel et al., 2012), changes in the organic carbon:carbonate ("the rain ratio") or carbon:silicate constitution of marine organisms (e.g. Archer and Maier-Reimer, 1994; Harrison, 2000), and increased biological utilisation of exposed shelf-derived nutrients such as phosphorus (e.g. Menviel et al., 2012)."

RC: What do you mean by composite mechanisms?

AC: we have amended this to "the aggregate effects of several mechanisms" throughout the document

RC: It would be good to also introduce the numerous modelling studies that have been done on the topic of G-IG changes in pCO2, and notably transient simulations of the G-IG trying to understand the changes in pCO2 (e.g. Ganopolski & Brovkin 2017, Menviel et al., 2012).

AC: Thanks, we have added to our introduction (P2 L23):

"Several studies have attempted to solve the problem of glacial-interglacial CO_2 by modelling either the last glacial-interglacial cycle in its entirety, or multiple glacial-interglacial cycles (e.g. Ganopolski et al., 2010; Menviel et al., 2012; Brovkin et al., 2012; Ganopolski and Brovkin, 2017). These studies highlight the roles of orbitally-forced Northern Hemisphere ice sheets in the onset of the glacial periods, and important feedbacks from ocean circulation, carbonate chemistry and marine biological productivity throughout the glacial cycle (Ganopolski et al., 2010; Brovkin et al., 2012; Ganopolski and Brovkin, 2017). Menviel et al. (2012) modelled a range of physical and biogechemical mechanisms to deliver the full amplitude of atmospheric CO_2 variation in the last glacial-interglacial cycle, using transient simulations with the Bern3D model. According to Brovkin et al. (2012), a ~50 ppm drop in atmospheric CO_2 early in the last glacial cycle was caused by cooling sea surface temperatures (SST), increased Northern hemisphere ice sheet cover, and expansion of southern-sourced abyssal waters in place of North Atlantic Deep Water (NADW) formation. Ganopolski and Brovkin (2017) modelled the last four glacial cycles with orbital forcing as the singular driver of carbon cycle feedbacks. They described the "carbon stew", a feedback of combined physical and biogeochemical changes in the carbon cycle, to drive the last four glacial-interglacial cycles of atmospheric CO_2."

And also, a few lines down to explain how our approach differs (P3 L23):

"Our modelling approach differs from other model studies of the last glacial-interglacial cycle (e.g. Ganopolski et al., 2010; Menviel et al., 2012; Brovkin et al., 2012; Ganopolski and Brovkin, 2017), in that we constrain several physical processes from observations (SST, sea level, sea-ice cover, salinity, coral reef fluxes of carbon), then solve for the values of model parameters for ocean circulation and biology based on an optimisation against atmospheric and ocean proxy data. "

And at P8 L14:

“Joos et al. (2004), Ganopolski et al. (2010), Menviel et al. (2012), Menviel and Joos (2012), Brovkin et al. (2012) and Ganopolski and Brovkin (2017) provide coverage of the termination period with transient simulations of the last glacial-interglacial cycle, using intermediate complexity models (more complex than our model). “

RC: 3) Methods: - Variables included in the model: surely the model includes Dissolved Inorganic Carbon.

AC: yes, the model includes DIC and we have added DIC to the sentence.

RC: By “CO2”, do you mean atmospheric CO2?

AC: yes, we have added “atmospheric” to the sentence at P3 L33.

RC: Does the model really includes “carbonate ions” as a prognostic tracer?

AC: Yes. SCP-M calculates CO^{2-}_3 concentration in umol kg^{-1}, by calculating the three species of DIC. First, pCO_2 is calculated using the method of Follows et al. (2006) which takes as inputs DIC, alkalinity, pH, SST, salinity and phosphorus in each box in the model. Then H_2CO_3, HCO_3^- and CO^{2-}_3 are calculated using coefficients for the solubility of CO_2 (K_0) and coefficients for carbonic acid of K_1 and K_2 using Lueker et al. (2000). In the model documentation paper (O’Neill et al., 2019) the SCP-M model estimates for CO^{2-}_3 in a modern ocean setting are demonstrated to align with modern data from the ocean, using data from Key at al (2004).

We have added a summary sentence to describe this, in section 2.1 “Model description” on P4.

RC: p4, L. 2: please refer to section 2.2.1 and Figure 2.

AC: Added

RC: p7: I am very confused by the treatment of the terrestrial biosphere in the model and the paragraph L. 19-27. It reads like there is an interactive terrestrial module. But how can NPP be calculated with significance if there is no atm. Temperature or precipitation in the model?

Our box model applies a simple representation of the terrestrial biosphere, whereby biological productivity responds to carbon fertilisation. Therefore, CO_2 is the driver of terrestrial biosphere productivity in this model. We use a two-box terrestrial box model scheme, presented in Harman et al. (2011). The inputs are starting estimates of net primary productivity (NPP), the terrestrial biosphere carbon stock, plant respiration rate and atmospheric CO_2. The approach of Harman et al. (2011) is to split the terrestrial biosphere into two boxes, a fast-response (grasslands and grassy components of savannah systems)

and a slow-response (woody trees) component. In this model, the productivity is mostly focussed on the plants/grasses component.

The formula is shown in the model documentation paper (O'Neill et al., 2019) and Harman et al. (2011), and extract is reproduced here:

$$dAtCO2/dt = -N_{pre}RP[1+\beta LN(AtCO2)] + Cstock/k + D_{forest}$$

Where Npre is NPP at a reference pre-industrial level of atmospheric CO2, RP is a parameter to split NPP between short-term terrestrial biosphere carbon stock and the longer term stock (Cstock1 and Cstock2). B is a parameter with a value typically in the range 0.4-0.8 (Harman et al., 2011). Cstock is the carbon stock in each terrestrial biosphere box, k is the respiration timeframe for each box. Dforest is the prescribed rate of deforestation emissions for present day simulations and projections. A terrestrial biosphere fractionation factor is applied for the carbon isotopes.

Harman et al. (2011) model the terrestrial biosphere primarily as a function of atmospheric CO_2. They also incorporate an optional temperature dependency. This is the same approach used in the simplest 4Box terrestrial biosphere module of the Bern Simple Carbon Model (Strassman and Joos, 2018; Seigenthaler and Joos, 1992; Kicklighter et al., 1999; Meyer et al., 1999), and described by Enting (1994) – although we understand that there are various terrestrial biosphere modules applied with the Bern models, and most are more complex. As far as we can discern, the simple carbon fertilisation approach is also used in Jelstch-Thommes et al. (2019), which also applies the simplest 4Box terrestrial biosphere of the simple Bern model.

There are other possible drivers of the NPP – temperature, precipitation, soil nutrient levels. In the context of our simple carbon cycle model, we are mainly interested in CO_2. We don't model atmospheric temperature, and if we were to try to incorporate atmospheric temperature as a driver of terrestrial biosphere, we would also need to incorporate it for terrestrial weathering. There is a limit to how much detail we want to include in the model given we are conducting many simulations (~80,000) in our model-data optimisations across the MIS of the last glacial-interglacial cycle.

We do note that there are studies devoted to determining whether the CO_2 fertilisation effect or climate is the dominant control on terrestrial biosphere NPP and the size of the terrestrial biosphere carbon stock. According to Hoogakker et al. (2016), CO_2 fertilization, rather than climate, is the primary driver of lower glacial net primary productivity by the terrestrial biosphere, accounting for around 85% of the reduction in global NPP at the LGM. Kaplan et al. (2002) also concluded that over glacial-interglacial timescales, global terrestrial carbon storage is controlled primarily by atmospheric CO_2, while the climate has more influence on the isotopic composition. Otto et al. (2002) also found that the CO_2 fertilization effect is mostly responsible for the total increase in vegetation and soil carbon stocks since the last glacial maximum. Kohler et al. (2010) prioritised CO_2 fertilisation as the driver of terrestrial biosphere in their "control" main simulation scenario for glacial-interglacial cycles over the last 740 kyr, but also ran scenarios with a climatic driver for the terrestrial biosphere to estimate the effects of "fast" climate changes on atmospheric $\delta^{13}C$. Other

studies arguing that atmospheric CO_2 is an important, or is the main driver of terrestrial biosphere productivity include Kicklighter et al. (1999), Joos et al. (2001), Schimel et al. (2015), Sitch et al. (2008), Arneth et al. (2017)). This view has been contested by Francois et al. (1999) and van der Sleen et al. (2015).

Given we don't model the atmospheric temperature or precipitation, we saw limited additional benefit to introduce them into our model of the terrestrial biosphere, although it would not be difficult to do this. Finally, given that CO_2 and atmospheric temperature co-vary closely, across glacial cycles, it seems of limited benefit to split these effects out in our simple carbon cycle modelling exercise. For example, Meyer et al. (1999) found similar results for modelling carbon uptake in the terrestrial biosphere whether only CO_2 fertilisation, or CO_2 fertilisation + climate, were included as drivers of NPP – but noting this was not tested for the LGM.

In summary, our aim is not to contribute new findings on the terrestrial biosphere, but we present the behaviour of the terrestrial biosphere in our manuscript to confirm that our exhaustively multi-proxy constrained model-data output is consistent with the range of literature estimates of variations in the terrestrial biosphere in the last glacial-interglacial cycle and LGM-Holocene period, and we show this. For example, our experiment shows a change in the terrestrial biosphere carbon stock of +630 PgC between the MIS 2 (LGM) and MIS 1 (Holocene) period. This compares with other estimates of +540 PgC (Brovkin et al., 2007), +~820-850 PgC (Joos et al., 2004) – with the majority by CO_2 fertilisation, ~+500 PgC (Kohler et al., 2010), +~500 PgC (Brovkin et al., 2012), +850 PgC (Jeltsch-Thommes et al., 2019), +511 +/- 289 PgC (Peterson et al., 2014), +378 +/- 88 PgC (Menviel et al., 2016). Another estimate of the LGM-Holocene terrestrial biosphere change is 550-694 Pg C, which our result of 630 Pg C sits comfortably within (Prentice et al., 2011)

Our estimate is actually towards the upper end of the literature ranges, suggesting if anything we could exaggerate the effects of the terrestrial biosphere from the LGM to the Holocene period, with perhaps little to gain by splitting out temperature and precipitation effects. If did, we would probably also need to consider other important features such as soil nutrients and local humidity.

While we have a simple, but explicit two-box representation of the terrestrial biosphere, we don't believe that this detracts from our model-data results, as shown in Figures 9-11 and Figure 12 specifically for the terrestrial biosphere.

If there is some reason to examine the terrestrial biosphere in more detail, we suggest for our study this would be done simply by a sensitivity, as applied in Menviel et al. (2016) with regard to C3/C4 plants and the relative proportional influence of C3 and C4 plants on terrestrial biosphere $\delta^{13}C$ fractionation.

We have added some text to explain that we have a simplified representation of the terrestrial biosphere employing CO_2 fertilisation, and that we don't take account of temperature and precipitation, in the methods section, P5 L24. This also includes discussion of the isotopic fractionation factor in response to one of the other reviewers:

"The terrestrial biosphere is represented in SCP-M as a stock of carbon that fluxes with the

atmosphere, governed by parameters for net primary productivity (NPP) and respiration. In SCP-M, NPP is calculated as a function of carbon fertilisation, which increases NPP as atmospheric CO_2 rises via a simple logarithmic relationship, using the model of Harman et al. (2011). This is a simplified approach, which omits the contribution of temperature and precipitation on NPP. Other, more complex models of the carbon cycle applied to glacial-interglacial cycles have a more detailed treatment of the terrestrial biosphere, including climate dependencies (e.g. Brovkin et al., 2002; Menviel et al., 2012). A number of studies emphasise the role of atmospheric CO_2 as the driver of terrestrial biosphere NPP on glacial-interglacial cycles (Kaplan et al., 2002; Otto et al., 2002; Joos et al., 2004; Hoogakker et al., 2016), although other studies cast doubt on the relative importance of atmospheric CO_2 versus temperature and precipitation (Francois et al., 1999; van de Sleen et al., 2015).

The isotopic fractionation behaviour of the terrestrial biosphere may also vary on glacial-interglacial timeframes. This has been studied for the LGM, Holocene and the present day (e.g. Collatz et al., 1998; Francois et al., 1999; Kaplan et al., 2002; Kohler and Fischer, 2004; Joos et al., 2004; Kohn, 2016). The variation in isotopic fractionation within the terrestrial biosphere reflects changes in the relative proportions of plants with the C3 and C4 photosynthetic pathways, but also strong variations within the same photosynthetic pathways themselves (Francois et al., 1999; Kohn, 2010; Schubert and Jahren, 2012; Kohn, 2016). The drivers for these changes include relative sea level and exposed land surface area (Francois et al., 1999), global tree-line extent (Kohler and Fischer, 2004), atmospheric temperature and CO_2 (Collatz et al., 1998; Francois et al., 1999; Kohler and Fischer, 2004; Kohn, 2010; Schubert and Jahren, 2012), global and localised precipitation and humidity (Huang et al., 2001; Kohn, 2010; Schubert and Jahren, 2012; Kohn, 2016), and also changes in the intercellular CO_2 pressure in the leaves of C3 plants (Francois et al., 1999).

Estimated changes in average terrestrial biosphere $\delta^{13}C$ signature between the LGM and the Holocene fall in the range -0.3-1.8‰ (less negative $\delta^{13}C$ signature in the LGM), with further changes estimated from the onset of the Holocene to the pre-industrial, and even greater changes to the present day (due to rising atmospheric CO_2). This feature has been covered in detail within studies that focussed on the terrestrial biosphere between the LGM and Holocene, but less so in modelling and model-data studies of the last glacial-interglacial cycle. Menviel et al. (2016) provided a sensitivity of -0.7+0.5‰ around an average LGM value of -23.3‰ for the LGM, based on previous modelling of the LGM-Holocene timeframe by Joos et al. (2004). Another modelling study (Menviel and Joos, 2012), assessed the variation in LGM-Holocene $\delta^{13}C$ of the terrestrial biosphere to be a minor factor and it was omitted. Kohler and Fischer (2004) assessed the changing $\delta^{13}C$ signature of plants between the LGM and Holocene to be a minor factor in setting $\delta^{13}C$ of marine DIC, compared to the change in the absolute size of the terrestrial biosphere across this period.

Given the uncertainty around the starting estimates of $\delta^{13}C$, the uncertain LGM-Holocene changes, the large number of potential drivers, and the further uncertainty in extrapolating the posited LGM-Holocene changes back for the preceding 100 kyr, and the modest changes relative to the average $\delta^{13}C$ signature (and the very large range in, for example, present day

estimates of C3 plant $\delta^{13}C$ (Kohn, 2010, 2016), we omit this feature with the caveat that there is added uncertainty in our terrestrial biosphere results with respect of the $\delta^{13}C$ signature applied. We apply an average $\delta^{13}C$ signature of -23‰, similar to values assumed by Menviel et al. (2016) and Jeltsch-Thommes et al. (2019) (23.3‰, -24‰ respectively), but more negative than assumed in Brovkin et al. (2002), Kohler and Fischer (2004) and Joos et al. (2004) (-16-(-17)‰).

Our aim is not to contribute new findings of the terrestrial biosphere, but to ensure that the simple representation of the terrestrial biosphere in SCP-M provides the appropriate feedbacks to our (exhaustive) glacial-interglacial cycle model-data optimisation experiments, that are in line with published estimates."

We have also updated the discussion of our model results for the terrestrial biosphere, to provide a bit more detail and some additional references (Section 5.3), plus an additional caveat in the "advantages and limitations section" (P34, L18).

"Furthermore, we apply a simple representation of the terrestrial biosphere in our model-data experiments, relying primarily on atmospheric CO_2 as the driver for NPP. This approach provided reasonable results for the terrestrial biosphere carbon stock and NPP, on the whole, but may miss some detail in the terrestrial biosphere during the last glacial-interglacial cycle."

RC: Why is "tundra" discussed with such emphasis in this paragraph?.

AC: Thanks for picking up on this. We have substantially revised this paragraph as follows (P10 L25):

"The terrestrial biosphere module in SCP-M does not explicitly represent the carbon stored in buried peat, permafrost and also cold-climate vegetation that may have expanded its footprint in the glaciation, such as tundra biomes (e.g. Tarnocai et al., 2009; Ciais et al., 2012; Schneider et al., 2013; Eggleston et al., 2016; Ganopolski and Brovkin, 2017; Treat et al., 2019). The freezing and burial of organic matter across the glacial cycle may significantly imprint the terrestrial biosphere CO_2 size and $\delta^{13}C$ signature (Tarnocai et al., 2009; Ciais et al., 2012; Schneider et al., 2013; Eggleston et al., 2016; Ganopolski and Brovkin, 2017; Mauritz et al., 2018; Treat et al., 2019). Schneider et al. (2013) and Eggleston et al. (2016) both observed a permanent increase in atmospheric $\delta^{13}C$ during the last glacial cycle, of ~0.4‰, and attributed its cause likely due to soil storage of carbon in peatlands which were buried or frozen as permafrost as the glacial cycle progressed. Ganopolski and Brovkin (2017) incorporated permafrost, peat, and buried carbon into their transient simulations of the last four glacial- interglacial cycles, observing that these features dampened the amplitude of glacial-interglacial variations in terrestrial biosphere carbon stock, in the CLIMBER-2 model. As a crude measure to account for this counter-CO_2 cycle storage of carbon in the terrestrial biosphere and frozen soils, we force the terrestrial biosphere productivity parameter in SCP-M in the range ~+5-10 PgC yr^{-1}, increasing into the LGM (MIS

2), and maintained in the Holocene (MIS 1). We maintain the forcing of the terrestrial biosphere in the Holocene, as the posited effects of buried peat and permafrost storage of carbon on atmospheric CO_2 and $\delta^{13}C$ during the lead-up and into the LGM, were likely not fully reversed after the glacial termination (Tarnocai et al., 2009; Eggleston et al., 2016; Mauritz et al., 2018; Treat et al., 2019), and were partially or wholly replaced by other soil stocks of carbon (e.g. Lindgren et al., 2018). SCP-M calculates net primary productivity (NPP) using this productivity input parameter, as a function of carbon fertilisation (Harman et al., 2011)."

RC: Tundra is not an "inert" carbon pool

AC: we've modified the sentence as per above excerpt to refer to carbon stored in frozen peat, permafrost soils.

RC: and I don't think "permafrost" is a vegetation type

AC: We've modified this sentence as per above excerpt, to remove the reference to permafrost as a vegetation type.

RC: What is "pre-carbon fertilisation"?

AC: This is just the N_{pre} in the equation for NPP from the model documentation, reproduced above. We can refer to this as "undisturbed" (by CO_2) NPP. The equations for NPP takes an input value N_{pre}, which is subsequently varied due to any change in atmospheric CO_2. This is our model representation of CO_2 fertilisation of the terrestrial biosphere.

RC: p8: what is the point of Table 1 if all the values of GOC, AMOC, biology are the same? It would be interesting to mention the PI control values though.

AC: Thanks, we've consolidated Table 1 to show the MIS model-data experiment ranges and the PI control values.

RC: - p10-11: The 'depth issue" should also be discussed in 2.3.1 and 2.3.2.

AC: Re 2.3.1 – there is a much greater coverage of $\delta^{13}C$ and $\Delta^{14}C$ data for the ocean boxes so we have not applied a default weighting for those data in our model-data optimisation. For CO^{2-}_3, a problem presents because there are only 1 or 2 data points in some boxes, and they are clustered near the box boundary, so we end up with unrepresentative data for some boxes for CO^{2-}_3. So, we applied a larger weighting for CO^{2-}_3 data, as discussed in 2.3.2.

4) Discussion:

RC: p20, L. 3-6: It is not what the simulations tell you, but the proxy data!

AC: We've removed this reference to the modelling and replaced with reference to the proxy data shown in Figure 4 (P23, L7).

RC: p21, L. 1-2: This is wrong → you are forcing your model with SST, Sea-ice. . .. so all these factors contribute to the pCO2 decrease. The experiments show that changes in oceanic circulation and SO biological productivity also contribute to that pCO2 de- crease.

AC: We have reworded this sentence to list the full set of changes modelled (P24 L7)

RC: Please take into consideration that G-IG pCO2 changes have been previously successfully simulated with models of intermediate complexity (e.g. e.g. Ganopolski & Brovkin 2017, Menviel et al., 2012) and box models.

AC: We have added a sentence at the start of the discussion to reference these studies (P23, L5) and they are referenced throughput the Discussion.

RC: p21, L. 3-4: I don't understand the meaning

AC: This sentence has been reworded (P24 L6).

RC: p21, L. 7: Might want to check Piotrowski et al., 2008, Yu et al., 2016. (Nat. Geo).

AC: We have picked up the citation of Yu et al. (2016) in reference to AMOC in the MIS 4, a little further down in the manuscript (P29 L28). We have added a reference to Piotrowski et al. (2009) in the same place (P29 L29).

We have also added the Piotrowski et al. (2009) $\delta^{13}C$ data to our dataset and cited it in the manuscript (Table 2).

RC: p21, L. 10 –p22, L. 5: This section really has to be discussed in light of all the work that has been done on the impact of iron fertilisation in the Southern Ocean. Some work on the topic: Watson et al., 2000, Nature; Jaccard et al., 2013, Science; Yamamoto et al., 2019, Climate of the Past;

AC: Text added (P31 L2):

"Our finding of increased biological productivity, while mostly constrained to MIS 2 and MIS 4, and a modest contributor to the overall glacial CO_2 drawdown, corroborates proxy data (e.g. Martinez-Garcia et al., 2014; Lambert et al., 2015; Kohfeld and Chase, 2017) and recent model-data exercises (e.g. Menviel et al., 2016; Muglia et al., 2018; Khatiwala, 2019). Martin (1990) pioneered the "iron hypothesis", which invoked the increased supply of continent-borne dusts to the Southern Ocean in glacial periods. Increased dust supply stimulated more plankton productivity where plankton were bio- limited in nutrients supplied in the dust, such as iron (Martin, 1990). Since then, the iron hypothesis has retained an important place in the debate over glacial-interglacial cycles of CO_2. Watson et al. (2000) took experimental data on the effects of iron supply on plankton productivity in the Southern Ocean (Boyd, 2000) and applied this to a carbon cycle model across glacial- interglacial cycles. Their modelling, informed by the ocean experiment data, suggested that variations in the

Southern Ocean iron supply and plankton productivity could account for large (~40 ppm) swings in atmospheric CO_2, with peak activity in the last glacial cycle at MIS 2 and MIS 4. Debate has continued over the magnitude of the contribution of Southern Ocean biological productivity to the glacial CO_2 drawdown. According to Kohfeld et al. (2005), based on sediment data, the Southern Ocean biological productivity mechanism could account for no more than half of the glacial CO_2 drawdown. Others emphasise that Southern Ocean biological export productivity fluxes may have been weaker in the LGM, in absolute terms, but that with weaker Southern Ocean upwelling, the iron-enhanced productivity contributed to a stronger biological pump of carbon and was a major contributor to the LGM CO_2 drawdown (Jaccard et al., 2013; Martinez-Garcia et al., 2014; Yamamoto et al., 2019). "

RC: p22, L. 18: "sea-ice cover"

AC: Thanks, corrected

RC: p23, L. 1-12: Figure 13 is interesting but care has to be taken here given the large size of the "boxes". This should at least be discussed in light of previous modelling studies on the subject (e.g. Menviel et al., 2015, GBC).

AC: This figure has changed from the original manuscript due to a change in our data method for $\delta^{13}C$, stemming from the other reviewer comments. We are now only using *Cibicides* species $\delta^{13}C$ data, and we re-ran our model-data experiments. There are only slight variations to our model-data results. However, a narrower spread of standard deviations of the $\delta^{13}C$ data necessitates us to change this Figure. We do think it's an important figure that provides some insights into our model, the results in this manuscript and how they might differ from other studies that simply rely on qualitative and simple statistical analysis of proxy data (without models).

Text added P29 L3:

"These observations from Fig. 13 could be exaggerated in SCP-M due to the large size of its ocean boxes and therefore relatively large spread of $\delta^{13}C$ values and standard deviations for each box. In addition, this experiment may reflect idiosyncrasies in the SCP-M model design and its simple parameterisation of ocean circulation and mixing. A finer resolution model may show a greater sensitivity of the ocean box $\delta^{13}C$ to variations in ocean circulation. Menviel et al. (2015) analysed the sensitivity of ocean and atmospheric $\delta^{13}C$ to variations in NADW, AABW and North Pacific Deep Water (NPDW) formation rates, in the context of rapid changes in atmospheric $\delta^{13}C$ and CO_2 observed during the last glacial termination. Their modelling, using the more spatially-detailed LOVECLIM and Bern3D models, showed modest but location-dependent sensitivities of ocean $\delta^{13}C$ to slowing ocean circulation, and particular sensitivity to AABW. These models are much higher resolution and show greater sensitivity of $\delta^{13}C$ to ocean circulation over depth intervals not

differentiated in the SCP-M boxes, but also quite a variation across the LOVECLIM and Bern3D models. However, our simple experiment illustrated in Fig. 13 does highlight the potential for important changes in the ocean during glacial-interglacial periods to go unnoticed, when focussed on one set of ocean proxy data and without validation by modelling."

References

Arneth, A., Sitch, S., and J. Pongratz, e. a.: Historical carbon dioxide emissions caused by land-use changes are possibly larger than assumed, Nature Geoscience, 10„ 79–84, 2017.

Brovkin, V., Claussen, J. B. M., Ganopolski, A., Kubatzki, C., Petoukhov, V., and Andreev, A.: Carbon cycle, vegetation, and climate dynamics in the Holocene: Experiments with the CLIMBER-2 model, Global Biogeochemical Cycles, 16, 1139, doi:10.1029/2001GB001 662, 2002.

Brovkin, V., Ganopolski, A., Archer, D., and Munhoven, G.: Glacial CO2 cycle as a succession of key physical and biogeochemical processes, Climate of the Past, 8, 251–264, 2012.

Ciais, P., Tagliabue, A., Cuntz, M., Bopp, L., Scholze, M., Hoffmann, G., Lourantou, A., Harrison, S. P., Prentice, I. C., Kelley, D. I., Koven, C., and Piao, S. L.: Large inert carbon pool in the terrestrial biosphere during the Last Glacial Maximum, Nature Geoscience, 5, 74–79, 2012.

Collatz, G., Berry, J., and Clark, J.: Effects of climate and atmospheric CO2 partial pressure on the global distribution of C4 grasses: present, past, and future, Oecologia, 114, 441–454, 1998.

Eggleston, S., Schmitt, J., Bereiter, B., Schneider, R., and Fischer, H.: Evolution of the stable carbon isotope composition of atmospheric CO2 over the last glacial cycle, Paleoceanography, 31, 434–452, 2016.

Enting, I. G., Wigley, T. M. L. and Heimann, M. 1994. Future emissions and concentrations of carbon dioxide: Key ocean/atmosphere/land analyses. CSIRO Division of Atmospheric Research Technical Paper No. 31.

Follows, M. J., Ito, T., and Dutkiewicz, S.: On the solution of the carbonate chemistry system in ocean biogeochemistry models, Ocean Modelling, 12, 290–30, 2006.

Francois, L., Godderis, Y., Warnant, P., Ramstein, G., de Noblet, N., and Lorenz, S.: Carbon stocks and isotopic budgets of the terrestrial biosphere at mid-Holocene and last glacial maximum times, Chemical Geology, 159, 163–199, 1999.

Ganopolski, A. and Brovkin, V.: Simulation of climate, ice sheets and CO2 evolution during the last four glacial cycles with an Earth system model of intermediate complexity, Climate of the Past, 13, 1695–1716, 2017.

Ganopolski, A., Calov, R., and Claussen, M.: Simulation of the last glacial cycle with a coupled climate ice-sheet model of intermediate complexity, Climate of the Past, 6, 229–244, 2010.

Harman, I., Trudinger, C., and Raupach, M.: SCCM – the Simple Carbon-Climate Model: Technical Documentation, CAWCR Technical Report 047, CSIRO Centre for Australian Weather and Climate Research, CSIRO Marine and Atmospheric Research, FC Pye Laboratory, GPO Box 3023, Canberra, ACT, 2601, Australia, 2011.

Hoogakker, B. et al.: Terrestrial biosphere changes over the last 120 kyr, Climate of the Past, 12, 51–73, 2016.

Huang, Y., Street-Perrott, F., Metcalfe, S., Brenner, M., Moreland, M., and Freeman, K.: Climate change as the dominant control on glacial-interglacial variations in C3 and C4 plant abundance, Science, 293, 1647–1651, 2001.

Jaccard, S., Hayes, C., Martínez-García, A., an R.F. Anderson, D. H., Sigman, D., and Haug, G.: Two Modes of Change in Southern Ocean Productivity Over the Past Million Years, Science, 339, 1419–1423, 2013.

Jeltsch-Thommes, A., Battaglia, G., Cartapanis, O., Jaccard, S., and Joos, F. J.: Low terrestrial carbon storage at the Last Glacial Maximum: constraints from multi-proxy data, Climate of the Past, 15, 849–879, 2019.

Joos, F., Gerber, S., Prentice, I. C., Otto-Bliesner, B., and Valdes, P.: Transient simulations of Holocene atmospheric carbon dioxide and terrestrial carbon since the Last Glacial Maximum, Global Biogeochemical Cycles, 18, GB2002, doi:10.1029/2003GB002 156, 2004.

Kaplan, J., Prentice, I., Knorr, W., and Valdes, P.: Modeling the dynamics of terrestrial carbon storage since the Last Glacial Maximum, Geophysical Research Letters, 22, 2074, doi:10.1029/2002GL015 230, 2002.

Kicklighter, D. W. et al., A first order analysis of the potential role of CO2 fertilization to affect the global carbon budget: A comparison study of four terrestrial biosphere models, Tellus, Set. B, 51, 343-366, 1999.

Kohler, P. and Fischer, H.: Simulating changes in the terrestrial biosphere during the last glacial/interglacial transition, Global and Planetary Change, 43, 33–55, 2004.

Köhler, P., Fischer, H., and Schmitt, J.: Atmospheric d13CO2 and its relation to pCO2 and deep ocean d13C during the late Pleistocene, Paleoceanography, 25, doi:10.1029/2008PA001 703, 2010.

Kohn, M.: Carbon isotope compositions of terrestrial C3 plants as indicators of (paleo)ecology and (paleo)climate, PNAS, 107, 19 691– 19 695, 2010.

Kohn, M.: Carbon isotope discrimination in C3 land plants is independent of natural variations in pCO2, Geochemical Perspectives Letters, 2, 35–43, 2016.

Lindgren, A., Hugelius, G., and Kuhry, P.: Extensive loss of past permafrost carbon but a net accumulation into present-day soils, Letters to Nature, 560, 219–222, 2018.

Lueker, T. J., Dickson, A. G., and Keeling, C. D.: Ocean pCO2 calculated from dissolved inorganic carbon, alkalinity, and equations for K-1 and K-2: validation based on laboratory measurements of CO2 in gas and seawater at equilibrium, Marine Chemistry, 70, 105–119, 2000.

Mauritz, M., Celis, G., Ebert, C., Hutchings, J., Ledman, J., Natali, S., Pegoraro, E., Salmon, V.,

Schädel, C., Taylor, M., , and Schuur, E.: Using stable carbon isotopes of seasonal ecosystem respiration to determine permafrost carbon loss, Journal of Geophysical Research: Biogeosciences, 124, 46–60, 2018.

Menviel, L. and Joos, F.: Toward explaining the Holocene carbon dioxide and carbon isotope records: Results from transient ocean carbon cycle-climate simulations, Paleoceanography, 27, PA1207, doi:10.1029/2011PA002 224, 2012.

Menviel, L., Joos, J., and Ritz, S.: Simulating atmospheric CO2, 13C and the marine carbon cycle during the Last Glacial-Interglacial cycle: possible role for a deepening of the mean remineralization depth and an increase in the oceanic nutrient inventory, Quaternary Science Reviews, 56, 46–68, 2012.

Menviel, L., Mouchet, A., Meissner, K. J., Joos, F., and England, M. H.: Impact of oceanic circulation changes on atmospheric d13CO2, Global Biogeochemical Cycles, 29, 1944–1961, 2015.

Menviel, L., Yu, J., Joos, F., Mouchet, A., Meissner, K. J., and England, M. H.: Poorly ventilated deep ocean at the Last Glacial Maximum inferred from carbon isotopes: A data-model comparison study, Paleoceanography, 31, 2–17, 2016.

Meyer, R., F. Joos, G. Esser, M. Heimann, G. Hooss, G. Kohlmaier, W. Sauf, R. Voss, and U. Wittenberg. The substitution of high-resolu- tion terrestrial biosphere models and carbon sequestration in response to changing CO2 and climate, Global Biogeochem. Cycles, 13, 785-802, 1999.

O'Neill, C., A. Mc. Hogg, M.J. Ellwood, S. E., and Opdyke, B.: The [simple carbon project] model v1.0, Geosci. Model Dev., 12, 1541–1572, https://doi.org/10.5194/gmd–12–1541–2019, 2019.

Otto, D., Rasse, D., Kaplan, J., Warnant, P., and Francois, L.: Biospheric carbon stocks reconstructed at the Last Glacial Maximum: com- parison between general circulation models using prescribed and computed sea surface temperatures, Global and Planetary Change, 33, 117–138, 2002.

Piotrowski, A., Banakar, V., Scrivner, A., Elderfield, H., Galy, A., and Dennis, A.: Indian Ocean circulation and productivity during the last glacial cycle, Earth and Planetary Science Letters, 285, 179–189, 2009.

Prentice, I. C., Harrison, S. P. & Bartlein, P. J. Global vegetation and terrestrial carbon cycle changes after the last ice age. New Phytologist (2011) 189: 988–998 doi: 10.1111/j.1469-8137.2010.03620.x

Schmitt, J., Schneider, R., Elsig, J., Leuenberger, D., Lourantou, A., Chappellaz, J., Köhler, P., Joos, F., Stocker, T., Leuenberger, M., and Fischer, H.: Carbon Isotope Constraints on the Deglacial CO2 Rise from Ice Cores, Science, 336, 711–714, 2012.

Schneider, R., Schmitt, J., Kohler, P., Joos, F., and Fischer, H.: A reconstruction of atmospheric carbon dioxide and its stable carbon isotopic composition from the

penultimate glacial maximum to the last glacial inception, Climate of the Past, 9, 2507–2523, 2013.

Schubert, B. and Jahren, A.: The effect of atmospheric CO2 concentration on carbon isotope fractionation in C3 land plants, Geochimica et Cosmochimica Acta, 96, 29–43, 2012.

Siegenthaler, U. & F. Joos (1992) Use of a simple model for studying oceanic tracer distributions and the global carbon cycle, Tellus B: Chemical and Physical Meteorology, 44:3, 186-207, DOI: 10.3402/tellusb.v44i3.15441

Strassmann, K. M. and Joos, F.: The Bern Simple Climate Model (BernSCM) v1.0: an extensible and fully documented open-source re-implementation of the Bern reduced-form model for global carbon cycle–climate simulations, Geosci. Model Dev., 11, 1887–1908, https://doi.org/10.5194/gmd-11-1887-2018, 2018.

Tarnocai, C., Canadell, J., Schuur, E., Kuhry, P., Mazhitova, G., and Zimov, S.: Soil organic carbon pools in the northern circumpolar permafrost region, Global Biogeochemical Cycles, 23, GB2023, doi:10.1029/2008GB003 327, 2009.

Treat, C., Kleinen, T., Broothaerts, N., Dalton, A., Dommain, R., Douglas, T., Drexler, J., Finkelstein, S., Grosse, G., Hope, G., Hutchings, J., Jones, M., Kuhry, P., Lacourse, T., Lähteenoja, O., Loisel, J., Notebaert, B., Payne, R., Peteet, D., Sannel, A., Stelling, J., Strauss, J., Swindles, G., Talbot, J., Tarnocai, C., Verstraeten, G., C.J. Williams, Z. X., Yu, Z., Väliranta, M., Hättestrand, M., Alexanderson, H., and Brovkin, V.: Widespread global peatland establishment and persistence over the last 130,000 y, PNAS, 116, 4822–4827, 2019.

van der Sleen, P., P. Groenendijk, M. Vlam, N. P. R. Anten, A. Boom, F. Bongers, T. L. Pons, G. Terburg, and P. A. Zuidema (2015), No growth stimulation of tropical trees by 150 years of CO2 fertilization but water-use efficiency increased, Nat. Geosci., 8(1), 24–28, doi:10.1038/Ngeo2313.

Watson, A., Bakker, D. C. E., Ridgwell, A. J., Boyd, P. W., and Law, C.: Effect of iron supply on Southern Ocean CO2 uptake and implications for glacial atmospheric CO2, Nature, 407, 730–733, 2000.

Yamamoto, A., Abe-Ouchi, A., Ohgaito, R., Ito, A., and Oka, A.: Glacial CO2 decrease and deep-water deoxygenation by iron fertilization from glaciogenic dust, Climate of the Past, 15, 981–996, 2019.

Yu, J., Menviel, L., Jin, Z. D., Thornalley, D., Barker, S., Marino, G., Rohling, E. J., Cai, Y., Zhang, F., Wang, X., Dai, Y., Chen, P., and Broecker, W. S.: Sequestration of carbon in the deep Atlantic during the last glaciation, Nature Geoscience, 9, 319–325, 2016.

Sequential changes in ocean circulation and biological export productivity during the last glacial cycle: a model-data study

Cameron M. O'Neill[1], Andrew McC. Hogg[1,2], Michael J. Ellwood[1], Bradley N. Opdyke[1], and Stephen M. Eggins[1]

[1]Research School of Earth Sciences, Australian National University, Canberra, Australia
[2]ARC Centre of Excellence for Climate Extremes, Australian National University, Canberra, Australia

Correspondence to: Cameron O'Neill (cameron.oneill@anu.edu.au)

Abstract.

We conduct a model-data analysis of the ~~ocean, atmosphere and terrestrial carbon system to understand their effects on~~ marine carbon cycle to understand and quantify the drivers of atmospheric CO_2 during the last glacial cycle. We use a carbon cycle box model "SCP-M", combined with multiple proxy data for the atmosphere and ocean, to test for variations in ocean circulation and ~~biological~~ Southern Ocean biological export productivity across marine isotope stages spanning 130 thousand years ago to the present. The model is constrained by proxy data associated with a range of environmental conditions including sea surface temperature, salinity, ocean volume, ~~sea ice~~ sea-ice cover and shallow water carbonate production. Model parameters for global ocean circulation, Atlantic meridional overturning circulation and Southern Ocean biological export productivity are optimised in each marine isotope stage, against proxy data for atmospheric CO_2, $\delta^{13}C$ and $\Delta^{14}C$ and deep ocean $\delta^{13}C$, $\Delta^{14}C$ and carbonate ion. Our model-data results suggest that global overturning circulation weakened at marine isotope stage 5d, coincident with a ~25 ppm fall in atmospheric CO_2 from the penultimate interglacial level. This change was followed by a further slowdown in Atlantic meridional overturning circulation and enhanced Southern Ocean biological export productivity at marine isotope stage 4 (~-30 ppm). There was also a transient slowdown in Atlantic meridional overturning circulation at MIS 5b. In this model, the last glacial maximum was characterised by relatively weak global ocean and Atlantic meridional overturning circulation, and increased Southern Ocean biological export productivity (~-20 ppm during MIS 2-4). Ocean circulation and Southern Ocean biology rebounded to modern values by the Holocene period. The terrestrial biosphere decreased by ~~500~~ 400 Pg C in the lead up to the last glacial maximum, followed by a period of intense regrowth during the Holocene (~~750~~ 630 Pg C). Slowing ocean circulation, a cooler ocean and, to a lesser extent, shallow carbonate dissolution, contributed ~-75 ppm to atmospheric CO_2 in the ~100 thousand-year lead-up to the last glacial maximum, with a further ~-10 ppm contributed during the glacial maximum. Our model results also suggest that an increase in Southern Ocean biological productivity was one of the ingredients required to achieve the last glacial maximum atmospheric CO_2 level. The incorporation of longer-timescale data into quantitative ocean transport models, provides useful insights into the timing of changes in ocean processes, enhancing our understanding of the last glacial maximum and Holocene carbon cycle transition.

1 Introduction

Large and regular fluctuations in atmospheric CO_2 and ocean proxy signals for carbon isotopes and carbonate ion concentration, over the last 800 kyr, are preserved in ice and marine core records. The most obvious of these fluctuations is the repeated oscillation of atmospheric CO_2 over the range of ~180-280 ppm every ~100 kyr. The magnitude and regularity of these oscillations in atmospheric CO_2, combined with proxy observations for carbon isotopes, point to the quasi-regular transfer of carbon between the main earth reservoirs: the ocean, atmosphere, terrestrial biosphere and marine sediments (Broecker, 1982; Sigman and Boyle, 2000; Toggweiler, 2008; Hogg, 2008; Kohfeld and Ridgewell, 2009; Kohfeld and Chase, 2017). The ocean, given its large size as a carbon store and ongoing exchange of CO_2 with the atmosphere, likely plays the key role in changing atmospheric CO_2 (Broecker, 1982; Knox and McElroy, 1984; Toggweiler and Sarmiento, 1985; Sigman and Boyle, 2000; Kohfeld and Ridgewell, 2009). Ocean-centric hypotheses for variation in atmospheric CO_2 have been examined in great detail for the last glacial maximum (LGM) and Holocene periods, supported by the abundance of paleo data from marine sediment coring and sampling activity ~~(e.g. Sikes et al., 2000; Curry and Oppo, 2005; Kohfeld and Ridgewell, 2009; Oliver et al., 2010; Peterson et al., 2014; Y~~ However, the hypotheses for variation in atmospheric CO_2 across the LGM-Holocene remain under debate ~~(e.g. Kohfeld et al., 2005; Martin~~ ~~Hypotheses include ocean biology (e.g. Martin et al., 1987; Martinez-Garcia et al., 2014)~~(e.g. Kohfeld et al., 2005; Martinez-Garcia et al., Established hypotheses include those emphasising ocean biology (e.g. Martin, 1990; Martinez-Garcia et al., 2014), ocean circulation (e.g. Burke and Robinson, 2012; Menviel et al., 2016; Skinner et al., 2017)~~and composite mechanisms (e.g. Kohfeld and Ridgewell~~ or the aggregate effect of several mechanisms (e.g. Kohfeld and Ridgewell, 2009; Hain et al., 2010; Ferrari et al., 2014; Ganopolski and Br explain the LGM-Holocene carbon cycle transition. Hypotheses for an ocean biological role include the effects of iron fertilisation on biological export productivity (e.g. Martin, 1990; Watson et al., 2000; Martinez-Garcia et al., 2014), the depth of remineralisation of particulate organic carbon (POC) (e.g. Matsumoto, 2007; Kwon et al., 2009; Menviel et al., 2012), changes in the organic carbon:carbonate ("the rain ratio") or carbon:silicate constitution of marine organisms (e.g. Archer and Maier-Reimer, 1994; Harrison, 2000 and increased biological utilisation of exposed shelf-derived nutrients such as phosphorus (e.g. Menviel et al., 2012).

~~Kohfeld and Chase (2017)~~ Several studies have attempted to solve the problem of glacial-interglacial CO_2 by modelling either the last glacial-interglacial cycle in its entirety, or multiple glacial-interglacial cycles (e.g. Ganopolski et al., 2010; Menviel et al., 201 These studies highlight the roles of orbitally-forced Northern Hemisphere ice sheets in the onset of the glacial periods, and important feedbacks from ocean circulation, carbonate chemistry and marine biological productivity throughout the glacial cycle (Ganopolski et al., 2010; Brovkin et al., 2012; Ganopolski and Brovkin, 2017). Menviel et al. (2012) modelled a range of physical and biogechemical mechanisms to deliver the full amplitude of atmospheric CO_2 variation in the last glacial-interglacial cycle, using transient simulations with the Bern3D model. According to Brovkin et al. (2012), a ~50 ppm drop in atmospheric CO_2 early in the last glacial cycle was caused by cooling sea surface temperatures (SST), increased Northern hemisphere ice sheet cover, and expansion of southern-sourced abyssal waters in place of North Atlantic Deep Water (NADW) formation. Ganopolski and Brovkin (2017) modelled the last four glacial cycles with orbital forcing as the singular driver of carbon cycle feedbacks. They described the "carbon stew", a feedback of combined physical and biogeochemical changes in the carbon cycle, to drive the last four glacial-interglacial cycles of atmospheric CO_2.

Kohfeld and Chase (2017) also extended the LGM-Holocene CO_2 debate further into the past, by evaluating proxy data over the period 18-115 thousand years before present (ka), a time that encompasses the gradual fall in atmospheric CO_2 of ~85-90 ppm from the penultimate interglacial period until the last glacial termination. Kohfeld and Chase (2017) identified time periods during which CO_2 decreased, and aligned these with concomitant changes in proxies for ~~sea surface temperature (SST), sea ice~~ SST, sea-ice extent, deep Atlantic Ocean circulation and mixing, and ocean biological productivity. Kohfeld and Chase (2017) observed that the ~100kyr transition to the LGM involved three discrete CO_2 events. Firstly, a drop in atmospheric CO_2 of ~35 ppm at ~115-100 ka (marine isotope stage, or MIS, 5c-5d) was accompanied by lower SST and the expansion of Antarctic ~~sea ice~~ sea-ice cover. A second phase of CO_2 drawdown took place ~72-65 ka (MIS 4-5a), of ~40ppm, and likely resulted from a slowdown in deep ocean circulation (Kohfeld and Chase, 2017). Finally, during the period 40-18 ka (MIS 2-4), atmospheric CO_2 dropped a further 5-10 ppm, which according to Kohfeld and Chase (2017), was the result of enhanced Southern Ocean biological productivity, and continually intensifying deep ocean stratification, including shoaling of North Atlantic Deep Water (NADW) and northward extension of Antarctic Bottom Water (AABW).

In this paper we quantitatively test the Kohfeld and Chase (2017) hypothesis by undertaking model-data experiments in each MIS across the last glacial cycle, and extend their analysis to include Pacific and Indian Ocean modelling and proxy data. We use the SST reconstructions compiled by Kohfeld and Chase (2017) and other glacial cycle proxies presented in that work. We apply a carbon cycle box model (O'Neill et al., 2019), constrained by available atmospheric and oceanic proxy data, to solve for optimal model-data parameter solutions for ocean circulation and biological export productivity. We also present a qualitative analysis of the compiled proxy data, to place the model-data experiment results in context. We thereby further constrain the timing and magnitude of posited CO_2 mechanisms operating during each MIS in the last glacial cycle ~~(e.g. Kohfeld and Ridgewell, 2009; Oliver et al., 2010; Yu et al., 2013; Eggleston et al., 2016; Yu et al., 2016; Kohfeld and Chase, 2017)~~(e This time series analysis complements recent multi-proxy model-data studies of the LGM and Holocene (e.g. Menviel et al., 2016; Kurahashi-Nakamura et al., 2017; Muglia et al., 2018; O'Neill et al., 2019) by testing for changes in the ocean carbon cycle in the lead-up to the LGM, in addition to the LGM-to-Holocene. Our modelling approach differs from other model studies of the last glacial-interglacial cycle (e.g. Ganopolski et al., 2010; Menviel et al., 2012; Brovkin et al., 2012; Ganopolski and Brovkin, 2017), in that we constrain several physical processes from observations (SST, sea level, sea-ice cover, salinity, coral reef fluxes of carbon), then solve for the values of model parameters for ocean circulation and biology based on an optimisation against atmospheric and ocean proxy data.

2 Materials and methods

2.1 Model description

We used the SCP-M carbon cycle box model in our model-data experiment (O'Neill et al., 2019). In summary, SCP-M contains simple parameterisations of the major fluxes in the Earth's surface carbon cycle (Fig. 1). SCP-M incorporates the ocean, atmosphere, terrestrial biosphere and marine/continental sediment carbon reservoirs, weathering and river fluxes, and a number of variables including atmospheric CO_2, DIC, phosphorus, alkalinity, carbon isotopes (^{13}C and ^{14}C) and the carbonate ion. SCP-

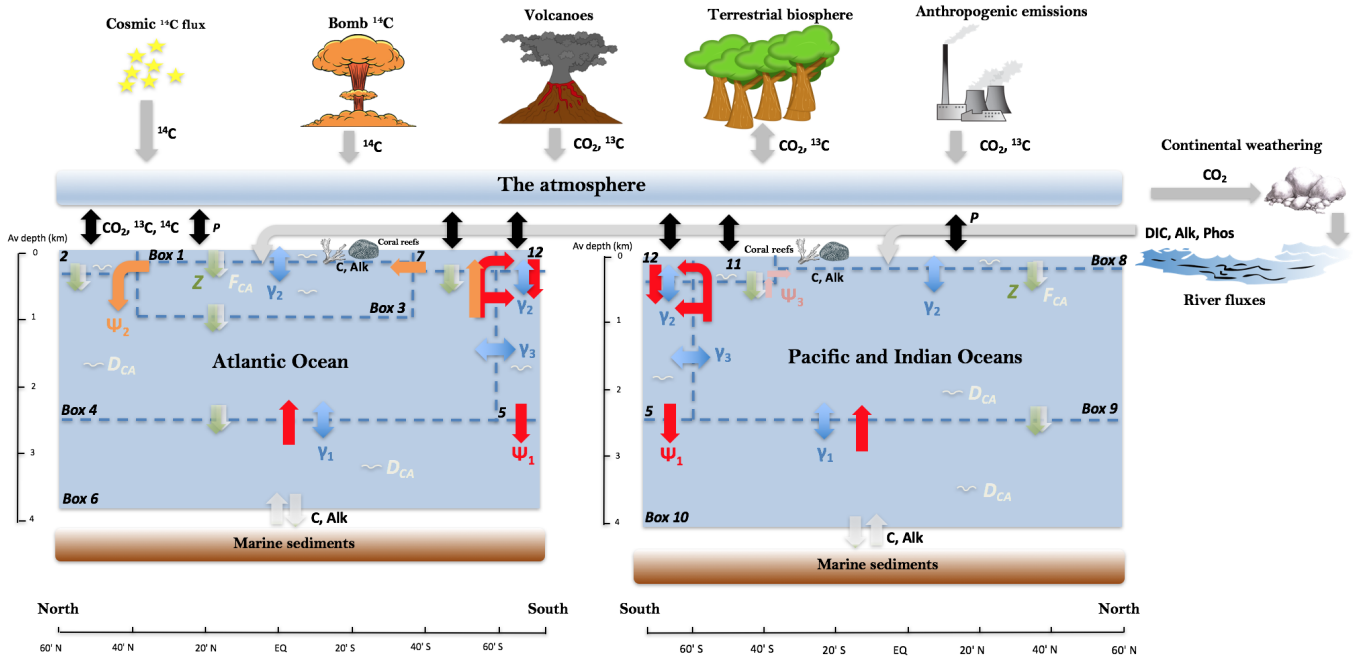

Figure 1. SCP-M configured as a twelve box ocean model-plus atmosphere with marine sediments, continents and the terrestrial biosphere. Exchange of elemental concentrations occur due to fluxes between boxes. Ψ_1 (red arrows) is global overturning circulation (GOC), Ψ_2 (orange arrows) is Atlantic meridional overturning circulation (AMOC). GOC upwelling in both basins is set by default to 50% split between upwelling into the subpolar and polar Southern Ocean. Ψ_3 (pink arrows) is Antarctic intermediate water (AAIW) and Subantarctic mode water (SAMW) formation in the Indian and Pacific Oceans (e.g. Talley, 2013). Blue arrows represent mixing fluxes between boxes. γ_1 and γ_3 parameterise deep-abyssal and Southern Ocean-deep topographically-induced mixing (e.g. De Boer and Hogg, 2014), while γ_2 is low-latitude thermohaline mixing (e.g. Liu et al., 2016). Z (green downward arrows) is the biological pump, F_{CA} (white downward arrows) is the carbonate pump, D_{CA} (white squiggles) is carbonate dissolution and P (black, bidirectional arrows) is the air-sea gas exchange. Key to boxes: Atlantic (box 1: low latitude/tropical surface ocean, 0-100m; box 2: northern surface ocean, 0-250m; box 3: intermediate ocean, 100-1,000m; box 4: deep ocean, 1,000-2,500m; box 6: abyssal ocean, 2,500-3,700m; box 7: subpolar southern surface ocean, 0-250m). Pacific-Indian (box 8: low latitude/tropical surface ocean, 0-100m; box 9: deep ocean, 100-2,500m; box 10: abyssal ocean, 2,500-4,000m; box 11: subpolar southern surface ocean, 0-250m). Southern Ocean (box 5: intermediate-deep; box 12: surface ocean). For a more detailed model description see O'Neill et al. (2019) and updated model code and data at https://doi.org/10.5281/zenodo.3559339.

M ~~'s fast run time and flexibility renders it useful for long term paleo-reconstructions involving large numbers of quantitative experiments and data integration (O'Neill et al., 2019)~~calculates ocean pCO_2 using the equations of Follows et al. (2006), and applies the first and second "dissociation constants" of carbonic acid estimated by Lueker et al. (2000), to calculate HCO_3^- and CO_3^{2-} concentrations, respectively, in units of μmol kg^{-1}, in each ocean box. The model employs partial differential equations for determining the concentration of elements in each box, with each box represented as a row and column in a matrix. In this

paper, we extend SCP-M by incorporating a separate basin for the combined Pacific and Indian Oceans (Fig. 1), following the conceptual model of Talley (2013), to incorporate modelling and proxy data for those regions of the ocean. This version of SCP-M ~~is a simple box model, which incorporates large regions of the ocean as averaged boxes~~ consists of 12 ocean boxes plus the atmosphere and terrestrial biosphere. SCP-M splits out depth regions of the ocean between surface boxes (100-250m average depth), intermediate (1,000m average depth), deep (2,500m average depth) and abyssal depth boxes (3,700 (Atlantic) - 4,000m (Pacific-Indian) average depth). The Southern Ocean is split into two boxes, including a polar box which covers latitude range 60-80 degrees South (box 12 in Fig. 1) and subpolar boxes in the Atlantic (box 7) and Pacific-Indian (box 12) basins, which cover latitude range 40-60 degrees South. See O'Neill et al. (2019) for a discussion of the choice of box depth and latitude dimensions.

The major ocean carbon flux parameters of interest in this model-data study, are global ocean circulation (GOC), Ψ_1, Atlantic meridional overturning circulation (AMOC), Ψ_2, and ocean biological export productivity, Z. The ocean circulation parameters Ψ_1 and ~~parameterised fluxes~~ Ψ_2 are simply prescribed in units of Sverdrups (Sv, 10^6 m^3 s^{-1}). Ocean biological export productivity Z is calculated using the method of Martin et al. (1987). The biological productivity flux, at 100m depth, is attenuated with depth for each box according to the decay rule of Martin et al. (1987). Each sub surface box receives a biological flux of an element at its ceiling depth, and loses a flux at its floor depth (lost to the boxes below it). The difference is the amount of element that is remineralised into each box. The input parameter is the value of export production at 100m depth, in units of mol C m^{-2} yr^{-1} as per Martin et al. (1987). Equation (1) shows the general form of the Martin et al. (1987) equation:

$$F = F_{100}(\frac{d}{100})^b \quad (1)$$

Where F is a flux of carbon in mol C m^{-2} yr^{-1}, F_{100} is an estimate of carbon flux at 100m depth, d is depth in metres and b is a depth scalar. In SCP-M, the Z parameter implements the Martin et al. (1987) equation. Z is an estimate of biological productivity at 100m depth (in mol C m^{-2} yr^{-1}), and coupled with the Martin et al. (1987) depth scalar, controls the amount of organic carbon that sinks from each model surface box to the boxes below.

The terrestrial biosphere is represented in SCP-M as a stock of carbon (a box) that fluxes with the atmosphere, governed by parameters for net primary productivity (NPP) and respiration. In SCP-M, NPP is calculated as a function of carbon fertilisation, which increases NPP as atmospheric CO_2 rises via a simple logarithmic relationship, using the model of Harman et al. (2011). This is a simplified approach, which omits the contribution of temperature and precipitation on NPP. Other, more complex models of the carbon cycle applied to glacial-interglacial cycles have a more detailed treatment of the terrestrial biosphere, including climate dependencies (e.g. Brovkin et al., 2002; Menviel et al., 2012). A number of studies emphasise the role of atmospheric CO_2 as the driver of terrestrial biosphere NPP on glacial-interglacial cycles (Kaplan et al., 2002; Otto et al., 2002; Joos et al., 2 although other studies cast doubt on the relative importance of atmospheric CO_2 versus temperature and precipitation (Francois et al., 1999;

The isotopic fractionation behaviour of the terrestrial biosphere may also vary on glacial-interglacial timeframes. This has been studied for the LGM, Holocene and the present day (e.g. Collatz et al., 1998; Francois et al., 1999; Kaplan et al., 2002; Kohler and Fis

The variation in isotopic fractionation within the terrestrial biosphere reflects changes in the relative proportions of plants with the C3 and C4 photosynthetic pathways, but also strong variations within the same photosynthetic pathways themselves (Francois et al., 1999; Kohn, 2010; Schubert and Jahren, 2012; Kohn, 2016). The drivers for these changes include relative sea level and exposed land surface area (Francois et al., 1999), global tree-line extent (Kohler and Fischer, 2004), atmospheric temperature and CO_2 (Collatz et al., 1998; Francois et al., 1999; Kohler and Fischer, 2004; Kohn, 2010; Schubert and Jahren, 2012), global and localised precipitation and humidity (Huang et al., 2001; Kohn, 2010; Schubert and Jahren, 2012; Kohn, 2016), and also changes in the intercellular CO_2 pressure in the leaves of C3 plants (Francois et al., 1999). Estimated changes in average terrestrial biosphere $\delta^{13}C$ signature between the LGM and the Holocene fall in the range -0.3-1.8‰ (less negative $\delta^{13}C$ signature in the LGM), with further changes estimated from the onset of the Holocene to the pre-industrial, and even greater changes to the present day (due to rising atmospheric CO_2). This feature has been covered in detail within studies that focussed on the terrestrial biosphere between the LGM and Holocene, but less so in modelling and model-data studies of the last glacial-interglacial cycle. Menviel et al. (2016) provided a sensitivity of -0.7+0.5‰ around an average LGM terrestrial biosphere value $\delta^{13}C$ of -23.3‰, based on previous modelling of the LGM-Holocene timeframe by Joos et al. (2004). Another modelling study (Menviel and Joos, 2012), assessed the variation in LGM-Holocene $\delta^{13}C$ of the terrestrial biosphere to be a minor factor and it was omitted. Kohler and Fischer (2004) assessed the changing $\delta^{13}C$ signature of plants between the LGM and Holocene to be a minor factor in setting $\delta^{13}C$ of marine DIC, compared to changes in the absolute size of the terrestrial biosphere across this period. Given the uncertainty and ranges of starting estimates of terrestrial biosphere $\delta^{13}C$, the uncertain LGM-Holocene changes, the large number of potential drivers, and the further uncertainty in extrapolating the posited LGM-Holocene changes back for the preceding 100 kyr, and the modest changes relative to the average $\delta^{13}C$ signature (and the very large range in, for example, present day estimates of C3 plant $\delta^{13}C$ (Kohn, 2010, 2016), we omit this feature with the caveat that there is added uncertainty in our terrestrial biosphere results with respect of the $\delta^{13}C$ signature applied. We apply an average $\delta^{13}C$ signature of -23‰, similar to values assumed by Menviel et al. (2016) and Jeltsch-Thommes et al. (2019) (23.3‰, -24‰ respectively), but more negative than assumed in Brovkin et al. (2002), Kohler and Fischer (2004) and Joos et al. (2004) (-16-(-17)‰). Our aim is not to contribute new findings of the terrestrial biosphere, but to ensure that the simple representation of the terrestrial biosphere in SCP-M provides the appropriate feedbacks to our (exhaustive) glacial-interglacial cycle model-data optimisation experiments, that are in line with published estimates.

Air-sea gas exchange is based on the relative pCO_2 in the surface ocean boxes and the atmosphere, and a parameter that sets its rate in m day^{-1}, P (Fig. 1), with ocean pCO_2 calculated using the method of Follows et al. (2006). SCP-M parameterises shallow water carbonate production, which is linked to the Z parameter by an assumption for the relative proportion of carbonate vs organic matter, known as "the rain ratio" (e.g. Archer and Maier-Reimer, 1994; Ridgwell, 2003). Carbonate dissolution is calculated based on the ocean box or marine surface sediment calcium carbonate concentration versus a depth-dependant saturation concentration (Morse and Berner, 1972; Millero, 1983). Most other carbon cycle processes are parameterised simply, such as volcanic emissions, continental weathering, anthropogenic emissions and cosmic ^{14}C fluxes. The isotopes of carbon are calculated applying various fractionation factors associated with the biological, physical and chemical

fluxes of carbon (see the Supporting Information and O'Neill et al. (2019)). ~~It is an appropriate tool for this study, in which we evaluate many simulations to explore possible parameter combinations, in conjunction with proxy data.~~

We have added a simple representation of shallow water carbonate fluxes of carbon and alkalinity in SCP-M's low latitude surface boxes, to cater for this feature in theories for glacial cycle CO_2 ~~(e.g. Opdyke and Walker, 1992; Ridgwell et al., 2003)~~(e.g. Berger, 1
using:

$$\left[\frac{dC_i}{dt}\right]_{reef} = C_{reef}/V_i \quad (2)$$

Where C_{reef} is the prescribed flux of carbon out of/into the low latitude surface ocean boxes during net reef accumulation/dissolution, in mol C yr^{-1}, and V_i is the volume of the low latitude surface box i. The alkalinity flux associated with reef production/dissolution is simply Eq. 2 multiplied by two (e.g. Sarmiento and Gruber, 2006). ~~The model~~

The major fluxes of carbon are parameterised simply in SCP-M to allow them to be solved by model-data optimisation with respect of atmospheric and ocean proxy data. In this study, the values for GOC, AMOC and biological export productivity at 100m depth, are outputs of the model-data experiments, as they are deduced from a data optimisation routine. Their input values for the experiments are ranges, as described in 2.2.1. SCP-M's fast run time and flexibility renders it useful for long term paleo-reconstructions involving large numbers of quantitative experiments and data integration (O'Neill et al., 2019). SCP-M is a simple box model, which incorporates large regions of the ocean as averaged boxes and parameterised fluxes. It is an appropriate tool for this study, in which we evaluate many tens of thousands of simulations to explore possible parameter combinations, in conjunction with proxy data. The model used for this paper is located at https://doi.org/10.5281/zenodo.3559339.

2.2 Model-data experiment design

We undertook a series of model-data experiments to solve for the values of ocean circulation and biology parameters at each MIS stage during the last glacial cycle (~~130-0~~ 0-130 ka). We targeted these parameters due to their central role in many LGM-Holocene CO_2 hypotheses ~~(e.g. Knox and McElroy, 1984; Toggweiler and Sarmiento, 1985; Martin et al., 1987; Kohfeld and Ridgewell, 2~~
We force SST, salinity, sea volume and ice cover, and reef carbonate production, in each MIS ~~,~~ (Section 2.2.1, Fig. 2), using values sourced from the literature (e.g. Opdyke and Walker, 1992; Key, 2001; Adkins et al., 2002; Ridgwell et al., 2003; Kohfeld and Ridgewell, 2009; Rohling et al., 2009; Wolff et al., 2010; Muscheler et al., 2014; Kohfeld and Chase, 2017). Then, we optimise the model parameters for ~~global overturning circulation (GOC), Atlantic meridional overturning circulation (AMOC)~~ GOC, AMOC and Southern Ocean biological export productivity in each MIS time slice. We chose GOC and AMOC due to the prevalence of varying ocean circulation in many theories for glacial cycles of CO_2 (e.g. Sarmiento and Toggweiler, 1984; Toggweiler, 1999; Kohfeld and Ridgewell, 2009; Burke and Robinson, 2012; Freeman et al., 2016; Menviel et al., 2016; Kohfeld and Chase, 2017; Skinner et al., 2017; Muglia et al., 2018), and its key role in distribution of carbon and other elements in the ocean (Talley, 2013). We chose to vary Southern Ocean biological export productivity due to its long-standing place and debate among theories of atmospheric CO_2 during the LGM and Holocene ~~(e.g. Martin et al., 1987; Knox and McElroy, 1984; Sarmiento and Toggweiler, 1984; Sigman and Boyle, 2000; Anderson et al., 2002; Ko~~

The GOC (Ψ_1), AMOC (Ψ_2) and Southern Ocean biology (Z) parameters are varied over ~59,000 possible combinations at each MIS, a total of ~80,000 simulations across MIS 1-5e. At the end of each experiment batch, the model results are solved for the best fit to the ocean and atmosphere proxy data using a least-squares optimisation, and the parameter values for Ψ_1, Ψ_2 and Z are returned. Our experiment time slices are the MIS of Lisiecki and Raymo (2005), with two minor modifications (see Fig. 2). MIS 2 (14-29 ka) as per Lisiecki and Raymo (2005) straddles the LGM (18-24 ka) and the last glacial termination (15-18 ka), while MIS 1 (0-14 ka) incorporates the Holocene period (0-11.7 ka) and the end of the termination. We are interested in the LGM and Holocene as discrete periods, so our experiment time slice for MIS 2 is truncated at 18 ka, and our MIS 1 simply covers the Holocene, removing overlaps with the glacial termination. ~~For MIS 5, we take the timing for peak glacial and interglacial substages of Lisiecki and Raymo (2005), ±5kyr for MIS 5c-5e, and ±2.5 kyr for MIS 5a-5b.~~ Therefore, our modelling excludes the last glacial termination (~11-18 ka). The glacial termination period was highly transient, with atmospheric CO_2 varying by ~85 ppm in <10 kyr, and large changes in carbon isotopes. Thus it is anticipated that in a model-data reconstruction, model parameters would vary substantially for this period. Our strategy of integrating the model forward to an equilibrium state for each MIS as intervals of discrete climate and CO_2, would be unsuitable when applied to the last glacial termination. Joos et al. (2004), Ganopolski et al. (2010), Menviel et al. (2012), Menviel and Joos (2012), Brovkin et al. (2012) and Ganopolski and Brovkin (2017) provide coverage of the termination period with transient simulations of the last glacial-interglacial cycle, using intermediate complexity models (more complex than our model). For MIS 5, we take the timing for peak glacial and interglacial substages of Lisiecki and Raymo (2005), ±5kyr for MIS 5c-5e, and ±2.5 kyr for MIS 5a-5b.

2.2.1 Model forcings and parameter variations

We took a reconstructed SST time series for the last 130 kyr (Kohfeld and Chase, 2017), mapped these to SCP-M's surface boxes, and averaged the time series across each MIS (Fig. 2(A)). We have extrapolated an Antarctic sea ice cover proxy as shown in Fig. 2(B) (Wolff et al., 2010) to the profiles for sea surface salinity (Fig. 2(C)) and the polar Southern Ocean box air-sea gas exchange parameter (Fig. 2(D). For example, our notional reduction in the strength of the polar Southern Ocean box air-sea gas exchange due to Antarctic sea ice cover (-30%) is linearly (negatively) profiled with the Antarctic sea ice proxy time series of Wolff et al. (2010). We also vary the North Atlantic air-sea gas exchange parameter to the same extent (-30%) to approximate the effects of increased sea ice during MIS 2 and MIS 4 (Hoff et al., 2015; Maffezzoli et al., 2018). Note the polar Southern Ocean box, which is forced with reduced air-sea exchange, is separate from the subpolar Southern Box in which the biological export productivity parameter is varied in the model-data experiment. Our treatment of sea-ice cover is simply as a regulator of air-sea gas exchange in the polar ocean surface boxes. This treatment misses important linkages that likely exist between sea-ice cover and Southern Ocean upwelling, wind-sea surface interactions, NADW formation, deep ocean stratification, nutrient distributions and biological productivity (Morrison and Hogg, 2013; Ferrari et al., 2014; Jansen, 2017; Kohfeld and Chase, 2017; Marzocc
Furthermore, our linear application of the sea-ice proxy data of Wolff et al. (2010) to our air-sea gas exchange parameter may serve to overestimate its effect on the model results early in the glacial period (MIS 5d), and underestimate it during MIS 2-4 (Wolff et al., 2010).

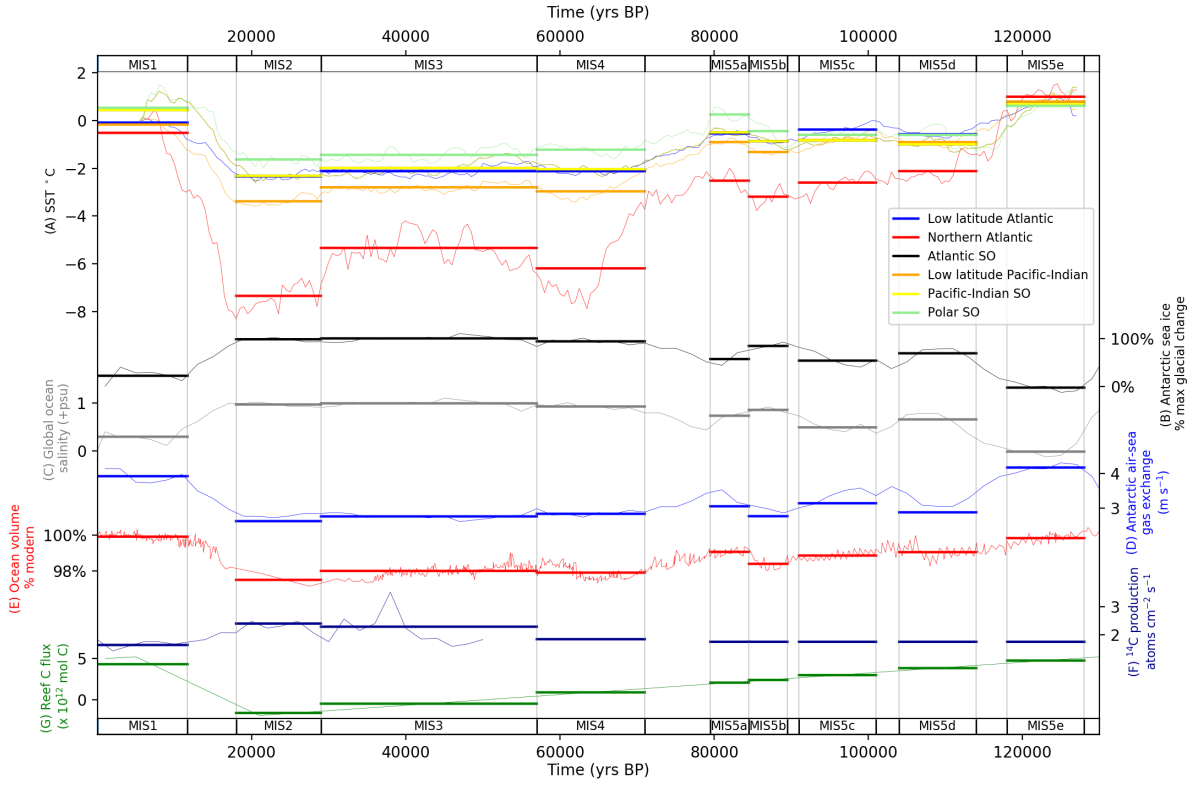

Figure 2. Model forcings for MIS across the last glacial cycle. (A) sea surface temperature reconstruction of (Kohfeld and Chase, 2017), mean values mapped into SCP-M surface boxes (fine lines) and averaged across MIS (bold lines). (B) Proxy for Antarctic ~~sea ice~~ sea-ice extent using ssNa fluxes from the EPICA Dome C ice core (Wolff et al., 2010), used to temporally contour MIS model forcings for (C) salinity (Adkins et al., 2002) and (D) polar Southern Ocean air-sea gas exchange. Global ocean salinity is forced to a glacial maximum of +1 psu (shown in (C)) and the polar Southern Ocean is forced to +2 psu (not shown), as modified from Adkins et al. (2002). Ocean volume (E) forced using global relative sea level reconstruction of Rohling et al. (2009). (F) Atmospheric ^{14}C production rate time series for 0-50 ka of Muscheler et al. (2014) . Long-term values assumed for ~~>~~≫50 ka (Key, 2001). (G) Shallow water carbonate flux of carbon from Ridgwell et al. (2003) profiled across the glacial cycle using a curve from Opdyke and Walker (1992). Fine lines are the time series data and bold lines are the model forcings in each MIS. Data behind the figure are shown in Supplementary Information.

Adkins et al. (2002) reconstructed LGM deep-sea salinity for the Southern, Atlantic and Pacific Oceans. They found increased salinity for the LGM at all locations, across a range of +0.95-2.4 practical salinity units (psu) above modern values, with an average value of +1.5 psu. The most saline LGM waters were in the Southern Ocean (+ 2.4 psu), with Atlantic and Pacific waters ranging +0.95-1.46 psu and an average of +1.2 psu. Adkins et al. (2002) also observed that within a (globally) more saline ocean, lower glacial temperatures would have caused less evaporation during the LGM, a negative feedback on salinity. We chose a global forcing for LGM sea surface salinity of +1 psu for the global ocean, and +2 psu for the polar South-

ern Ocean, relative to the interglacial period. These values conservatively reflect the hypothesis that surface evaporation may have been less in the LGM, hence a lesser magnitude of change in salinity in the surface ocean relative to the deep ocean values estimated by Adkins et al. (2002), and also that the most voluminous parts of the ocean were less saline than the Southern Ocean (Adkins et al., 2002). In our model-data experiments, the estimated glacial change in sea surface salinity (Fig. 2(C)), is also contoured through time with the variation in Antarctic ~~sea ice~~ sea-ice cover of Wolff et al. (2010). Adkins et al. (2002) observed that glacial salinity is a poor predictor of global mean sea level, due to storage of saline waters in ice shelves and groundwater reserves, hence the proxy for Antarctic ~~sea ice~~ sea-ice cover may have a more direct linkage to sea surface salinity than using global sea level, for our purposes of estimating temporal evolution in salinity.

Rohling et al. (2009) reconstructed global relative sea level (RSL) over the past five glacial cycles. According to Rohling et al. (2009), the glacial RSL minimum was ∼-115m at ∼27 ka, immediately prior to the LGM. We perform a simple calculation to reduce ocean depth and volume in SCP-M, in line with the Rohling et al. (2009) time series. In a box model this is only an approximation, given the lack of topographical detail. Varying ocean box volume and surface area, effects the ocean surface area available for in-gassing and de-gassing, and overall ocean capacity to store CO_2, which impacts atmospheric CO_2, $\delta^{13}C$ and $\Delta^{14}C$ ~~(O'Neill et al., 2019)~~(Köhler et al., 2010; O'Neill et al., 2019). Opdyke and Walker (1992) reconstructed coral reef carbonate fluxes of $CaCO_3$ for the last glacial cycle, for the purposes of modelling the "coral reef hypothesis". According to Opdyke and Walker (1992), reef carbon fluxes (out of the ocean) declined through the glacial cycle, with net dissolution in MIS 2 and MIS 3 leading to positive fluxes of carbon and alkalinity into the ocean in those periods. Fluxes of carbon and alkalinity out of the ocean into coral reefs, rebounded from the LGM (MIS 2) into the Holocene (MIS 1), driven by increased sea level and temperature (Kleypas, 1997). Given that Opdyke and Walker (1992) evaluated the possibility for coral reefs to drive the entire glacial-interglacial CO_2 variation, we have taken the more conservative modelling assumption of Ridgwell et al. (2003) of 0.5 x 10^{17} mol C, for postglacial accumulation of coral reefs. We have profiled this value across the glacial cycle accumulation/dissolution curve of Opdyke and Walker (1992), as shown in Fig. 2. We applied the estimated atmospheric production rate for ^{14}C for the last 50 kyr of Muscheler et al. (2014), with a long term average production rate of ∼1.7 atoms cm^{-2} s^{-1} assumed for 50-130 ka (Key, 2001).

The terrestrial biosphere module in SCP-M does not explicitly represent the ~~large glacial "inert" carbon pool in permafrost and tundra (e.g. Ciais et al., 2012). These vegetation types~~ carbon stored in buried peat, permafrost and also cold-climate vegetation that may have expanded its footprint in the glaciation, such as tundra biomes (e.g. Tarnocai et al., 2009; Ciais et al., 2012; Schnei The freezing and burial of organic matter across the glacial cycle may significantly imprint the ~~glacial cycle~~ terrestrial biosphere CO_2 size and $\delta^{13}C$ ~~signatures (Ciais et al., 2012; Hoogakker et al., 2016; Eggleston et al., 2016). Eggleston et al. (2016)~~ signature (Tarnocai et al., 2009; Ciais et al., 2012; Schneider et al., 2013; Eggleston et al., 2016; Ganopolski and Brovkin, 2017; Mauritz et al., 201 Schneider et al. (2013) and Eggleston et al. (2016) both observed a permanent increase in atmospheric $\delta^{13}C$ during the last glacial cycle, of ∼~~0.5~~0.4‰, and attributed its ~~likely cause to glacial growth in tundra~~cause likely due to soil storage of carbon in peatlands which were buried or frozen as permafrost as the glacial cycle progressed. Ganopolski and Brovkin (2017) incorporated permafrost, peat, and buried carbon into their transient simulations of the last four glacial-interglacial cycles, observing that these features dampened the amplitude of glacial-interglacial variations in terrestrial biosphere carbon stock, in the

CLIMBER-2 model. As a crude measure to account for ~~the~~ this counter-CO_2 cycle ~~growth in tundra in the LGM~~storage of carbon in the terrestrial biosphere and frozen soils, we force the ~~'pre-carbon fertilisation' terrestrial biosphere~~ terrestrial biosphere productivity parameter in SCP-M in the range ~~+4-10~~ 5-10 PgC yr^{-1}, increasing into the LGM (MIS 2), and maintained in the Holocene (MIS 1). ~~It is appropriate to~~ We maintain the forcing of the terrestrial biosphere in the Holocene, as the posited effects of ~~tundra growth on atmospheric~~ buried peat and permafrost storage of carbon on atmospheric CO_2 and $\delta^{13}C$ during the lead-up and into the LGM, ~~are not~~ were likely not fully reversed after the ~~termination (Eggleston et al., 2016)~~glacial termination (Tarnocai et al., 2009; Eggleston et al., 2016; Mauritz et al., 2018; Treat et al., 2019), and were partially or wholly replaced by other soil stocks of carbon (e.g. Lindgren et al., 2018). SCP-M calculates net primary productivity (NPP) using this ~~input~~productivity input parameter, as a function of carbon fertilisation (Harman et al., 2011).

~~5~~9,000 model simulations were undertaken across the parameter ranges in Table 1 for each MIS. Parameters were varied simultaneously to allow coverage of all possible combinations of the parameter values within their respective experiment ranges. Within these ranges, values are incremented by 1 Sv for GOC (Ψ_1) and AMOC (Ψ_2), and ~0.5 mol C m^{-2} yr^{-1} for Atlantic Southern Ocean biological export productivity (Z). Each simulation was run for 10 kyr to enable the model to achieve steady state. We show the experiment ranges for the biological export productivity parameter Z for the Atlantic and Pacific-Indian sectors of the Southern Ocean (Table 1). In SCP-M, the Pacific-Indian Southern Ocean biological export productivity parameter (in mol C m^{-2} yr^{-1}) is set by default at a value of ~~40~~70% of the corresponding Atlantic sector Southern Ocean box, to align with natural observations of variations in the Southern Ocean biological export productivity (e.g. Dunne et al., 2005; Sarmiento and Gruber, 2006; Henson et al., 2011; Siegel et al., 2014; DeVries and Weber, 2017). This variation is reflected in the values in Table 1. In the experiments, the values for Z in the Pacific-Indian Southern Ocean surface box scale linearly with the values for the Atlantic Southern Ocean surface box (Table 1). Herein we focus our presentation and discussion of the experiment results for the Z parameter on the Atlantic Southern Ocean, due to it's prominence in glacial cycle hypotheses for increased biological productivity ~~(e.g. Martinez-Garcia et al., 2014; Lambert et al., 2015; Muglia et al., 2018)~~(e.g. Martinez-Garcia et al., 2014; Lambert et al., 20

2.2.2 Optimisation procedure

We performed a least squares optimisation of the model experiment output against MIS data for atmospheric CO_2, atmospheric and deep and abyssal ocean $\Delta^{14}C$ and $\delta^{13}C$, and deep and abyssal ocean carbonate ion proxy, to source the best-fit parameter values for GOC, AMOC and Southern Ocean biological productivity in each time slice - a brute force form of the *gradient descent* method for optimisation (e.g. Strutz, 2016). The equation for least fit applied was:

$$Opt_n = Min \sum_{i,k=1}^{N} (\frac{R_{i,k} - D_{i,k}}{\sigma_{i,k}})^2 \quad (3)$$

where: Opt_n = optimal value of parameters n (e.g. GOC, AMOC and Southern Ocean biological productivity), $R_{i,k}$ = model output for concentration of each element i in box k, $D_{i,k}$ = average data concentration each element i in box k and $\sigma_{i,k}$ =

Table 1. Free-floating parameter ranges in the model-data experiments, for global overturning circulation (Ψ_1), Atlantic meridional overturning circulation (Ψ_2) and Southern Ocean biological export productivity (Z). Parameters were varied simultaneously across these ranges and then optimised against proxy data in each MIS. Also shown are pre-industrial control values for GOC (Talley, 2013), AMOC (Talley, 2013) and Southern Ocean biological export productivity (Dunne et al., 2005; Sarmiento and Gruber, 2006; Henson et al., 2011; Siegel et al., 2014; DeVries and Weber, 2017). The Pacific-Indian Southern Ocean biology parameter is set at a base value of ∼70% Atlantic Southern Ocean box, but scales linearly with the Atlantic Ocean parameter in the experiments. The smaller values for Pacific-Indian Southern Ocean takes account of natural observations of a relatively stronger biological export productivity in the Atlantic sector of the subpolar Southern Ocean (e.g. Dunne et al., 2005; Sarmiento and Gruber, 2006; Henson et al., 2011; Siegel et al., 2014; DeVries and Weber, 2017).

Time period	**GOC (Ψ_1) Sv**	**AMOC (Ψ_2) Sv**	**Southern Atlantic (Pacific-Indian) Ocean biology (Z) mol C m^{-2} yr^{-1}**
PI control values	29	19	3.2 (2.2)
MIS experiment ranges	10-35	10-25	0.5-6.5 (0.3-4.5)

standard deviation of the data for each element *i* in box *k*. The standard deviation performs two roles. It normalises for different unit scales (e.g. ppm, ‰ and μmol kg^{-1}), which allows multiple proxies to be incorporated in the optimisation, and reduces the weighting of a proxy data point with a high standard deviation, and therefore an uncertain value. The weighting by proxy data standard deviation also fulfils the important role of accounting for data variance in the optimised parameter results, such that the effects of data variance are embedded in the optimised parameter values. Where proxy data is unavailable for a box, that data and box combination is automatically omitted from the optimisation routine. The experiment routine returns the model run with the best fit to the data, and the model's parameters and results.

2.3 Data

The model-data optimisation rests on compilations of atmospheric and ocean paleo proxy data. We compile and apply published proxy data for atmospheric CO_2, δ^{13}C and Δ^{14}C and ocean δ^{13}C, Δ^{14}C and carbonate ion. Sources of proxy data are shown in Table 2 and data locations in Fig. 3.

2.3.1 Ocean carbon isotopes

We gathered published marine Δ^{14}C data extending back to ∼40 ka (Table 2). Our dataset incorporates individual records contributed over the last ∼thirty years and supplemented by the recent compilations of Skinner et al. (2017) and Zhao et al. (2017). The data total ∼75 individual location estimates for benthic and planktonic foraminifera, and deep sea corals. We have restricted our efforts to time series which contain independent calendar ages, and therefore corrections for radioactive decay

Table 2. Ocean and atmosphere proxy data sources for the last glacial cycle

Indicator	Time period coverage	Reference
Atmosphere CO_2	0-800 ka	Bereiter et al. (2015)
Atmosphere $\delta^{13}C$	0-155 ka	Eggleston et al. (2016)
Atmosphere $\Delta^{14}C$	0-50 ka	Reimer et al. (2009)
Ocean $\delta^{13}C$	0-120 ka	Oliver et al. (2010), Govin et al. (2009), Piotrowski et al. (2009)
Ocean $\Delta^{14}C$	0-40 ka	Skinner and Shackleton (2004), Marchitto et al. (2007), Barker et al. (2010), Bryan et al. (2010), Skinner et al. (2010), Burke and Robinson (2012), Davies-Walczak et al. (2014), Skinner et al. (2015), Chen et al. (2015), Hines et al. (2015), Sikes et al. (2016), Ronge et al. (2016), Skinner et al. (2017), Zhao et al. (2017)
Ocean carbonate ion proxy	0-705 ka	Yu et al. (2010), Yu et al. (2013), Yu et al. (2014b), Yu et al. (2014a), Broecker et al. (2015), Yu et al. (2016), Qin et al. (2017), Qin et al. (2018), Chalk et al. (2019)

in the time since the sample was deposited (yielding $\Delta^{14}C$). Figure 3 shows the geographic distribution of the $\Delta^{14}C$ data, which is generally concentrated on ocean basin margins. Some regions, such as the central Pacific, southern Indian and polar Southern Ocean, are devoid of data.

Oliver et al. (2010) compiled a global dataset of 240 cores of marine $\delta^{13}C$ data encompassing benthic and planktonic species over the last ~150 kyrs. Oliver et al. (2010) observed considerable uncertainties associated with the broad range of species included, particularly for the planktonic foraminifera. By comparison, Peterson et al. (2014) aggregated marine $\delta^{13}C$ for the LGM and late Holocene periods, as time period averages, exclusively sampling ~~the~~ benthic *C. wuellerstorfi* data, which is a more reliable indicator of marine $\delta^{13}C$ (Oliver et al., 2010; Peterson et al., 2014). To narrow the range of uncertainty, we constrain our use of marine $\delta^{13}C$ data to the deep and abyssal ~~benthic~~ (>2,500m) benthic *Cibicides* species foraminifera samples in the Oliver et al. (2010) dataset, supplemented with *Cibicides* species $\delta^{13}C$ proxy data from Govin et al. (2009) and Piotrowski et al. (2009) (Table 2). Figure 3 shows the $\delta^{13}C$ data locations from Oliver et al. (2010), which are concentrated in the Atlantic Ocean. We mapped and averaged the carbon isotope data into SCP-M's boxes on depth and latitude coordinates (Fig. 1), and averaged for each MIS time slice.

2.3.2 Carbonate ion proxy

We aggregated ocean carbonate ion proxy data from the sources shown in Table 2 and locations in Fig. 3, mapped into SCP-M box coordinates and averaged the data across MIS. The data coverage for CO_3^{2-} is relatively sparse, with <20 individual

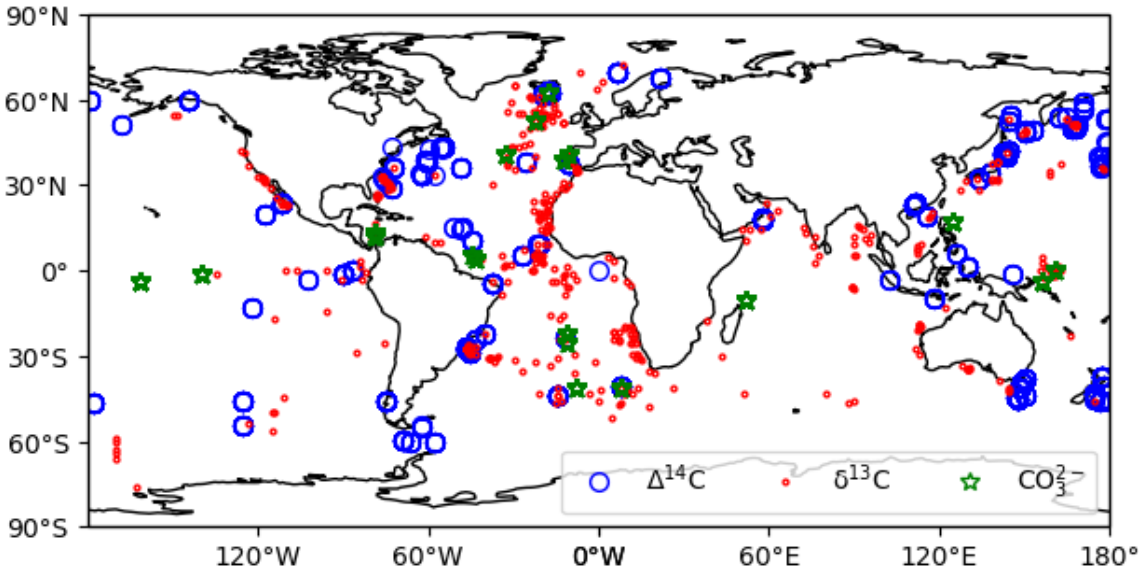

Figure 3. $\Delta^{14}C$, $\delta^{13}C$ and CO_3^{2-} data locations. $\Delta^{14}C$ and CO_3^{2-} data was compiled from published estimates. For $\delta^{13}C$ we take the compilation of Oliver et al. (2010).

site locations across the global ocean. However, the depth and lateral coverage of SCP-M's boxes is large, particularly in the case of the deep ocean boxes, which cover the full lateral extent of the Pacific-Indian and Atlantic oceans, and depth ranges of 100-2,500m (Pacific-Indian) and 250-2,500m (Atlantic). CO_3^{2-} can vary by more than 100 μmol kg^{-1} across the depth range 100-2,500m, and can vary by up to $\sim$200 μmol kg^{-1} in the shallow ocean (e.g. Sarmiento and Gruber, 2006; Yu et al., 2014b, a). Some boxes contain only one core, creating an exceptionally low standard deviation range relative to the other proxies. In other cases, such as the deep Atlantic ocean, the data points are clustered within the 2,000-2,500m depth range, the bottom third of the corresponding SCP-M box. This clustering becomes a problem for the SCP-M box model, which outputs average concentrations over the complete depth range of each box - a drawback of using a large resolution box model to analyse proxy data at a global ocean level. Furthermore, the very low standard deviations associated with the CO_3^{2-} data (data shown in Supplementary Information) cause it to assume a disproportionate weighting in the model-data optimisation, which uses standard deviation for weighting of proxies, relative to ocean $\delta^{13}C$ and $\Delta^{14}C$. The latter proxies often have box standard deviations up to 100% of their mean value, when averaged across a box. This issue is also an artefact of our procedure necessary to normalise the different proxies (each in unique units) in a multi-proxy model-data optimisation, by using the standard deviation as a weighting. To deal with this, we have assigned an arbitrary standard deviation (weighting) of ~~50~~ 15 μmol kg^{-1} to CO_3^{2-} data observations in our model-data optimisations, which acts as a feasible weighting for the processing of the CO_3^{2-} ~~data, and of a similar proportion to other proxy data, in our model-data optimisation~~relative to the other ocean proxy data. This value is ~~approximately half~~ a small fraction of the variation in CO_3^{2-} concentrations observed over the depth range 100-2,500m in the modern ocean (e.g. Key et al., 2004; Yu et al., 2014b).

3 Data analysis

Figure 4 shows the atmospheric data used to constrain the model, ~~mapped~~ averaged into MIS time slices. There are ~~three major~~ many fluctuations and transient changes, but three major sustained reductions in atmospheric CO_2 in the lead-up to the LGM (Fig. 4(A)). A drop of ∼25 ppm in MIS 5d, a further drop of ∼30 ppm in MIS 4, and finally a fall of ∼20 ppm in the period leading up to the LGM (between MIS 2 and 4). These are the three major CO_2 events described in Kohfeld and Chase (2017), and, combined with additional reductions of ∼-10 ppm throughout the period, yield a total drop of ∼-85 ppm from the penultimate interglacial to the LGM. ~~There is also a transient drop~~ Transient changes in atmospheric CO_2 ~~, of 14 ppm, at~~ are littered throughout the glacial cycle, including in MIS 5b~~.~~, MIS 4 and throughout MIS 3. CO_2 increases by ∼85 ppm in the glacial termination and Holocene periods.

Atmospheric $\delta^{13}C$ (Fig. 4(B)) ~~increases~~ increased by ∼~~0.5~~0.4‰ between the penultimate interglacial (MIS 5e) and the Holocene (MIS 1), with temporary falls at MIS 5d, MIS 4 ~~, MIS 3~~ and in the last glacial termination (between MIS 1 and 2). The ~~increase in~~ cause of the observed increase in atmospheric $\delta^{13}C$ across the ~~glacial cycle , is attributed to the growth of tundra at high latitudes (e.g. Ciais et al., 2012; Eggleston et al., 2016; Hoogakker et al., 2016).~~ last glacial-interglacial cycle may be the effect of accumulation and freezing, or burial in glacial sediments, of peat and other soil organic matter at the high latitudes (e.g. Tarnocai et al., 2009; Ciais et al., 2012; Schneider et al., 2013; Eggleston et al., 2016; Ganopolski and Brovkin, 2017; Treat et al., 20 According to Treat et al. (2019), peatlands and other vegetation accumulated carbon in the relatively warm periods, and these carbon stocks were then frozen and/or buried in glacial and other sediments during the cooler periods, throughout the last glacial cycle. This buried or frozen stock of carbon persists to the present day (Tarnocai et al., 2009), although according to Ciais et al. (2012) it may be smaller now than in the LGM. Schneider et al. (2013) evaluated several possible candidates for the rising atmospheric $\delta^{13}C$ pattern across the last glacial-interglacial cycle and could not discount any of (1) changes in the carbon isotope fluxes of carbonate weathering and sedimentation on the seafloor, (2) variations in volcanic outgassing or (3) peat and permafrost build-up throughout the last glacial-interglacial cycle.

The large drop in $\delta^{13}C$ in ~~MIS 4 accompanies a~~ MIS4, reverses in MIS 3 (Fig. 4(B)). This excursion in the ~~∼δ^{13}30 ppm fall in CO~~C pattern likely resulted from sequential changes in SST (cooling), AMOC, Southern Ocean upwelling and marine biological productivity (Eggleston et al., 2016). Eggleston et al. (2016) parsed the atmospheric ~~$_2\delta^{13}$~~. ~~The drop in~~ C signal into its component drivers across MIS 3-5, using a stack of proxy indicators, and highlighted the sequence of events between the end of MIS 5 and beginning of MIS 3, and their cumulative effects to deliver the full change in atmospheric δ^{13}~~C is likely caused by a reduction in the terrestrial biosphere, itself driven by the fall in CO~~C. Our MIS-averaging approach fails to capture the full amplitude of the changes in atmospheric ~~$_2\delta^{13}$~~ ~~(Hoogakker et al., 2016).~~ C during MIS 3-5, and only captures the changes in the mean-MIS value, serving to understate the full extent of transient changes in responsible processes. In addition, the MIS-averaging approach misses the sequential timing of changes in processes within each MIS. These are limitations of our steady-state, MIS-averaging approach. The reduction in atmospheric $\delta^{13}C$ at the last glacial termination, ~~coincident with~~ between MIS 1 and MIS 2, coincident with a large atmospheric CO_2 increase, is attributed to the release of deep-ocean carbon to the atmosphere ~~as a result of~~ resulting from increased ocean circulation and Southern Ocean upwelling (Schmitt

et al., 2012). The subsequent rebound of $\delta^{13}C$ in the termination period and the Holocene is believed to result from terrestrial biosphere regrowth, in response to increased CO_2 and carbon fertilisation (Schmitt et al., 2012; Hoogakker et al., 2016).

The atmospheric $\Delta^{14}C$ data covers the period 0-50ka (Reimer et al., 2009). During this period, $\Delta^{14}C$ is heavily influenced by declining atmospheric ^{14}C production (Broecker and Barker, 2007; Muscheler et al., 2014). In addition, an acceleration in atmospheric $\Delta^{14}C$ decline at the last glacial termination is attributed to the release of old, ^{14}C-depleted waters from the deep ocean, due ~~to increased GOC and/or AMOC (Sikes et al., 2000; Marchitto et al., 2007; Skinner et al., 2010; Burke and Robinson, 2012; Sk~~ to increased Southern Ocean upwelling (e.g. Sikes et al., 2000; Marchitto et al., 2007; Skinner et al., 2010; Burke and Robinson, 2012; Sia

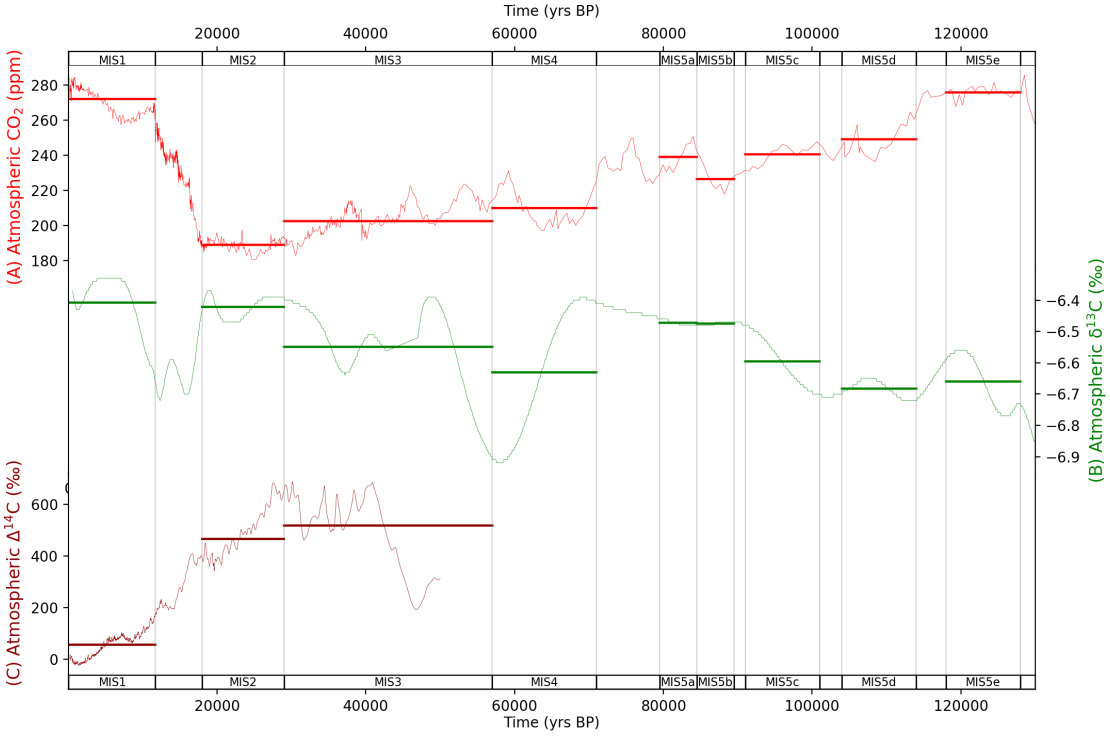

Figure 4. MIS atmosphere data for (A) atmospheric CO_2 (Bereiter et al., 2015), (B) $\delta^{13}C$ (Eggleston et al., 2016) and (C) $\Delta^{14}C$ (Reimer et al., 2009). Data are shown in fine lines, with bold horizontal lines for MIS-sliced data. Natural observations for $\Delta^{14}C$ do not exist beyond $\sim$50 ka due to the radioactive decay of ^{14}C. Data behind the figure are shown in Supplementary Information.

Figure 5 shows deep and abyssal ocean $\delta^{13}C$ data mapped into SCP-M box model space and averaged across MIS. The visual offset between deep and abyssal proxy data values is regularly interpreted as an indicator of the strength of deep ocean circulation and/or mixing, or biological productivity, during the LGM and the Holocene (e.g. Sikes et al., 2000; Curry and Oppo, 2005; Marchitto et al., 2007; Oliver et al., 2010; Skinner et al., 2010; Burke and Robinson, 2012; Yu et al., 2013, 2014a; Skinner et al., 2015, 2017). The deep-abyssal Atlantic $\delta^{13}C$ time series (Fig. 5(A)) exhibits modest widening in the deep and

abyssal offset between MIS 5d and 5e, again at MIS 5b, and a ~~further~~ more substantial widening at MIS 4 and at MIS 2 (the LGM). The widening of the offset during MIS 2-4 is caused primarily by more negative abyssal $\delta^{13}C$ values. The offset is almost closed in MIS 1 (the Holocene). The deep Atlantic $\delta^{13}C$ range itself also widens considerably from MIS 4, and narrows after the LGM. Oliver et al. (2010) and Kohfeld and Chase (2017) interpreted these patterns as the result of weakened deep Atlantic ocean circulation at MIS 4 and at the LGM, rebounding in the post glacial period.

The Pacific-Indian $\delta^{13}C$ data (Fig. 5(B)) shows a drop in abyssal $\delta^{13}C$ and ~~modest~~ widening in the deep-abyssal offset at MIS 5d, continuing ~~to MIS 5a~~throughout the last glacial cycle. Importantly, the more negative abyssal $\delta^{13}C$ values during MIS 5a-5d, occur at the same time that atmospheric $\delta^{13}C$ becomes more positive (Fig. 4(B)), suggesting that the abyssal Pacific-Indian ocean became more isolated from the atmosphere during this period. This is qualitative evidence for slowing ocean circulation or increased biological export productivity in the Pacific-Indian ocean, at that time. This also corresponds with a $\sim$35 ppm fall in CO_2 across MIS 5a-5e (Fig. 4(A)). Abyssal Pacific-Indian $\delta^{13}C$ drops further and most noticeably at MIS 4, and again at the LGM, and then rebounds from the LGM into the Holocene period, as also observed in the Atlantic Ocean $\delta^{13}C$ data. Statistical analysis of the $\delta^{13}C$ data, provided in the Supplementary Information (Fig. S1 and Table S8), supports our qualitative interpretation of the data.

Ocean $\Delta^{14}C$ data covers the MIS 1-3 periods, and the LGM and Holocene in most detail (Fig. 6). We show ocean $\Delta\Delta^{14}C$, which is atmospheric less ocean $\Delta^{14}C$. This calculation is made in attempt to normalise the effects of varying atmospheric ^{14}C production through the glacial cycle (Broecker and Barker, 2007; Muscheler et al., 2014), which imparts a dominant influence on the ocean $\Delta^{14}C$ trajectory. Given the sparse data coverage for MIS 3, we focus our analysis on MIS 1 and 2. The $\Delta\Delta^{14}C$ time series exhibits two key features across the LGM (MIS 2) and Holocene periods (MIS 1). First, there is a narrowing in the spread of values between the shallow and abyssal ocean from the LGM to the Holocene, in both the Atlantic (Fig. 6(A)) and Pacific-Indian (B) basins. Second, all ocean boxes display an increase in $\Delta\Delta^{14}C$ from the LGM to the Holocene, towards equilibrium with the atmosphere. These patterns are believed to represent increased overturning circulation in the Atlantic and Pacific-Indian basins across the LGM-Holocene. Increased ocean overturning brought old, $\Delta^{14}C$-negative water up from the deep and abyssal oceans, mixing with shallow and intermediate waters, and eventually into contact with the atmosphere, where ^{14}C is produced - known as "increased ventilation" (e.g. Sikes et al., 2000; Marchitto et al., 2007; Bryan et al., 2010; Skinner et al., 2010; Burke and Robinson, 2012; Davies-Walczak et al., 2014; Skinner et al., 2014; Hines et al., 2015; Freeman et al., 2016; Sikes et al., 2016; Skinner et al., 2017).

The Atlantic ocean CO_3^{2-} time series shows a similar pattern to $\Delta\Delta^{14}C$ and $\delta^{13}C$, with a wide dispersion of shallow-abyssal and deep-abyssal concentrations at the LGM, which narrows at the Holocene (Fig. ~~6~~7). This pattern has been interpreted as varying strength and/or depth of AMOC and biological productivity in the Atlantic Ocean (e.g. Yu et al., 2013, 2014b, a, 2016). The abyssal Atlantic CO_3^{2-} pattern, which spans the last glacial cycle, is punctuated by two downward excursions (Fig. ~~6~~7). These occur at MIS 4 and MIS 2, corresponding to the second major atmospheric CO_2 drop in the glacial cycle, and the LGM, respectively. The lower CO_3^{2-} value at MIS 4 was interpreted by Yu et al. (2016) as shoaling of AMOC and increased carbon storage in the deep-abyssal Atlantic Ocean. This signal is repeated at the LGM, where further shoaling and slowing AMOC ~~is believed to have~~ contributed to deep oceanic drawdown of CO_2 from the atmosphere (Yu et al., 2013, 2014b, a). There is a

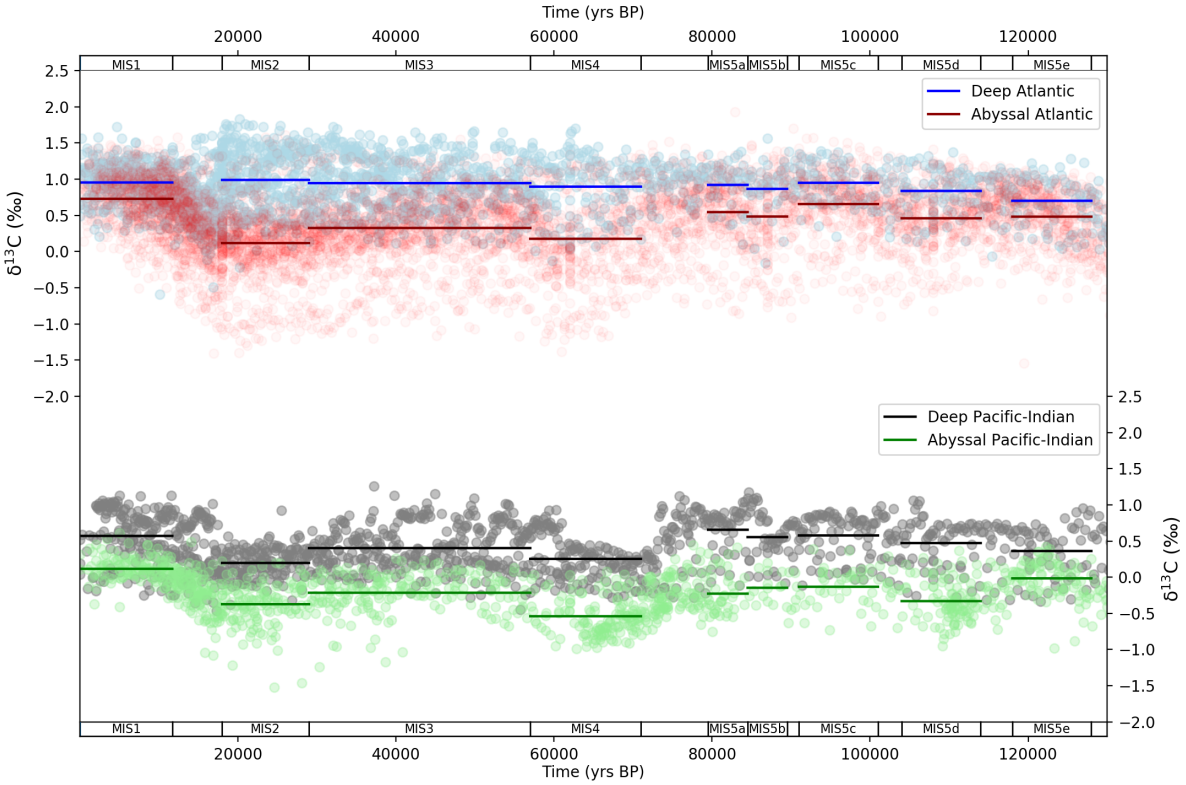

Figure 5. MIS ocean data mapped into SCP-M box model dimensions for δ^{13}C (Oliver et al., 2010). Data (round circles) are mapped into deep (2,500m average depth) and abyssal (3,700 (Atlantic) - 4,000m (Pacific-Indian) average depth) model boxes and averaged across MIS slices (bold lines). ~~Sources listed in Table 2.~~ Data behind the figure are shown in Supplementary Information.

~~transient~~ modest drop in abyssal Atlantic ~~ocean~~ Ocean CO_3^{2-} at MIS 5b (-13 μmol kg^{-1} relative to MIS 5c), which coincides with a ~~transient~~ minor drop in abyssal Atlantic ~~ocean~~ Ocean δ^{13}C (-0.19‰) and atmospheric CO_2 (-14 ppm), ~~suggesting~~ indicating a common link. Menviel et al. (2012) modelled a transient slowdown in North Atlantic overturning circulation for this period, which could explain these features.

The Pacific Ocean is thought to partially buffer the effects of ocean circulation on CO_3^{2-} concentrations (Fig. 7) via changes in shallow (reef) and deep carbonate production and dissolution, and therefore displays less variation across the MIS (Yu et al., 2014b; Qin et al., 2017, 2018). The deep and abyssal Pacific-Indian ocean data shows a ~~persistent~~ gradual trend of increasing CO_3^{2-} through the glacial cycle (Fig. 7), suggesting that it is influenced by variations in shallow and deep sea carbonate production and dissolution, ~~rather than~~ and less by deep ocean circulation (Yu et al., 2014b; Qin et al., 2017, 2018). Notable exceptions are MIS 5d and MIS 4. At MIS 5d, both deep and abyssal Pacific-Indian ocean CO_3^{2-} drop (Fig. 7), aligning with the contemporary drop in abyssal δ^{13}C and atmospheric CO_2 (Fig. 5 and Fig. 5(B)), suggesting a possible common driver,

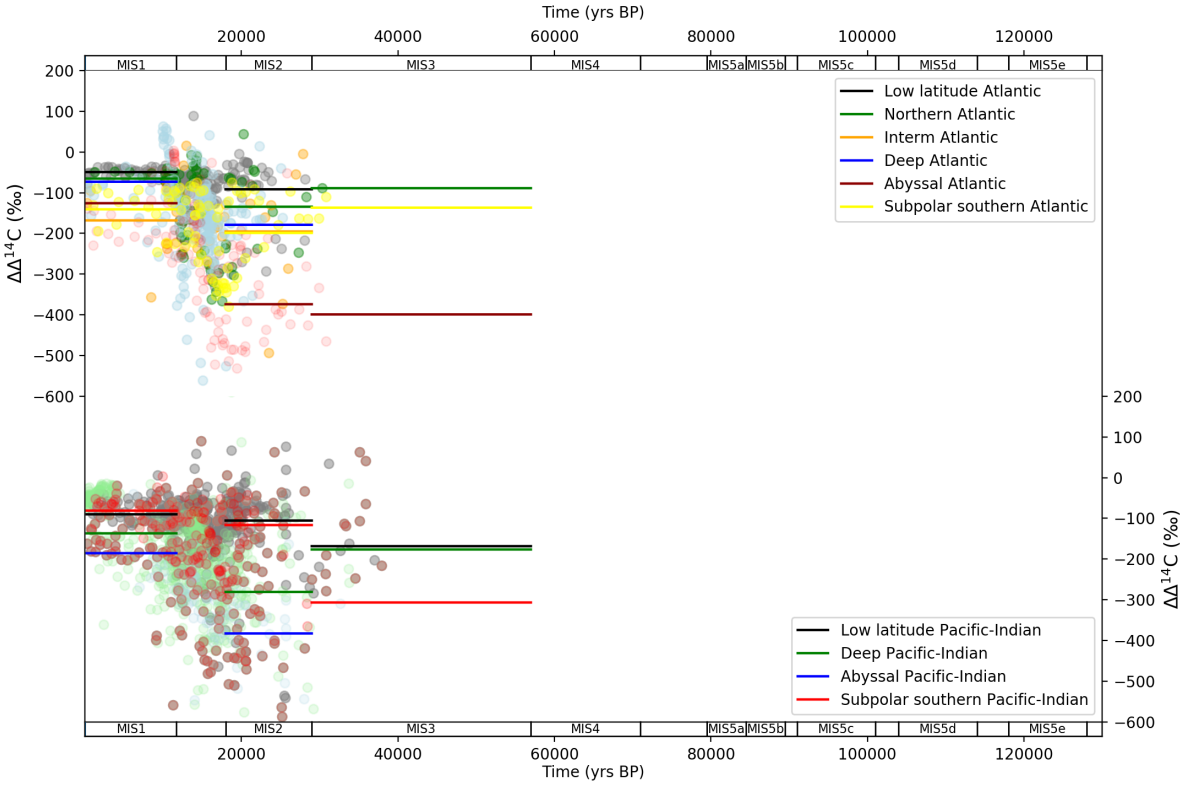

Figure 6. MIS stage ocean data mapped into box model dimensions for $\Delta\Delta^{14}C$. Data (round circles) are mapped into deep (2,500m average depth) and abyssal (3,700 (Atlantic) - 4,000m (Pacific-Indian) average depth) model boxes and averaged across MIS slices (bold lines). ~~Sources listed in Table 2.~~ Natural observations do not exist beyond ~50 ka due to the radioactive decay of ^{14}C. Data behind the figure are shown in Supplementary Information.

and providing additional qualitative evidence for changes in either Pacific-Indian ocean circulation or biology, at this time. At MIS 4, there is a drop in deep Pacific-Indian CO_3^{2-} and a modest widening in the deep-abyssal offset from prior periods, also suggestive of the influence of deep ocean circulation and/or biological export productivity ~~.~~ (Fig. 7). The widest Pacific-Indian deep-abyssal offset CO_3^{2-} is observed in MIS 3, also seen in the $\delta^{13}C$ and $\Delta\Delta^{14}C$ data (Figs 5-7), indicating it is a persistent feature of the proxy records, and suggesting MIS 3 may be the nadir of Pacific-Indian ocean circulation and/or the peak in biological activity in the glacial cycle, and at least that most changes in this part of the ocean took place prior to the LGM.

4 Results

Figure 8 shows the data-optimised values returned from the model-data experiments for GOC, AMOC and Atlantic Southern Ocean biological productivity parameters, in each MIS ("X" symbols). The optimised values take account of data variance, due

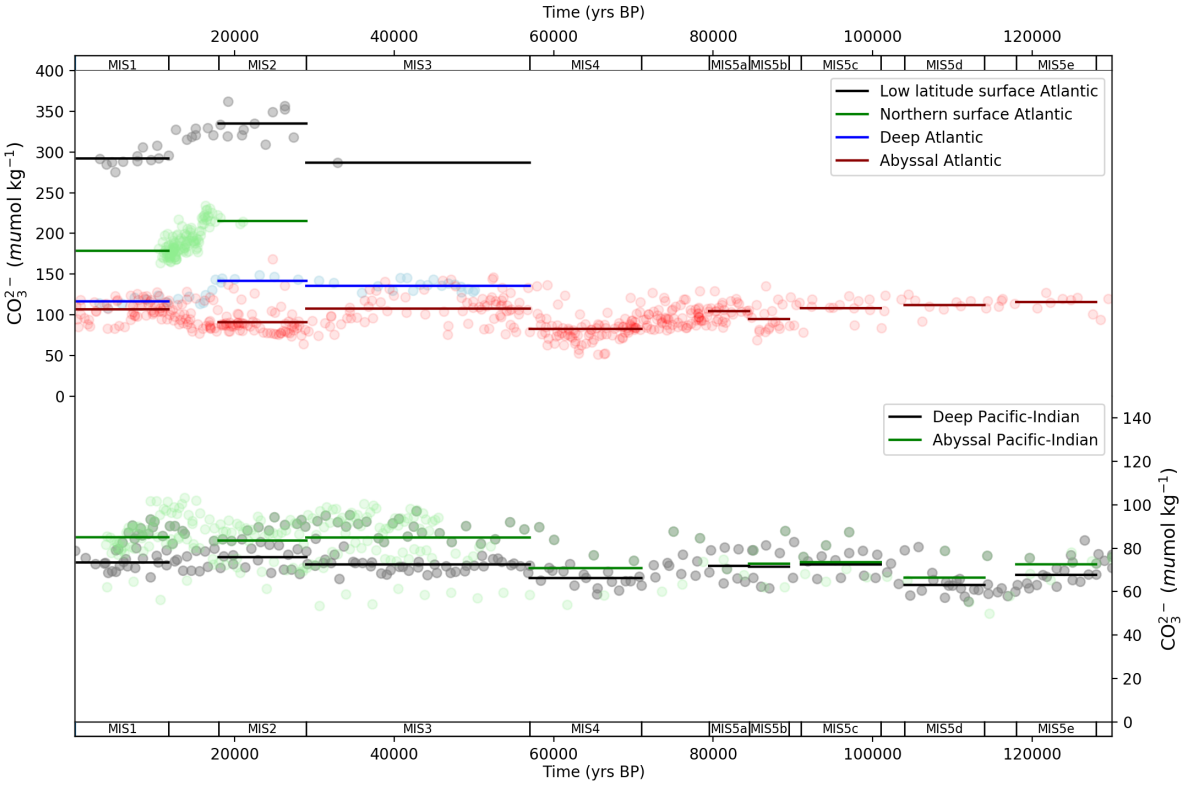

Figure 7. MIS stage ocean data mapped into box model dimensions for carbonate ion proxy. Data (round circles) are mapped into deep Data (round circles) are mapped into deep (2,500m average depth) and abyssal (3,700 (Atlantic) - 4,000m (Pacific-Indian) average depth) model boxes and averaged across MIS slices (bold lines). ~~Sources listed in Table 2~~and abyssal (3,700 (Atlantic) - 4,000m (Pacific-Indian) average depth) model boxes and averaged across MIS slices (bold lines). Data behind the figure are shown in Supplementary Information.

to the weighting of proxy data points by their standard deviation in the model-data optimisation equation (Eq. 3). The full range of model-data experiment results are shown in the Supplementary Information. The GOC parameter (Ψ_1) value falls from ~~28 Sv to 19~~ 29 Sv to 22 Sv between MIS ~~5d and~~ 5e and 5d, with gradual declines during MIS ~~5b-5c, followed by stabilisation at MIS 4-5a, and a further drop at MIS 3. It remains steady at the LGM, just above~~ 5a-5c and a slight acceleration in the rate of decline during MIS 3-4. GOC reaches it's minimum glacial value ~~at~~ (16 Sv) in MIS 3, maintained in MIS 2 (LGM), and then increases to ~~26~~ 31 Sv in MIS 1. AMOC (Ψ_2) ~~remains largely unchanged across the period MIS 5a-5e~~weakens modestly in MIS 5d, with a ~~transient~~ larger drop at MIS 5b ~~. A pronounced fall (-6 Sv) takes place~~ that is partially reversed in MIS 5a. AMOC weakens further in MIS 4, achieving its glacial nadir, which is maintained until the LGM, ~~with a transient increase at MIS 3,~~ before increasing to ~~20~~ 18 Sv in MIS 1. Importantly, Ψ_2 closely follows the abyssal Atlantic $\delta^{13}C$ and CO_3^{2-} data pattern across the glacial cycle, and $\Delta\Delta^{14}C$ from the LGM to the Holocene (Figs 5-7). Ψ_2 remains ~~elevated~~ near it's modelled

penultimate interglacial value (MIS 5e, 18 Sv), during MIS 5c and 5d, ~~increasingly slightly, before dropping temporarily~~ before dropping in MIS 5b (abyssal Atlantic $\delta^{13}C$ and CO_3^{2-}, and atmospheric CO_2, also drop at this point), before partly rebounding at MIS 5a and then falling synchronously with abyssal Atlantic $\delta^{13}C$ and CO_3^{2-} concentrations during MIS ~~4 and MIS 2.~~ 2-4. Southern Ocean biological export productivity (Z) ~~drops early in the glacial cycle (MIS 5d) , then steadily~~ fluctuates around its penultimate interglacial (MIS 5e) value during MIS 5a-5d, then increases during MIS ~~4 and MIS 3.~~ 4. Atlantic (Pacific-Indian) Southern Ocean Z spikes to ~~6 (2~~4.7 (3.3) mol C m^{-2} yr^{-1} in the LGM, then falls to ~~2.3 (0.8~~3.8 (2.6) mol C m^{-2} yr^{-1} in MIS 1. ~~The value for Zat MIS 4 is the same as for MIS 5e, however is 1.3 mol C $m^{-2}yr^{-1}$higher than MIS 1, indicating elevated values for Zin MIS 4 when compared with the Holocene.~~

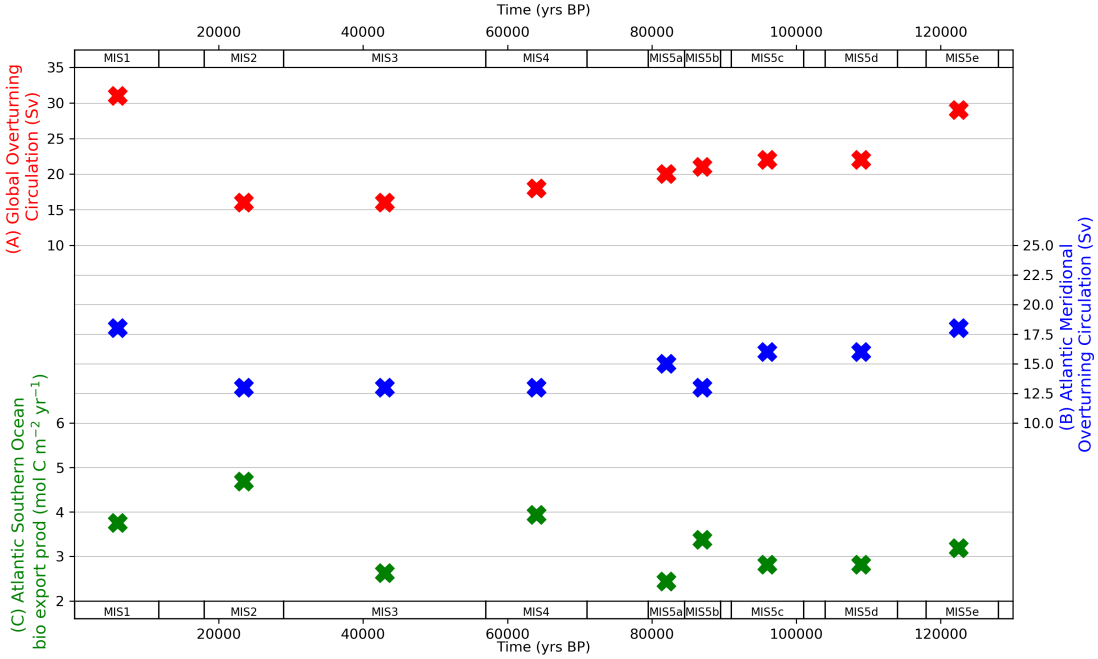

Figure 8. Model-data experiment results for global overturning circulation (A), Atlantic meridional overturning circulation (B) and Atlantic Southern Ocean biological export productivity (C). "X" symbols mark the optimal parameter values returned from the model-data experiments. The optimised values take account of data variance, due to the weighting of proxy data points by their standard deviation in the model-data optimisation equation (Eq. 3). Data for optimised parameter values shown in the figure are contained in Supplementary Information.

Figure 9 show the optimised model-data output for atmospheric CO_2 and ocean carbonate ion proxy, compared with the data observations, in each MIS. This shows how well the model is constrained by the proxy data, and also how well the model-data output of parameter values can explain the proxy data patterns as described in the data analysis section. The model-data results

fall within one standard deviation of atmospheric CO_2 and deep and abyssal CO_3^{2-} data, and mostly on the MIS means, across the MIS periods ~~. The results for the deep~~ (Fig. 9). The modelled abyssal Pacific-Indian ~~box~~ CO_3^{2-} ~~fall near the top of the standard deviation of the data, which we have notionally set at 50 μmol kg^{-1}due to the sparse coverage of data , clustering of the data near the bottom of that box and low standard deviation ranges around the box mean. The combined effect increases the difficulty of data-matching across all of the proxies, hence our adoption of the default standard deviation of 50 μmol kg^{-1}to allow sufficient tolerance and an appropriate weighting of the CO_3^{2-} data, relative to ocean δ^{13}C and Δ^{14}C, in the model-data optimisation. This issue could be resolved with a higher resolution model, more data, and/or a more complex treatment of~~ falls close to the MIS proxy data means across the glacial-interglacial cycle, but misses some of the variations in the data - particularly across MIS 3-4 (Fig. 9). This is a result of the abyssal ocean box carbonate dissolution equations in SCP-M, which effectively buffer any changes in the relative balance of DIC and alkalinity from ocean physical and biological changes, and possibly the large box sizes in SCP-M, which misses some detail for CO_3^{2-} ~~variation with depth~~.

The model-data results show good agreement with atmospheric, deep and abyssal δ^{13}C data throughout the MIS (Fig. 10). The results mostly fall on the mean and all are within the standard deviation for atmospheric δ^{13}C data in the MIS. All results fall within standard deviation for the deep and abyssal Atlantic and Pacific-Indian oceans. The modelled abyssal Pacific-Indian box δ^{13}C underestimates mean MIS δ^{13}C in most MIS time slices, which may reflect a discrepancy between the average depth of the δ^{13}C proxy data and SCP-M abyssal ocean box, or a bias in the model's equations.

~~Fig.~~ Figure 11 shows model-data results for atmospheric Δ^{14}C and ocean $\Delta\Delta^{14}$C compared with data, for MIS 1-3. Model-data results fall within one standard deviation of the data for all observations that were modelled~~.~~, and replicate the dramatic compression in deep-abyssal $\Delta\Delta^{14}$C and ocean-atmosphere offsets, between MIS 2 (LGM) and MIS 1 (the Holocene) as shown in the data (Fig. 11).

Figure 12 shows model-data output for the terrestrial biosphere net primary productivity (NPP) and carbon stock during the ~~glacial~~ last glacial-interglacial cycle. The NPP and carbon stock follow atmospheric CO_2 down in the lead-up to the LGM and rebound from the LGM to the Holocene. This is the effect of carbon fertilisation (Harman et al., 2011; Hoogakker et al., 2016). Notably, there is a distinct drop in NPP at MIS 4, a period where atmospheric CO_2 falls by ~30 ppm (Fig. 4(A)). ~~Falling NPP and persistent respiration of the terrestrial biosphere carbon stock during MIS 4, which releases δ^{13}C-negative carbon to the atmosphere, can explain the steep drop in atmospheric δ^{13}C during the same period (Fig. 4(B)).~~ Hoogakker et al. (2016) provided a reconstruction of NPP through the glacial cycle using pollen data and climate models, shown for comparison in Fig. 12(A). Our model-data results ~~underestimate the Hoogakker et al. (2016) compilation in MIS 5e, but otherwise fall within~~ for NPP periodically fall in the upper and lower end, but within of the range of ~~upper and lower estimates for the other MIS, with slight over-estimation at MIS 5b, 5a, 2 and 1.~~ values from the Hoogakker et al. (2016) compilation, with the exception of MIS 5e where our results likely underestimate those of Hoogakker et al. (2016) (which extend only to 120 ka). We model the terrestrial biosphere carbon stock to fall by ~~500~~ 400 PgC from the penultimate interglacial to the LGM, and increase by ~~750~~ 630 PgC from the LGM to the Holocene (Fig. 12(B)).

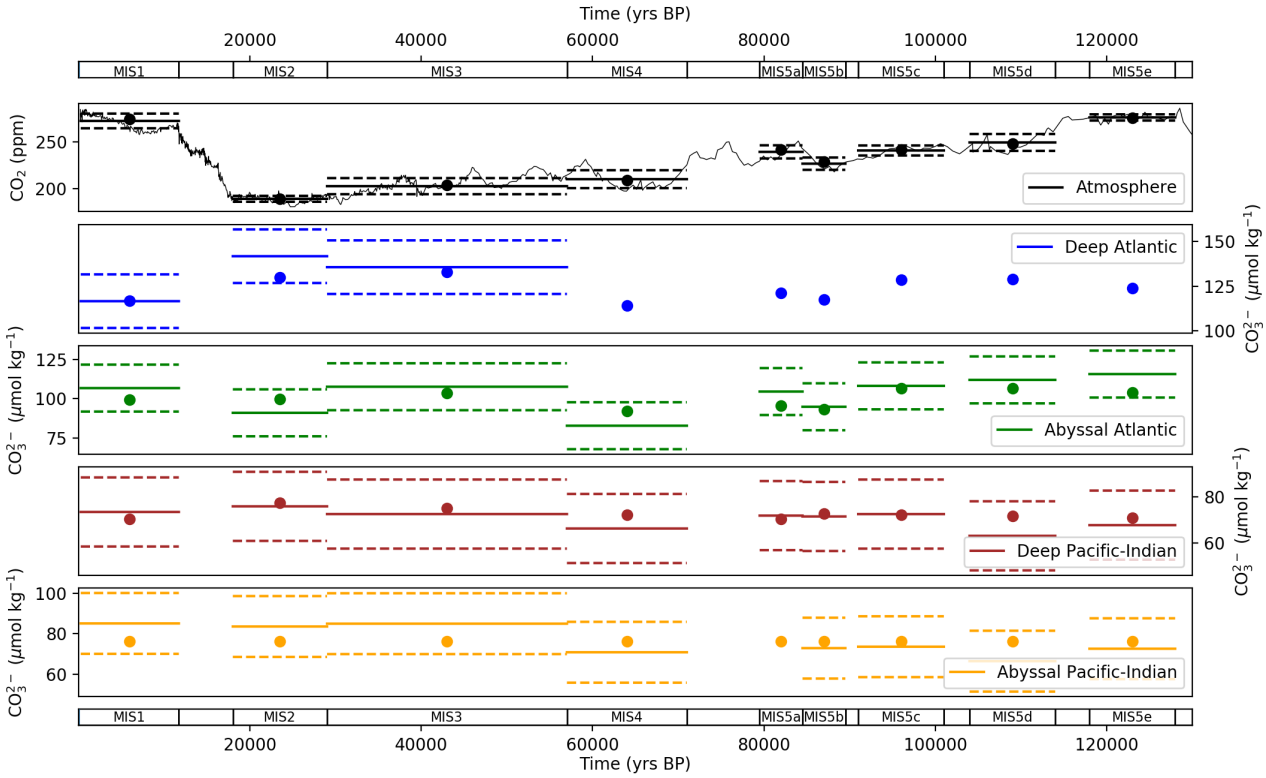

Figure 9. Values returned from the model-data experiment for (A) atmospheric CO_2 and carbonate ion proxy for (B) deep Atlantic (2,500m average depth), (C) abyssal Atlantic (3,700m average depth), (D) deep Pacific-Indian (2,500m average depth) and (E) abyssal Pacific-Indian (4,000m average depth). Model-data experiment results are shown as dots, with mean proxy data shown as solid lines, and one standard deviation range by dashed lines, in each MIS. A default standard deviation of ~~50~~ 15 μmol kg^{-1} is used as discussed in the text. CO_3^{2-} data for the SCP-M deep Atlantic box in (B) does not extend beyond 50 ka.

5 Discussion

5.1 Last ~~glacial~~ glacial-interglacial cycle

~~Model simulations constrained by the available datasuggest that there~~ This study applies a carbon cycle box model to diagnose the values for ocean circulation and Southern Ocean biological export productivity during the last glacial-interglacial cycle, optimised for ocean and atmospheric proxy data. This study continues efforts to simulate the last glacial-interglacial cycle of atmospheric CO_2 (e.g. Ganopolski et al., 2010; Brovkin et al., 2012; Menviel et al., 2012; Ganopolski and Brovkin, 2017), but with a simpler box model and using a non-transient model-data optimisation to estimate parameter values. There were three

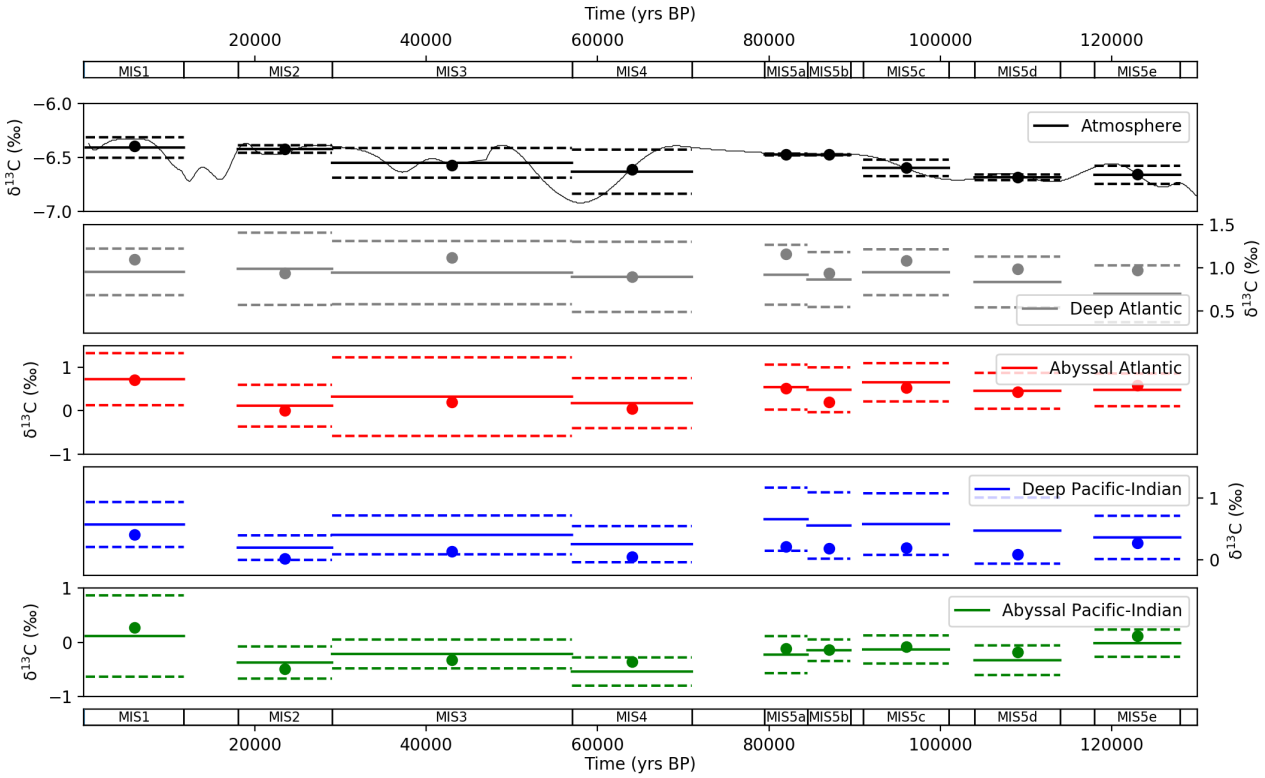

Figure 10. Values returned from the model-data experiment for δ^{13}C for (A) atmosphere, (B) deep Atlantic (2,500m average depth), (C) abyssal Atlantic (3,700m average depth), (D) deep Pacific-Indian (2,500m average depth) and (E) abyssal Pacific-Indian (4,000m average depth). Model-data experiment results are shown as dots, with proxy data mean (solid lines) and one standard deviation (dashed lines) in each MIS.

major episodes in which atmospheric CO_2 fell during the last glacial cycle ~~.~~ (Fig. 4(A)). The first spanned ~~120-100~~ 100-120 ka (MIS 5d-5e), which resulted in a decrease of ~25 ppm. A second drop of ~30ppm occurred during the period ~~80-60~~ 60-80 ka (MIS 4-5a), and finally, a drop of ~20 ppm took place more gradually during the period ~~40-20~~ 20-40 ka in the lead up to the LGM (MIS 2-4). The cumulative effect of these discrete events, combined with other minor changes of ~10 ppm throughout the glacial lead-up, was a drop in atmospheric CO_2 of ~85 ppm below the penultimate interglacial period, ~~130-120~~ 120-130 ka. Our model-data results show that atmospheric CO_2 and other proxy patterns ~~can be delivered solely by variations in~~ are delivered by a host of physical and biogeochemical changes. These changes include weakened GOC, AMOC and strengthened Southern Ocean biological export productivity (Figs. 8,9,10,11)~~. Critically, there were also~~ , and changes in SST, salinity, ocean volume, the terrestrial biosphere, reef carbonates and atmospheric ^{14}C production (Fig. 2).

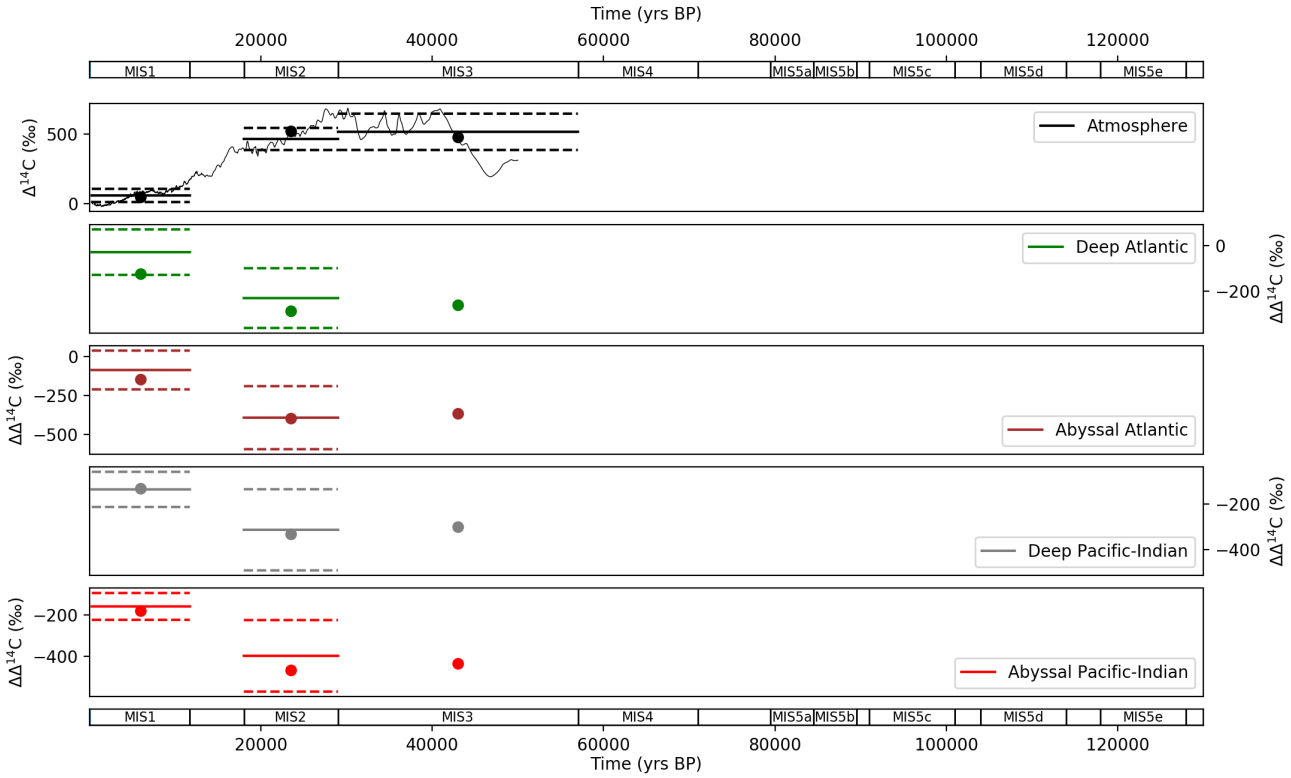

Figure 11. Values returned from the model-data experiment for (A) atmospheric Δ^{14}C and $\Delta\Delta^{14}$C for (B) deep Atlantic (2,500m average depth), (C) abyssal Atlantic (3,700m average depth), (D) deep Pacific-Indian (2,500m average depth) and (E) abyssal Pacific-Indian (4,000m average depth). $\Delta\Delta^{14}$C is atmospheric minus ocean Δ^{14}C, to correct for the varying atmospheric Δ^{14}C signal. Model-data experiment results are shown as dots, with proxy data mean (solid lines) and one standard deviation (dashed lines) in each MIS. Model-data experiment results prior to MIS 4 are omitted, due to the radioactive decay of ^{14}C which precludes natural observations prior to ∼50 ka.

Our model-data results show that ~~the~~ an initial fall in GOC took place at MIS 5d (Fig. 8), as atmospheric CO_2 ~~at MIS 5d was delivered principally by a weakening GOC~~ fell by ∼30 ppm. This was also a time of substantial cooling in SST (Fig. ~~8). GOC continued to weaken until MIS 5a, then stabilised at MIS 4, before weakening in MIS 3.~~ 2(A)). GOC drifted lower until achieving its glacial minimum level in MIS 3 and MIS 2. A pronounced fall in AMOC took place at MIS 4, at the same time that North Atlantic SST cooled dramatically (Fig. 2(A)) and atmospheric CO_2 fell ∼30 ppm. GOC and AMOC were both ~~near their~~ equal to their glacial lows at the LGM, and accompanied by increased Southern Ocean biological export productivity, yielding the LGM minima in atmospheric CO_2 and the final fall in CO_2 during the glacial cycle. We model elevated Southern Ocean biological productivity during MIS ~~2-4~~2 and MIS 4, relative to ~~model results for the Holocene (in~~

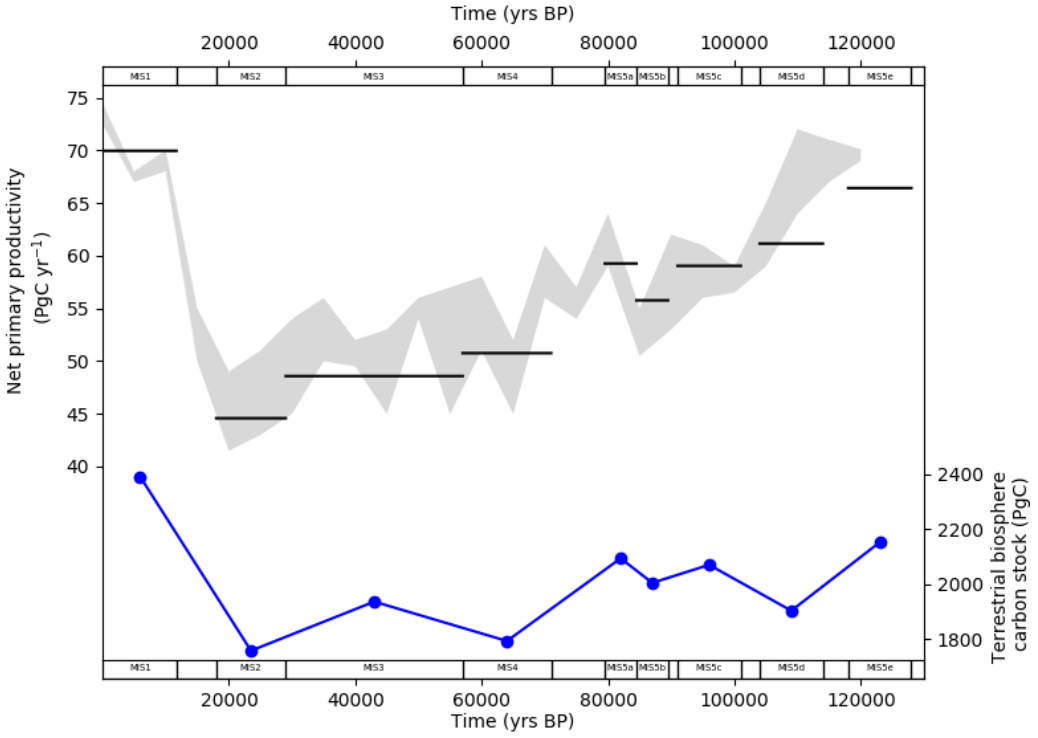

Figure 12. (A) Model-data output for the terrestrial biosphere net primary productivity (NPP) in each MIS time slice (black lines) compared with the range of estimates provided by Hoogakker et al. (2016) (grey area) and (B) model-data output for the terrestrial biosphere carbon stock for each MIS time slice.

~~particular) and for MIS 5a-5d~~interglacial values (MIS 1 and 5e). Importantly, the transition from MIS 3 to MIS 2, which incorporates the LGM and increased Southern Ocean biological productivity, only accounted for an average 13 ppm reduction in CO_2 (Figs. 4, 9). Therefore, our results suggest an increase in Southern Ocean biological productivity during this period was an additional 'kicker' to achieve the LGM CO_2 minima, following prior reductions of ~70 ppm in the lead-up which were delivered mainly by ocean physical processes and SST. The finding of increased biological productivity, while mostly constrained to MIS 2-4, and a modest yet essential contributor to the overall glacial CO_2 drawdown, corroborates proxy data ~~(e.g. Martinez-Garcia et al., 2014; Lambert et al., 2015; Kohfeld and Chase, 2017)~~ (e.g. Martinez-Garcia et al., 2014; Lambert et al., 2015 recent model-data exercises (e.g. Menviel et al., 2016; Muglia et al., 2018). According to Shaffer and Lambert (2018), varying dust fertilisation of the surface ocean, and dust scattering effects on solar radiation, helped to push atmospheric CO_2 into and out of its glacial minima, for example at the LGM and last glacial termination.

~~In~~ For the Holocene, we model GOC and AMOC returning to values similar to the modern ocean estimates of Talley (2013). Our Holocene result for Atlantic (Pacific-Indian) Southern Ocean biological export productivity, of ~~2.3 (0.8~~3.8 (2.6) mol C

m^{-2} yr^{-1} (Fig. 8), falls within modern observations for the Southern Ocean of 0.5-6 mol C m^{-2} yr^{-1} (e.g. Lourey and Trull, 2001; Weeding and Trull, 2004; Ebersbach et al., 2011; Jacquet et al., 2011; Cassar et al., 2015; Arteaga et al., 2019). Our model-data experiment results also reproduce values that fall within one standard deviation of the mean value in each model box, for all of the atmosphere and ocean proxies in each MIS (Figs. 9-11).

Kohfeld and Chase (2017) suggested that sequential falls in atmospheric CO_2 were first the result of temperature, ~~sea ice~~ sea-ice cover and potentially Atlantic Southern Ocean "barrier mechanisms" or shallow stratification, during MIS 5d-5e, and second, followed by falls in deep Atlantic ocean circulation and potentially dust-driven Southern Ocean biological productivity at MIS 4-5a. Finally, a synthesis of those factors with enhanced Southern Ocean biology, delivered the LGM CO_2 minimum. Our model-data results mostly agree with the Kohfeld and Chase (2017) hypothesis for glacial cycle CO_2, however we emphasise the role of ocean circulation in the Pacific and Indian oceans, in addition to the Atlantic Ocean. Stephens and Keeling (2000) proposed that expansive ~~sea-cover~~ sea-ice cover around Antarctica, could deliver LGM CO_2 changes on its own as a result of reduced air-sea gas exchange, or in combination with ice-driven ocean stratification. However, Köhler et al. (2010) demonstrated with a carbon cycle box model that increased sea-ice cover leads to increased atmospheric CO_2, due to less in-gassing of CO_2 into the cold waters surrounding Antarctica. Kohfeld and Ridgewell (2009) reviewed estimates of the effects of *decreased* ~~sea ice~~ sea-ice cover at the last glacial termination and found a best estimate of -5 ppm within a range of -14-0 ppm, which is in the opposite direction to that envisaged by Stephens and Keeling (2000) and Kohfeld and Chase (2017). The modelling work by Stephens and Keeling (2000) was discounted by Kohfeld and Ridgewell (2009), because it assumed nearly all ocean-degassing of CO_2 was confined to the polar Antarctic region, when modern observations suggest the locus of outgassing is in the equatorial ocean (Takahashi et al., 2003). In SCP-M, the effects of polar Southern Ocean sea-ice cover, modelled as a slowing down in air-sea gas exchange in the polar surface box, are modest. This modelling result reflects the offsetting effects of upwelled nutrient- (and carbon) and rich waters (degassing and higher CO_2), against the effects of cooler temperatures and biological export productivity (in-gassing and lower CO_2). ~~Therefore,~~ This finding may reflect our approach to treat polar sea-ice cover simply as a regulator of the rate of air-sea gas exchange in the polar oceans. This approach may neglect other effects of sea-ice cover including as a trigger for changes in Southern Ocean upwelling, NADW formation rates, deep ocean stratification, nutrient distributions and biological productivity (Morrison et al., 2011; Brovkin et al., 2012; Ferrari et al., 2014; Kohfeld and Chase, 2017; Jansen, 2017; Marzocchi and Jansen, 2017). For example, Brovkin et al. (2012) found that in the CLIMBER-2 model, atmospheric CO_2 was more sensitive to sea ice cover when it was linked to weakened vertical diffusivity in the Southern Ocean of tracers such as DIC, thereby reducing outgassing of CO_2.

In addition to cooling SST, increased-sea ice cover and other changes, SCP-M requires other changes in the ocean, to deliver the ~25 ppm fall in CO_2 at MIS 5d-5e, and satisfy the other atmospheric and ocean proxy data. We model a weakening in GOC of ~~9~~ 7 Sv at MIS 5d and ~~minor,~~ further weakening until the LGM, a substantial change outside the Atlantic Basin and underscoring the importance of this feature in any hypothesis for the last glacial cycle or LGM-Holocene (Fig. 8). We note that our simplified representation of slowing GOC, as per Talley (2013), includes features that may be separated out or characterised differently in other models or hypotheses, such as AABW formation rate, Southern Ocean upwelling or shallow

mixing/stratification, Pacific and Indian deepwater formation (PDW/IDW), or northward extension of AABW versus NADW formation of abyssal waters in the Atlantic Ocean (e.g. Menviel et al., 2016; Kohfeld and Chase, 2017).

The period MIS 5d-5e does not feature in many oceanographic theories of glacial inception, largely due to a focus on Atlantic ocean data and a lack of any obvious changes in the Atlantic shallow-deep-abyssal proxy offsets at that period, as observed clearly at MIS 4 and the LGM (e.g. Oliver et al., 2010; Yu et al., 2016; Kohfeld and Chase, 2017). However, Govin et al. (2009) proposed an expansion of AABW across the Southern Ocean at MIS 5d, and weakening of circumpolar deep water upwelling, based on qualitative analysis of deep ocean δ^{13}C from the Atlantic and Indian basins. ~~This proxy evidence supports the model of De Boer and Hogg (2014)~~The proxy evidence of Govin et al. (2009) supports the concept of De Boer and Hogg (2014), that the glacial ocean could have exhibited slower~~formation~~, and at the same time more expansive~~volume, ~~, formation of AABW. Ganopolski et al. (2010) and Brovkin et al. (2012) modelled cooling SST and substitution of North Atlantic Deep Water by denser waters of Antarctic origin, in the abyssal ocean, as the main drivers of falling atmospheric CO_2 at the last glacial inception. Menviel et al. (2012) modelled a transient slowdown in the rate of overturning circulation in the North Atlantic across MIS 5d-5e. Despite these findings, changes in ocean circulation at the last glacial inception are not obvious in Atlantic Ocean δ^{13}C proxy data (Oliver et al., 2010; Kohfeld and Chase, 2017).

To illustrate the plausibility of a slowdown in GOC at the last glacial inception, in the context of deep ocean δ^{13}C proxy data, we show a model experiment testing the sensitivity of atmospheric CO_2 and abyssal ocean δ^{13}C to slowed GOC under MIS 5d and MIS 5e conditions (~~Figure~~ Fig. 13). Shown for comparison are the standard deviation of data values for abyssal ocean δ^{13}C for MIS 5e ~~.~~ (Fig. 13(B)). The experiment shows that slowing GOC from the MIS 5e model-data optimised value of ~~28~~ 29 Sv (e.g. Fig. 8), delivers lower values for CO_2 ~~and~~ (Fig. 13A) and more negative abyssal Pacific-Indian δ^{13}C ~~. However, despite a range of GOC that almost covers the entire glacial~~ (Fig. 13B). However, in the experiment of decreasing GOC, modelled Atmospheric CO_2 ~~drawdown, the abyssal Atlantic~~ crosses the ~25 ppm change of the MIS 5d-5e transition, well before the model's abyssal Pacific-Indian box δ^{13}C ~~result stays within its standard deviation for MIS 5e. Atmospheric CO~~breaches one standard deviation of the abyssal Pacific-Indian δ^{13}C data (Fig. 13(B)). Changes in the deep-abyssal δ^{13}C offsets are also muted (Figure 13(C)) relative to atmospheric CO_2~~falls~~, and particularly for the Atlantic Ocean. The observation is even more obvious when including other ocean changes for the MIS 5d-5e transition, such as SST, in the experiment. When these changes are incorporated (shown as the "x" symbols in Fig. 13(A and B), the atmospheric CO~~~~$_2$ ~~35 ppm (~~change across MIS 5d-5e ~~change is~~ is even more quickly satisfied by the modelled reduction in GOC, while abyssal ocean ~~δ^{13}25 ppm) before~~ C remains near its MIS 5d box average, and well within one standard deviation~~is reached for abyssal~~ . Despite a range of GOC variation that surpasses the MIS 5d-5e CO_2 reduction, the abyssal Atlantic δ^{13}C ~~data, while changes in~~ result hardly varies, a particularly interesting finding. In SCP-M this can be explained by a reduced rate of AABW formation as a part of slowing GOC, leading to relatively greater influence of other Atlantic Ocean processes, such as the deep-abyssal mixing and AMOC, which mixes deep water with a more positive δ^{13}C ~~offsets remain muted (Figure 13(C), particularly for the Atlantic Ocean). Therefore,~~ into the abyssal Atlantic and offsets the effects of slowing GOC. Slowing GOC by itself leads to a more negative abyssal δ^{13}C, as per the Pacific-Indian Basin results. This type of dynamic could help explain why hypothesised or modelled changes in the ocean

at the last glacial inception (e.g. Govin et al., 2009; Menviel et al., 2012; Brovkin et al., 2012) don't show up more obviously in the deep and abyssal Atlantic Ocean δ^{13}C proxy data (Oliver et al., 2010; Kohfeld and Chase, 2017).

These observations from Fig. 13 could be exaggerated in SCP-M due to the large size of its ocean boxes and therefore relatively large spread of δ^{13}C values and standard deviations for each box. In addition, this experiment may reflect idiosyncrasies in the SCP-M model design and its simple parameterisation of ocean circulation and mixing. A finer resolution model may show a greater sensitivity of the ocean box δ^{13}C to variations in ocean circulation. Menviel et al. (2015) analysed the sensitivity of ocean and atmospheric δ^{13}C to variations in NADW, AABW and North Pacific Deep Water (NPDW) formation rates, in the context of rapid changes in atmospheric δ^{13}C and CO_2 observed during the last glacial termination. Their modelling, using the more spatially-detailed LOVECLIM and Bern3D models, showed modest but location-dependent sensitivities of ocean δ^{13}C to slowing ocean circulation, and particular sensitivity to AABW. These models are much higher resolution and show greater sensitivity of δ^{13}C to ocean circulation over depth intervals not differentiated in the SCP-M boxes, but also quite a variation across the LOVECLIM and Bern3D models. However, our simple experiment illustrated in Fig. 13 does highlight the potential for important changes in the ocean during glacial-interglacial periods to go unnoticed, when focussed on one set of ocean proxy data and without validation by modelling.

As shown in Fig. 13, analysing Atlantic Ocean data in isolation, and only qualitatively assessing ocean proxy ~~offsets, more generally, may obscure GOC as a feature~~ data offsets (e.g. solely relying on standard deviations), may obscure features that could have contributed meaningfully to glacial falls in atmospheric CO_2 ~~.~~ (e.g. GOC). According to (Talley, 2013) GOC is a key part of the global ocean carbon cycle, operating in the Atlantic, Pacific and Indian ocean basins. Given it's a global feature, spread across all basins, its global changes may not show up as dramatic changes in proxy data offsets in any particular basin, despite it exerting a strong influence on atmospheric CO_2. A number of authors highlight changes in Δ^{14}C distributions in the Pacific Ocean during the LGM and Holocene, providing qualitative evidence of changes in ocean circulation in this basin and of it being a potential driver for post-glacial increase in atmospheric CO_2 (e.g. Sikes et al., 2000; Marchitto et al., 2007; Stott et al., 2009; Cook and Keigwin, 2015; Skinner et al., 2015; Ronge et al., 2016; Skinner et al., 2017). Ocean Δ^{14}C values are particularly sensitive to ocean circulation rates (Broecker et al., 1980). However, Δ^{14}C proxy records in periods prior to the LGM and Holocene are sparse, because they can only extend to ~50 ka due to their radioactive decay in nature, therefore cannot be applied to the glacial inception period.

There is qualitative multi-proxy evidence for a slowdown or shoaling of AMOC at MIS 4. Kohfeld and Chase (2017) evaluated Atlantic basin δ^{13}C data and surmised that Atlantic deep ocean circulation slowed or shoaled at MIS ~~4, and~~ 4. Yu et al. (2016) and Chalk et al. (2019) came to similar conclusions from analysis of carbonate proxy records. Piotrowski et al. (2009) further suggested a reduced proportion of AMOC-sourced waters in the deep Indian Ocean at MIS 4, as deduced from Indian Ocean δ^{13}C data. Our model-data results corroborate these findings, with a pronounced weakening in AMOC at MIS ~~4, but we~~ 4. SCP-M does not take explicit account of AMOC shoaling due to it's rigid box boundaries, and therefore the change in proxy data across MIS 4-5a is resolved as weakening AMOC, which could understate the importance of this event. We also model a ~~minor, transient~~ drop in AMOC at MIS 5b which replicates abyssal Atlantic δ^{13}C and CO_3^{2-} observations (Fig. 5 and Fig. ~~5~~7), and also accompanies a ~~temporary~~ transient fall in atmospheric CO_2 of 14 ppm at that period (Fig. 4). ~~SCP-M does not take~~

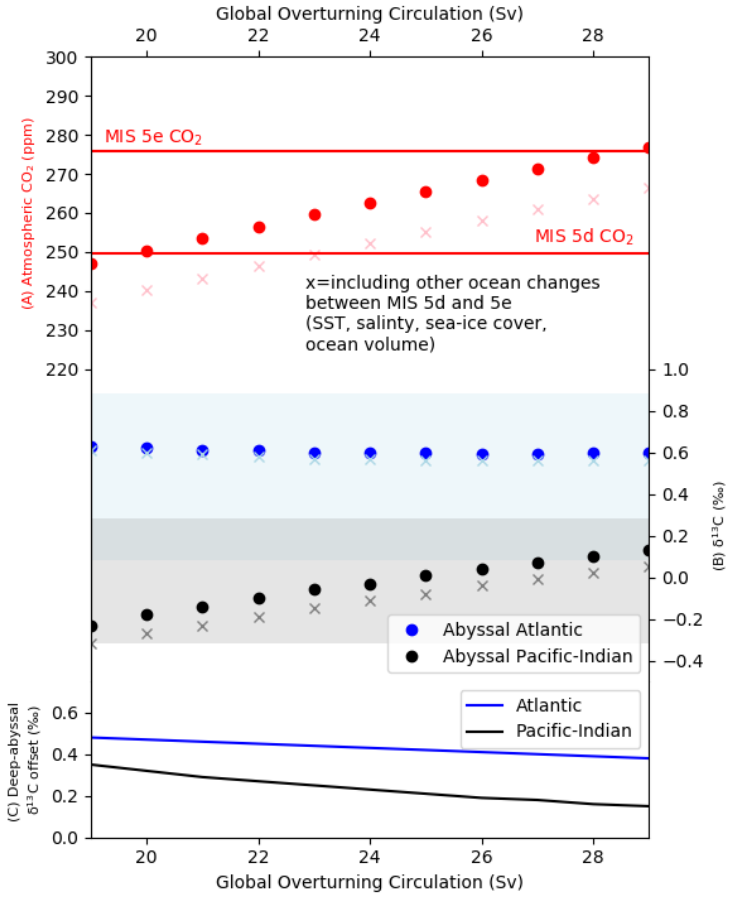

Figure 13. Sensitivity of atmospheric CO_2 and ocean $\delta^{13}C$ to a downward variation in global ocean circulation parameter Ψ_1 in MIS 5e in SCP-M. x-axis shows the range of variation in Ψ_1 in Sv and the y-axes show the model results for (A) atmospheric CO_2 and (B) abyssal ocean $\delta^{13}C$ in each basin. Shaded areas are the $\pm$ standard deviations for abyssal $\delta^{13}C$ in MIS 5e. (C) shows the deep-abyssal $\delta^{13}C$ offset for each basin. Atmospheric CO_2 in MIS 5d and 5e is shown for reference. ~~All~~ The "x" symbols in (A) and (B) show the same experiment including other ~~model settings per~~ changes in the ocean across MIS ~~5e~~5d-5e: SST, salinity, sea-ice cover, ocean volume and coral reef carbonate production. Southern Ocean biological export productivity is not varied in this experiment.

~~account of AMOC shoaling due to it's rigid box boundaries, and therefore the change in proxy data across MIS 4-5a is resolved as weakening AMOC, which could understate the importance of this event~~Menviel et al. (2012) modelled a transient, but more dramatic decline in the rate of overturning circulation in the Atlantic Ocean at MIS 5b, and a more protracted but similarly large decline during MIS 4 (also modelled by Ganopolski et al. (2010)), in addition to a deepening in the remineralisation depth of organic carbon.

Our model-data results indicate a role for increased Southern Ocean biological export productivity in achieving glacial troughs in atmospheric CO_2 in MIS 4 and MIS 2. Our finding of increased biological productivity, while mostly constrained to MIS 2 and MIS 4, and a modest contributor to the overall glacial CO_2 drawdown, aligns with proxy data for increased iron-rich continental dust supply to the Southern Ocean in these periods (e.g. Martinez-Garcia et al., 2014; Lambert et al., 2015; Kohfeld and Chase, recent model-data exercises (e.g. Menviel et al., 2016; Muglia et al., 2018; Khatiwala et al., 2019). Martin (1990) pioneered the "iron hypothesis", which invoked the increased supply of continent-borne dusts to the Southern Ocean in glacial periods. Increased dust supply stimulated more plankton productivity where plankton were bio-limited in nutrients supplied in the dust, such as iron (Martin, 1990). Since then, the iron hypothesis has retained an important place in the debate over glacial-interglacial cycles of CO_2. Watson et al. (2000) took experimental data on the effects of iron supply on plankton productivity in the Southern Ocean (Boyd, 2000) and applied this to a carbon cycle model across glacial-interglacial cycles. Their modelling, informed by the ocean experiment data, suggested that variations in the Southern Ocean iron supply and plankton productivity could account for large (~40 ppm) swings in atmospheric CO_2, with peak activity in the last glacial cycle at MIS 2 and MIS 4. Debate has continued over the magnitude of the contribution of Southern Ocean biological productivity to the glacial CO_2 drawdown. According to Kohfeld et al. (2005), based on sediment data, the Southern Ocean biological productivity mechanism could account for no more than half of the glacial CO_2 drawdown. Others emphasise that Southern Ocean biological export productivity fluxes may have been weaker in the LGM, in absolute terms, but that with weaker Southern Ocean upwelling, the iron-enhanced productivity contributed to a stronger biological pump of carbon and was a major contributor to the LGM CO_2 drawdown (Jaccard et al., 2013; Martinez-Garcia et al., 2014; Yamamoto et al., 2019).

Figure 14 shows the contribution to the glacial drawdown in atmospheric CO_2 by each mechanism we modelled, relative to the penultimate interglacial period (MIS 5e), in SCP-M. Our model-data study finds that approximately half of the glacial atmospheric CO_2 drawdown is contributed by weakened ocean circulation (GOC and AMOC), with the other half contributed by a combination of cooler SST, increased Southern Ocean biological export productivity, varying coral reef carbonate production and dissolution, and increased sea-ice cover. Weakened GOC delivers the highest contribution to falling CO_2, followed by cooler SST, weakened AMOC and stronger Southern Ocean biological export productivity. Lower SST leads to modest reductions in CO_2 early in the glacial cycle, increasing as the ocean cools further in MIS 4, and is an important contributor to decreased CO_2 in the LGM (Kohfeld and Chase, 2017). Southern Ocean biological export productivity ~~weakens initially, from MIS 5e to 5d, then strengthens relative to MIS 5a-5d,~~ strengthens at MIS 4, and contributes ~~-~12 ppm during~~ a peak of -10 ppm by MIS 2 (LGM). Other parameters contribute minor increases in CO_2 (salinity, polar ~~sea ice~~sea-ice, ocean volume) and decreases (coral reefs) during the cycle. Our estimate for coral reefs, of ~~-7 -~8 ppm CO_2, is at the lower end of the range of 6-20 ppm summarised in Kohfeld and Ridgewell (2009), suggesting that our simple parameterisation of the coral reef carbon and alkalinity fluxes could underestimate its effect, likely due to the assumed fast mixing rates of reef carbon and alkalinity into the surface boxes in SCP-M. Ridgwell et al. (2003) modelled +20 ppm CO_2 from coral reef accumulation in the Holocene period, noting a high sensitivity of their model to coral reef accumulation rates.

These attributions in Fig. 14 include the effects of feedbacks in the carbon cycle, such as carbonate compensation in the ocean, and the terrestrial biosphere - which responds to declining atmospheric CO_2. The terrestrial biosphere is discussed in

more detail below. It is likely that our model-data results underestimate the contribution of AMOC, which is hypothesised to slow and/or shoal during the period MIS 2-4 (e.g. Menviel et al., 2012; Brovkin et al., 2012; Yu et al., 2016; Eggleston et al., 2016; Kohfeld Our model does not explicitly resolve shoaling, other than a linear-positive linkage between the AMOC circulation parameter and a deep-abyssal Atlantic box mixing term (less mixing between the deep and abyssal Atlantic boxes as AMOC slows), and therefore may serve to miss additional parts of the AMOC mechanism which could contribute to greater atmospheric CO_2 drawdown in Fig. 14. The contribution of the model parameters to the glacial atmospheric CO_2 drawdown shown in Fig. 14, incorporate the effects of various feedbacks in the model such as the terrestrial biosphere, continental weathering, and calcium carbonate compensation. Shown for comparison on the right axis of Fig. 14 is the impact on atmospheric CO_2 from the contraction of the terrestrial biosphere through the glacial cycle from MIS 5e. The effects are similar yet modestly higher than Ganopolski and Brovkin (2017), reflecting the larger change in the terrestrial biosphere carbon stock in the lead up to the LGM from MIS 5e, from this study (-400 Pg C (and ~+630 Pg C from MIS 2 to MIS 1)), compared with the glacial-interglacial estimate of Ganopolski and Brovkin (2017) (-350 Pg C).

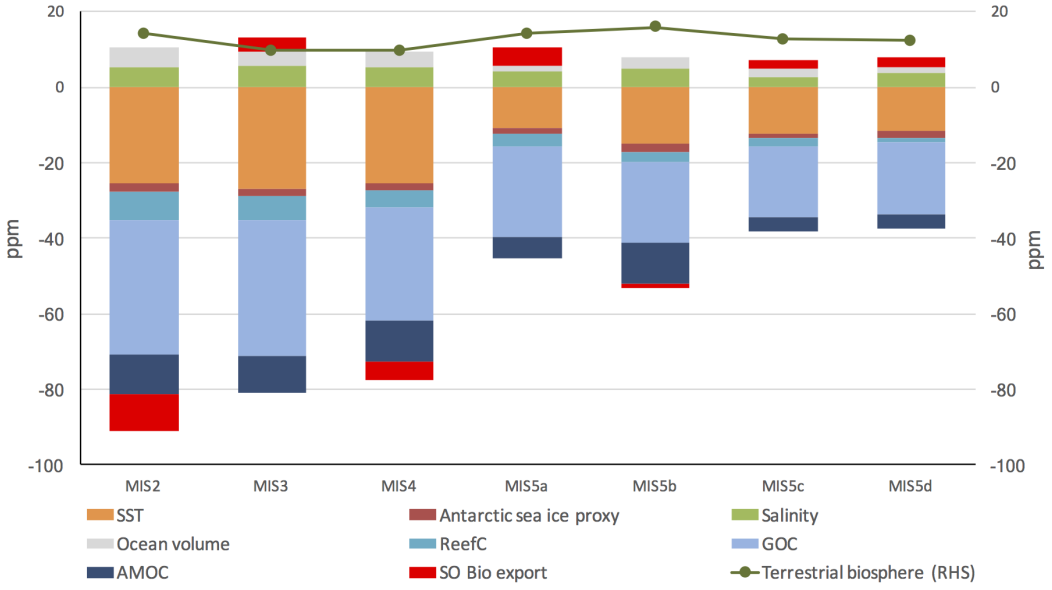

Figure 14. Impacts on CO_2 of model parameters from the model-data experiment results, from the penultimate interglacial period (MIS 5e) to the Last Glacial Maximum (MIS 2). SST = sea surface temperature, ReefC = shallow carbonate production/dissolution, GOC = global ocean circulation, AMOC = Atlantic Meridional Overturning Circulation, SO Bio Export = Southern Ocean Biological export productivity. Shown for comparison is the impact of the terrestrial biosphere in each MIS stage (comparison between model runs with and without terrestrial biosphere).

5.2 The LGM and Holocene

Within the context of LGM-Holocene studies, our findings corroborate the hypothesis that a number of mechanisms, not one singular factor, delivered the ~85 ppm increase in atmospheric CO_2 from the LGM to the Holocene ~~(e.g. Kohfeld and Ridgewell, 2009; Sig~~ This finding is more obvious when the sequential nature of changes is observed over the full glacial cycle, as distinct from analysing the LGM and Holocene in isolation. Our model-data results agree with those of Menviel et al. (2016): that variations primarily in GOC and AMOC, SST, and alongside Southern Ocean biological productivity, can account for for atmospheric CO_2 variation from the LGM to the Holocene, with an opposing feedback provided by the terrestrial biosphere. The longer time timescale of our analysis highlights that changes in GOC and AMOC took place much earlier in the glacial cycle than the LGM, and were at or near their glacial minima prior to the LGM. Our model-data results also constrain the effects of Southern Ocean biological export productivity in the glacial cycle CO_2, to MIS 2-4. Enhanced wind-borne iron dust deposits over the Southern Ocean are believed to have fed increased phytoplankton growth in the LGM and possibly MIS 4 (Martin, 1990; Martinez-Garcia et al., 2014; Kohfeld and Chase, 2017; Muglia et al., 2018).

5.3 The terrestrial biosphere

Our modelled ~~variation~~ increase in the terrestrial biosphere carbon stock from the LGM to Holocene, of ~~750~~ 630 Pg C (Fig. 12), ~~is at the upper bound of~~falls within, but towards the upper end of, recent estimates of this change, of ~~0-700 Pg C (e.g. Ciais et al., 2012), Peterson et al. (2014)), but within uncertainty bounds~~300-850 Pg C (e.g. Joos et al., 2004; Brovkin et al., 2007; Köh For example, Peterson et al. (2014) estimated a variation of 511 $\pm$ 289 Pg C in the terrestrial biosphere carbon stock, based on whole of ocean δ^{13}C data. Brovkin et al. (2007), Brovkin et al. (2012) and Köhler et al. (2010) all modelled ~500-550 Pg C increase in the terrestrial biosphere between the LGM and Holocene (Prentice et al. (2011) estimated (550-694 Pg C)). According to Francois et al. (1999), palynological and sediment data infer that the terrestrial biosphere carbon stock was 700-1350 ~~PgC~~ Pg C smaller in the LGM than the present. Ciais et al. (2012) pointed to a growth of a large ~~inert~~ carbon pool in steppes and tundra during the LGM as an offsetting feature to the declining tropical biosphere, a feature also included in reconstructed last glacial terrestrial biosphere by Hoogakker et al. (2016)~~.~~, leading to a smaller estimate of ~330 Pg C (Ganopolski and Brovkin (2017) modelled a similar estimate of 350 Pg C). Jeltsch-Thommes et al. (2019) estimated a glacial-interglacial change in terrestrial biosphere of 850 Pg C (median estimate; range 450 to 1250 Pg C), a similar estimate to that of Joos et al. (2004) of 820-850 Pg C. Jeltsch-Thommes et al. (2019) demonstrated the importance of including ocean-sediment and weathering fluxes in their modelling estimates, and suggested other studies may underestimate the full deglacial change in the terrestrial biosphere carbon stock. While our model results ~~are at the upper end of recent modelled and qualitative~~ (~630 Pg C) are higher than some estimates of the LGM-Holocene change in the terrestrial biosphere (e.g. Ciais et al., 2012; Me they are ~~in agreement~~ mostly in good agreement (e.g. Joos et al., 2004; Brovkin et al., 2007; Köhler et al., 2010; Prentice et al., 2011; Brov and our NPP estimates mostly align with the glacial cycle ~~reconstruction of NPP of~~ NPP reconstruction of Hoogakker et al. (2016) as shown in Fig. 12. The driver for NPP in the simple terrestrial biosphere module in SCP-M is atmospheric CO_2, via carbon fertilisation. According to several authors (e.g. Otto et al., 2002; Kaplan et al., 2002; Joos et al., 2004; Hoogakker et al., 2016),

carbon fertilisation is the primary driver of global variation in the terrestrial biosphere NPP during the last glacial-interglacial cycle. However, the importance of carbon fertilisation versus temperature and precipitation, and other factors, as drivers of NPP, are debated (e.g. Francois et al., 1999; van der Sleen et al., 2015).

5.4 Advantages and limitations of this study

The use of a simple box model for this model-data study, SCP-M, enabled a range of proxies to be incorporated into the MIS reconstructions, and a large number of simulations (~~5~~9,000) to explore possible parameter combinations in each MIS. However, given the large spatial coverage of the SCP-M boxes, data for large areas of the ocean are averaged, and some detail is lost. For example, in the case of the carbonate ion proxy, we apply a default estimate of standard deviation to account for the large volume of ocean covered by SCP-M's boxes relative to the proxy data locations, and to enable the normalisation of the carbonate ion proxy data in a procedure that uses the data standard deviation as a weighting. Despite this caveat, we believe that the model-data experiment results provide a good match to the data across the various atmospheric and ocean proxies as shown in Figs 9-11.

Most major processes in the SCP-M model are simply parameterised, allowing them to be free-floated in model-data experiments. ~~The~~ However, the driving factors behind parameter value changes can only be speculated. For example, slowdown in GOC may be the result of changing wind patterns or buoyancy fluxes around Antarctica (Morrison and Hogg, 2013), Antarctic sea-ice cover (Ferrari et al., 2014), or may be the result of shoaling AMOC leading to extensive filling of the abyssal ocean by waters sourced from GOC (Curry and Oppo, 2005; De Boer and Hogg, 2014; Jansen, 2017). Probing the root cause of our model-data findings would require a more detailed physical and/or biogeochemical model. Furthermore, we apply a simple representation of the terrestrial biosphere in our model-data experiments, relying primarily on atmospheric CO_2 as the driver for NPP. This approach provided reasonable results for the terrestrial biosphere carbon stock and NPP, on the whole, but may miss some detail in the terrestrial biosphere during the last glacial-interglacial cycle. Our MIS time-slicing ~~may obscure detail~~ obscures details in the proxy records within MIS. For example, Yu et al. (2013) observed a transient drop in carbonate ion concentrations in the deep Pacific Ocean during MIS ~~4. We omit~~ 4, and there are large transient changes in atmospheric $\delta^{13}C$ during MIS 3-4. Ganopolski et al. (2010) and Menviel et al. (2012) modelled transient collapses and rebounds in AMOC during MIS 4 (and other short-term changes in atmospheric dust supply and depth of biological nutrient remineralisation), which could have contributed to the full observed magnitude of changes in atmospheric $\delta^{13}C$ across this period (e.g. Eggleston et al., 2016) - not captured with our MIS-averaging approach. We omitted the transient last glacial termination from our analysis, a period in which atmospheric CO_2 rose ~85 ppm in 8 kyr. Future model-data optimisation work could probe this period at 1 kyr intervals, or with transient, data-optimised simulations, to profile the unwinding of processes that led to the last glacial cycle CO_2 drawdown. In summary, while the model we applied is high level in nature, the modelling itself is heavily constrained by natural observations and proxy data from the carbon cycle. Therefore, this work presents a plausible set of modelled outcomes for the last glacial-interglacial cycle.

6 Conclusions

Multiple processes drove atmospheric CO_2 fluctuations during the last glacial cycle. Against a backdrop of varied SST, salinity, sea-ice cover, ocean volume and reef carbonates, we modelled sequentially weaker GOC (first) and AMOC (second) to reduce atmospheric CO_2 in the lead up to the LGM. At the LGM, increased Southern Ocean biological export productivity delivered an incremental fall in CO_2, resulting in the glacial cycle CO_2 minimum. GOC, AMOC, Southern Ocean biology and SST rebounded to modern values between the LGM and Holocene, contributing to the sharp post-glacial increase in CO_2. The terrestrial biosphere played an important negative feedback role during the glacial cycle, releasing δ^{13}C-negative CO_2 to the atmosphere at times during the glaciation, and taking up CO_2 during the termination and Holocene. These model-data results were achieved with a simple carbon cycle box optimised for proxy data for CO_2, δ^{13}C, Δ^{14}C and $CO^{2-}{}_3$. Our results agree with ~~composite hypotheses for glacial~~ hypotheses for glacial-interglacial cycle CO_2 that emphasise varying ocean circulation~~(e.g. Kohfeld and Ridgewell, 2009; Sigman et al., 2010; Ferrari et al., 2014; Menviel et al., 2016; Kohfeld and Chase, 2017)~~, include marine biological productivity, and amidst many other physical and biogeochemical changes in the marine and terrestrial carbon cycle (e.g. Kohfeld and Ridgewell, 2009; Sigman et al., 2010; Ganopolski et al., 2010; Brovkin et al., 2012; Menviel et al., 20
We emphasise the need to include the Pacific and Indian oceans in evaluation of the oceanic carbon cycle, particularly in relation to the last glacial cycle and the LGM-Holocene transition.

Many uncertainties exist in the data and the prescribed nature of the processes in a box model. However, such uncertainty is largely inescapable when dealing with models and proxy data. We propose these model-data results as one set of plausible results for the last glacial carbon cycle, in agreement with available proxy data, and see them as encouraging for the use of models and data to help constrain hypotheses for the paleo- carbon cycle.

7 Code and data availability

The model code, processed data files, model-data experiment results, and any (published) raw proxy data gathered in the course of this work, are located at https://doi.org/10.5281/zenodo.3559339. No original data was created, or unpublished data used, in this work. This paper's Supplementary Information contains an overview of the files contained in the repository. For more detail on the SCP-M equations, see O'Neill et al. (2019).

Author contributions. CO undertook model development work, data-gathering, modelling and model-data experiments. AH provided the oceanographic interpretation and guided modelling and data analysis. ME designed model-data experiments and provided input into data analysis and the modelling of the marine biology and isotopes. BO contributed glacial cycle model forcings and input to modelling of the reef carbonates. SE oversaw the modelling of the marine biology and carbonate pump. All authors contributed to drafting and reviewing the document.

Competing interests. The authors declare that they have no conflict of interest.

Acknowledgements. Stewart Fallon provided input to the processing of radiocarbon data. Malcolm Sambridge provided input on model-data optimisation and inversions. Jimin Yu provided helpful discussions and carbonate ion proxy data.

References

Adkins, J., McIntyre, K., and Schrag, D.: The Salinity, Temperature, and 18O of the Glacial Deep Ocean, Science, 298, 1769–1773, 2002.

Anderson, R., Chase, Z., Fleisher, M., and Sachs, J.: The Southern Ocean's biological pump during the Last Glacial Maximum, Deep Sea Research Part II: Topical Studies in Oceanography, 49, 1909–1938, 2002.

Archer, D. and Maier-Reimer, E.: Effect of deep-sea sedimentary calcite preservation on atmospheric CO2 concentration, Nature, 367, 260–263, 1994.

Arteaga, L., Pahlow, M., Bushinsky, S., and Sarmiento, J.: Nutrient Controls on Export Production in the Southern Ocean, Global Biogeochemical Cycles, 33, 942–956, 2019.

Barker, S., Knorr, G., Vautravers, M., Diz, P., and Skinner, L.: Extreme deepening of the Atlantic overturning circulation during deglaciation, Nature Geoscience, 3, 567–571, 2010.

Bereiter, B., Eggleston, S., Schmitt, J., Nehrbass-Ahles, C., Stocker, T., Fischer, H., Kipfstuhl, S., and Chappellaz, J.: Revision of the EPICA Dome C CO2 record from 800 to 600kyr before present, Geophys. Res. Lett, 2015.

Berger, W.: Increase of carbon dioxide in the atmosphere during deglaciation: The coral reef hypothesis, Naturwissenschaften, 69, 87–88, 1982.

Boyd, P. e. a.: A mesoscale phytoplankton bloom in the polar Southern Ocean stimulated by iron fertilization, Nature, pp. 695–702, 2000.

Broecker, W., Yu, J., and Putnam, A.: Two contributors to the glacial CO2 decline, Earth and Planetary Science Letters, pp. 191–196, 2015.

Broecker, W. S.: Ocean chemistry during glacial time, Geochim. Cosmochim. Acta, 46, 1689–1705, 1982.

Broecker, W. S. and Barker, S.: A 190‰ drop in atmosphere's Δ14C during the "Mystery Interval" (17.5 to 14.5 kyr), Earth and Planetary Science Letters, 256, 90–99, 2007.

Broecker, W. S., Peng, T. H., and Engh, R.: Modeling the carbon system, Radiocarbon, 22, 565–598, 1980.

Brovkin, V., Claussen, J. B. M., Ganopolski, A., Kubatzki, C., Petoukhov, V., and Andreev, A.: Carbon cycle, vegetation, and climate dynamics in the Holocene: Experiments with the CLIMBER-2 model, Global Biogeochemical Cycles, 16, 1139, doi:10.1029/2001GB001 662, 2002.

Brovkin, V., Ganopolski, A., Archer, D., and Rahmstorf, S.: Lowering of glacial atmospheric CO2 in response to changes in oceanic circulation and marine biogeochemistry, Paleoceanography, 22, PA4202, doi:10.1029/2006PA001 380, 2007.

Brovkin, V., Ganopolski, A., Archer, D., and Munhoven, G.: Glacial CO2 cycle as a succession of key physical and biogeochemical processes, Climate of the Past, 8, 251–264, 2012.

Bryan, S., Marchitto, T., and Lehman, S.: The release of 14C-depleted carbon from the deep ocean during the last deglaciation: Evidence from the Arabian Sea, Earth and Planetary Science Letters, 298, 244–254, 2010.

Burke, A. and Robinson, L.: The Southern Ocean's Role in Carbon Exchange During the Last Deglaciation, Science, 335, 557–561, 2012.

Cassar, N., Wright, S., Thomson, P., Trull, T., Westwood, K., de Salas, M., Davidson, A., Pearce, I., Davies, D., and Matear, R.: The relation of mixed-layer carbon export production to plankton community in the Southern Ocean, Global Biogeochemical Cycles, 29, 446–462, 2015.

Chalk, T., Foster, G., and Wilson, P.: Dynamic storage of glacial CO2 in the Atlantic Ocean revealed by boron [CO2-3] and pH records, Earth and Planetary Science Letters, 510, 1–11, 2019.

Chen, T., Robinson, L., Burke, A., Southon, J., Spooner, P., Morris, P., and Ng, H.: Synchronous centennial abrupt events in the ocean and atmosphere during the last deglaciation, Science, 349, 1537–1541, 2015.

Ciais, P., Tagliabue, A., Cuntz, M., Bopp, L., Scholze, M., Hoffmann, G., Lourantou, A., Harrison, S. P., Prentice, I. C., Kelley, D. I., Koven, C., and Piao, S. L.: Large inert carbon pool in the terrestrial biosphere during the Last Glacial Maximum, Nature Geoscience, 5, 74–79, 2012.

Collatz, G., Berry, J., and Clark, J.: Effects of climate and atmospheric CO2 partial pressure on the global distribution of C4 grasses: present, past, and future, Oecologia, 114, 441–454, 1998.

Cook, M. and Keigwin, L.: Radiocarbon profiles of the NW Pacific from the LGM and deglaciation: Evaluating ventilation metrics and the effect of uncertain surface reservoir ages, Paleoceanography, pp. 174–195, 2015.

Curry, W. B. and Oppo, D. W.: Glacial water mass geometry and the distribution of d13C of CO2 in the western Atlantic Ocean, Paleoceanography, 20, PA1017, doi:10.1029/2004PA001 021, 2005.

Davies-Walczak, M., Mix, A., Stoner, J., Southon, J., Cheseby, M., and Xuan, C.: Late Glacial to Holocene radiocarbon constraints on North Pacific Intermediate Water ventilation and deglacial atmospheric CO2 sources, Earth and Planetary Science Letters, 397, 57–66, 2014.

De Boer, A. M. and Hogg, A. M. C.: Control of the glacial carbon budget by topographically induced mixing, Geophys. Res. Lett, 41, 4277–4284, 2014.

DeVries, T. and Weber, T.: The export and fate of organic matter in the ocean: New constraints from combining satellite and oceanographic tracer observations, Paleoceanography, 31, 535–555, 2017.

Dunne, J. P., Armstrong, R. A., Gnanadesikan, A., and Sarmiento, J. L.: Empirical and mechanistic models for the particle export ratio, Global Biogeochemical Cycles, 19, GB4026, doi:10.1029/2004GB002 390, 2005.

Ebersbach, F., Trull, W., Davies, D., and Bray, S.: Controls on mesopelagic particle fluxes in the Sub-Antarctic and Polar Frontal Zones in the Southern Ocean south of Australia in summer - Perspectives from free-drifting sediment traps, Deep Sea Research Part II: Topical Studies in Oceanography, 58, 2260–2276, 2011.

Eggleston, S., Schmitt, J., Bereiter, B., Schneider, R., and Fischer, H.: Evolution of the stable carbon isotope composition of atmospheric CO2 over the last glacial cycle, Paleoceanography, 31, 434–452, 2016.

Ferrari, R., Jansen, M., Adkins, J., Burke, A., Stewart, A. L., and Thompson, A.: Antarctic sea ice control on ocean circulation in present and glacial climates, PNAS, 111, 8753–8758, 2014.

Follows, M. J., Ito, T., and Dutkiewicz, S.: On the solution of the carbonate chemistry system in ocean biogeochemistry models, Ocean Modelling, 12, 290–30, 2006.

Francois, L., Godderis, Y., Warnant, P., Ramstein, G., de Noblet, N., and Lorenz, S.: Carbon stocks and isotopic budgets of the terrestrial biosphere at mid-Holocene and last glacial maximum times, Chemical Geology, 159, 163–199, 1999.

Freeman, E., Skinner, L., Waelbroeck, C., and Hodell, D.: Radiocarbon evidence for enhanced respired carbon storage in the Atlantic at the Last Glacial Maximum, Nature Communications, 2016.

Ganopolski, A. and Brovkin, V.: Simulation of climate, ice sheets and CO2 evolution during the last four glacial cycles with an Earth system model of intermediate complexity, Climate of the Past, 13, 1695–1716, 2017.

Ganopolski, A., Calov, R., and Claussen, M.: Simulation of the last glacial cycle with a coupled climate ice-sheet model of intermediate complexity, Climate of the Past, 6, 229–244, 2010.

Govin, A., Michel, E., Labeyrie, L., Waelbroeck, C., Dewilde, F., and Jansen, E.: Evidence for northward expansion of Antarctic Bottom Water mass in the Southern Ocean during the last glacial inception, Paleoceanography, 24, doi:10.1029/2008PA001 603, 2009.

Hain, M. P., Sigman, D. M., and Haug, G. H.: Carbon dioxide effects of Antarctic stratification, North Atlantic Intermediate Water formation, and subantarctic nutrient drawdown during the last ice age: Diagnosis and synthesis in a geochemical box model, Global Biogeochem. Cycles, 24, GB4023, doi:10.1029/2010GB003 790, 2010.

Harman, I., Trudinger, C., and Raupach, M.: SCCM – the Simple Carbon-Climate Model: Technical Documentation, CAWCR Technical Report 047, CSIRO Centre for Australian Weather and Climate Research, CSIRO Marine and Atmospheric Research, FC Pye Laboratory, GPO Box 3023, Canberra, ACT, 2601, Australia, 2011.

Harrison, K. G.: Role of increased marine silica input on paleo-pCO2 levels, Paleoceanography, 15, 292–298, 2000.

Henson, S. A., Sanders, R., Madsen, E., Morris, P. J., Moigne, F. L., and Quartly, G. D.: A reduced estimate of the strength of the ocean's biological carbon pump, Geophys. Res. Lett., 38, L04 606, doi:10.1029/2011GL046 735, 2011.

Hines, S., Southon, J., and Adkins, J.: A high-resolution record of Southern Ocean intermediate water radiocarbon over the past 30,000 years, Earth and Planetary Science Letters, 432, 46–48, 2015.

Hoff, U., Rasmussen, T., Stein, R., Ezat, M., and Fahl, K.: Sea ice and millennial-scale climate variability in the Nordic seas 90 kyr ago to present, Nature Communications, 7, DOI: 10.1038/ncomms12 247, 2015.

Hogg, A. M.: Glacial cycles and carbon dioxide: A conceptual model, Geophys. Res. Lett., 35, L01 701, doi:10.1029/2007GL032 071, 2008.

Hoogakker, B. et al.: Terrestrial biosphere changes over the last 120 kyr, Climate of the Past, 12, 51–73, 2016.

Huang, Y., Street-Perrott, F., Metcalfe, S., Brenner, M., Moreland, M., and Freeman, K.: Climate change as the dominant control on glacial-interglacial variations in C3 and C4 plant abundance, Science, 293, 1647–1651, 2001.

Jaccard, S., Hayes, C., Martínez-García, A., an R.F. Anderson, D. H., Sigman, D., and Haug, G.: Two Modes of Change in Southern Ocean Productivity Over the Past Million Years, Science, 339, 1419–1423, 2013.

Jacquet, S., Lam, P., Trull, T., and Dehairs, F.: Carbon export production in the Polar Front Zone and Subantarctic Zone south of Tasmania, Deep Sea Research Part II: Topical Studies in Oceanography, 58, 2277–2292, 2011.

Jansen, M.: Glacial ocean circulation and stratification explained by reduced atmospheric temperature, PNAS, 114, 45–50, 2017.

Jeltsch-Thommes, A., Battaglia, G., Cartapanis, O., Jaccard, S., and Joos, F. J.: Low terrestrial carbon storage at the Last Glacial Maximum: constraints from multi-proxy data, Climate of the Past, 15, 849–879, 2019.

Joos, F., Gerber, S., Prentice, I. C., Otto-Bliesner, B., and Valdes, P.: Transient simulations of Holocene atmospheric carbon dioxide and terrestrial carbon since the Last Glacial Maximum, Global Biogeochemical Cycles, 18, GB2002, doi:10.1029/2003GB002 156, 2004.

Kaplan, J., Prentice, I., Knorr, W., and Valdes, P.: Modeling the dynamics of terrestrial carbon storage since the Last Glacial Maximum, Geophysical Research Letters, 22, 2074, doi:10.1029/2002GL015 230, 2002.

Key, R.: Ocean process tracers: Radiocarbon. In: Encyclopedia of Ocean Sciences, pp. 2338–2353, Academic Press, London, 2001.

Key, R., Kozyr, A., Sabine, C. L., Lee, K., Wanninkhof, R., Bullister, J. L., Feely, R. A., Millero, F. J., Mordy, C., and Peng, T.-H.: A global ocean carbon climatology: Results from Global Data Analysis Project (GLODAP), Global Biogeochemical Cycles, 18, GB4031, doi:10.1029/2004GB002 247, 2004.

Khatiwala, S., Schmittner, A., and Muglia, J.: Air-sea disequilibrium enhances ocean carbon storage during glacial periods, Science Advances, 5, doi:10.1126/sciadv.aaw4981, https://advances.sciencemag.org/content/5/6/eaaw4981, 2019.

Kleypas, J.: Modeled estimates of global reef habitat and carbonate production since the Last Glacial Maximum, Paleoceanography and Paleoclimatology, 12, 533–545, 1997.

Knox, F. and McElroy, M.: Changes in Atmospheric CO2: Influence of the Marine Biota at High Latitude, Journal of Geophysical Research, 89, 4269–4637, 1984.

Kohfeld, K. and Chase, Z.: Temporal evolution of mechanisms controlling ocean carbon uptake during the last glacial cycle, Earth and Planetary Science Letters, 472, 206–215, 2017.

Kohfeld, K. and Ridgewell, A.: Glacial-Interglacial Variability in Atmospheric CO2, Surface Ocean–Lower Atmosphere Processes, Geophysical Research Series, 187, 251–286, 2009.

Kohfeld, K., Quéré, C. L., Harrison, S., and Anderson, R.: Role of Marine Biology in Glacial-Interglacial CO2 Cycles, Science, 308, 74–78, 2005.

Kohler, P. and Fischer, H.: Simulating changes in the terrestrial biosphere during the last glacial/interglacial transition, Global and Planetary Change, 43, 33–55, 2004.

Köhler, P., Fischer, H., and Schmitt, J.: Atmospheric d13CO2 and its relation to pCO2 and deep ocean d13C during the late Pleistocene, Paleoceanography, 25, doi:10.1029/2008PA001 703, 2010.

Kohn, M.: Carbon isotope compositions of terrestrial C3 plants as indicators of (paleo)ecology and (paleo)climate, PNAS, 107, 19 691–19 695, 2010.

Kohn, M.: Carbon isotope discrimination in C3 land plants is independent of natural variations in pCO2, Geochemical Perspectives Letters, 2, 35–43, 2016.

Kurahashi-Nakamura, T., Paul, A., and Losch, M.: Dynamical reconstruction of the global ocean state during the Last Glacial Maximum, Paleoceanography, 32, 326–350, 2017.

Kwon, E., Primeau, F., and Sarmiento, J.: The impact of remineralization depth on the air–sea carbon balance, Nature Geoscience, 2, 630–635, 2009.

Lambert, F., Tagliabue, A., Shaffer, G., Lamy, F., Winckler, G., Farias, L., Gallardo, L., and Pol-Holz, D.: Dust fluxes and iron fertilization in Holocene and Last Glacial Maximum climates, Geophysical Research Letters, 42, 6014–6023, 2015.

Lindgren, A., Hugelius, G., and Kuhry, P.: Extensive loss of past permafrost carbon but a net accumulation into present-day soils, Letters to Nature, 560, 219–222, 2018.

Lisiecki, L. E. and Raymo, M. E.: A Pliocene-Pleistocene stack of 57 globally distributed benthic d18O records, Paleoceanography, 20, doi:10.1029/2004PA001 071, 2005.

Liu, C., Kohl, A., Liu, Z., Wang, F., and Stammer, D.: Deep-reaching thermocline mixing in the equatorial pacific cold tongue, Nature Communications, 7, 11 576, doi:10.1038/ncomms11 576, 2016.

Lourey, M. J. and Trull, W.: Seasonal nutrient depletion and carbon export in the Subantarctic and Polar Frontal Zones of the Southern Ocean south of Australia, Journal of Geophysical Research: Oceans, 106, 31 463–31 487, 2001.

Lueker, T. J., Dickson, A. G., and Keeling, C. D.: Ocean pCO2 calculated from dissolved inorganic carbon, alkalinity, and equations for K-1 and K-2: validation based on laboratory measurements of CO2 in gas and seawater at equilibrium, Marine Chemistry, 70, 105–119, 2000.

Maffezzoli, N., Vallelonga, P., Edwards, R., Saiz-Lopez, A., Turetta, C., Kjær, H. A., Barbante, C., Vinther, B., and Spolaor, A.: 120,000 year record of sea ice in the North Atlantic, Climate of the Past, 2018, 1–19, 2018.

Marchitto, T., Lehman, S., Ortiz, J., Flückiger, J., and van Geen, A.: Marine Radiocarbon Evidence for the Mechanism of Deglacial Atmospheric CO2 Rise, Science, 316, 1456–1459, 2007.

Martin, J.: Glacial-interglacial CO2 change: The Iron Hypothesis, Paleoceanography, 5, 1–13, 1990.

Martin, J. H., Knauer, G., Karl, D., and Broenkow, W.: VERTEX: carbon cycling in the northeast Pacific, Deep-Sea Research, 34, 267–285, 1987.

Martinez-Garcia, A., Sigman, D., H.Ren, Anderson, R., Straub, M., Hodell, D., Jaccard, S., Eglinton, T., and Haug, G.: Iron Fertilization of the Subantarctic Ocean During the Last Ice Age, Science, 343, 1347–1350, 2014.

Marzocchi, A. and Jansen, M. F.: Connecting Antarctic sea ice to deep-ocean circulation in modern and glacial climate simulations, Geophysical Research Letters, 44, 2017.

Matsumoto, K.: Biology-mediated temperature control on atmospheric pCO2 and ocean biogeochemistry, Journal of Geophysical Research, 34, L20 605, doi:10.1029/2007GL031 301, 2007.

Mauritz, M., Celis, G., Ebert, C., Hutchings, J., Ledman, J., Natali, S., Pegoraro, E., Salmon, V., Schädel, C., Taylor, M., , and Schuur, E.: Using stable carbon isotopes of seasonal ecosystem respiration to determine permafrost carbon loss, Journal of Geophysical Research: Biogeosciences, 124, 46–60, 2018.

Menviel, L. and Joos, F.: Toward explaining the Holocene carbon dioxide and carbon isotope records: Results from transient ocean carbon cycle-climate simulations, Paleoceanography, 27, PA1207, doi:10.1029/2011PA002 224, 2012.

Menviel, L., Joos, F., and Ritz, S.: Simulating atmospheric CO2, 13C and the marine carbon cycle during the Last Glacial-Interglacial cycle: possible role for a deepening of the mean remineralization depth and an increase in the oceanic nutrient inventory, Quaternary Science Reviews, 56, 46–68, 2012.

Menviel, L., Mouchet, A., Meissner, K. J., Joos, F., and England, M. H.: Impact of oceanic circulation changes on atmospheric d13CO2, Global Biogeochemical Cycles, 29, 1944–1961, 2015.

Menviel, L., Yu, J., Joos, F., Mouchet, A., Meissner, K. J., and England, M. H.: Poorly ventilated deep ocean at the Last Glacial Maximum inferred from carbon isotopes: A data-model comparison study, Paleoceanography, 31, 2–17, 2016.

Millero, F. J.: Influence of pressure on chemical processes in the sea. In Chemical Oceanography, 2nd edn, vol. 8, Academic Press, New York, 1983.

Morrison, A. and Hogg, A.: On the Relationship between Southern Ocean Overturning and ACC Transport, Journal of Physical Oceanography, 43, 140–148, 2013.

Morrison, A., Hogg, A., and Ward, M.: Sensitivity of the Southern Ocean overturning circulation to surface buoyancy forcing, Geophysical Research Letters, 38, L14 602, doi:10.1029/2011GL048 031, 2011.

Morse, J. W. and Berner, R. A.: Dissolution kinetics of calcium carbonate in sea water. II: A kinetic origin for the lysocline, Am J Sci, 272, 1972.

Muglia, J., Skinner, L., and Schmittner, A.: Weak overturning circulation and high Southern Ocean nutrient utilization maximized glacial ocean carbon, Earth and Planetary Science Letters, 496, 47–56, 2018.

Muscheler, R., Beer, J., Wagner, G., Laj, C., Kissel, C., Raisbeck, G., Yioud, F., and Kubik, P.: Changes in the carbon cycle during the last deglaciation as indicated by the comparison of 10Be and 14C records, Earth and Planetary Science Letters, 219, 325–340, 2014.

Oliver, K., Hoogakker, B., Crowhurst, S., Henderson, G., Rickaby, R., Edwards, N., and Elderfield, H.: A synthesis of marine sediment core d13C data over the last 150 000 years, Climate of the Past, 6, 645–673, 2010.

O'Neill, C., A. Mc. Hogg, M.J. Ellwood, S. E., and Opdyke, B.: The [simple carbon project] model v1.0, Geosci. Model Dev., 12, 1541–1572, https://doi.org/10.5194/gmd–12–1541–2019, 2019.

Opdyke, B. and Walker, J.: Return of the coral reef hypothesis: Basin to shelf partitioning of CaCO3 and its effect on atmospheric CO2, Geology, 20, 733–736, 1992.

Otto, D., Rasse, D., Kaplan, J., Warnant, P., and Francois, L.: Biospheric carbon stocks reconstructed at the Last Glacial Maximum: comparison between general circulation models using prescribed and computed sea surface temperatures, Global and Planetary Change, 33, 117–138, 2002.

Peterson, C. D., Lisiecki, L. E., and Stern, J. V.: Deglacial whole-ocean d13C change estimated from 480 benthic foraminiferal records, Paleoceanography, 29, 549–563, 2014.

Piotrowski, A., Banakar, V., Scrivner, A., Elderfield, H., Galy, A., and Dennis, A.: Indian Ocean circulation and productivity during the last glacial cycle, Earth and Planetary Science Letters, 285, 179–189, 2009.

Prentice, I. C., Harrison, S., and Bartlein, P.: Global vegetation and terrestrial carbon cycle changes after the last ice age, New Phytologist, 189, 988–998, 2011.

Qin, B., Li, T., Xiong, Z., Algeo, T. J., and Chang, F.: Deepwater carbonate ion concentrations in the western tropical Pacific since 250 ka: Evidence for oceanic carbon storage and global climate influence, Paleoceanography, 32, 351–370, 2017.

Qin, B., Li, T., Xiong, Z., Algeo, T., and Jia, Q.: Deep-Water Carbonate Ion Concentrations in the Western Tropical Pacific Since the Mid-Pleistocene: A Major Perturbation During the Mid-Brunhes, Journal of Geophysical Research: Oceans, 123, https://doi.org/10.1029/2018JC014 084, 2018.

Reimer, P., Baillie, M., Bard, E., Bayliss, A., Beck, J., Blackwell, P., Ramsey, C. B., Buck, C., Burr, G., Edwards, R., Friedrich, M., Grootes, P., Guilderson, T., Hajdas, I., Heaton, T., Hogg, A., Hughen, K., Kaiser, K., Kromer, B., McCormac, F., Manning, S., Reimer, R., Richards, D., Southon, J., Talamo, S., Turney, C., van der Plicht, J., and Weyhenmeyer, C.: IntCal09 and Marine09 radiocarbon age calibration curves, 0-50,000 years cal BP., Radiocarbon, 51, 1111–50, 2009.

Ridgwell, A.: An end to the "rain ratio" reign?, Geochem. Geophys. Geosyst., 4, 1051, doi:10.1029/2003GC000 512, 2003.

Ridgwell, A., Watson, A., Maslin, M., and Kaplan, J.: Implications of coral reef buildup for the controls on atmospheric CO2 since the Last Glacial Maximum, Paleoceanography, 18, 1083, doi:10.1029/2003PA000 893, 2003.

Rohling, E., Grant, K., Bolshaw, M., Roberts, A., Siddall, M., Hemleben, C., and Kucera, M.: Antarctic temperature and global sea level closely coupled over the past five glacial cycles, Nature Geoscience, 2, 500–504, 2009.

Ronge, T., Tiedemann, R., Lamy, F., Kohler, P., Alloway, B., Pol-Holz, R. D., Pahnke, K., Southon, J., and Wacker, L.: Radiocarbon constraints on the extent and evolution of the South Pacific glacial carbon pool, Nature Communications, 7, 11 487, doi:10.1038/ncomms11 487, 2016.

Sarmiento, J. L. and Gruber, N.: Ocean biogeochemical dynamics, Princeton University Press, 2006.

Sarmiento, J. L. and Toggweiler, J. R.: A new model for the role of the oceans in determining atmospheric CO2, Nature, 308, 621–624, 1984.

Schmitt, J., Schneider, R., Elsig, J., Leuenberger, D., Lourantou, A., Chappellaz, J., Köhler, P., Joos, F., Stocker, T., Leuenberger, M., and Fischer, H.: Carbon Isotope Constraints on the Deglacial CO2 Rise from Ice Cores, Science, 336, 711–714, 2012.

Schneider, R., Schmitt, J., Kohler, P., Joos, F., and Fischer, H.: A reconstruction of atmospheric carbon dioxide and its stable carbon isotopic composition from the penultimate glacial maximum to the last glacial inception, Climate of the Past, 9, 2507–2523, 2013.

Schubert, B. and Jahren, A.: The effect of atmospheric CO2 concentration on carbon isotope fractionation in C3 land plants, Geochimica et Cosmochimica Acta, 96, 29–43, 2012.

Shaffer, G. and Lambert, F.: In and out of glacial extremes by way of dust-climate feedbacks, PNAS, 115, 2026–2031, 2018.

Siani, E., Michel, E., Pol-Holz, R. D., DeVries, T., Lamy, F., Carel, M., Isguder, G., Dewilde, F., and Lourantou, A.: Carbon isotope records reveal precise timing of enhanced Southern Ocean upwelling during the last deglaciation, Nature Communications, 4, 1–9, DOI:10.1038/ncomms3758, 2013.

Siegel, D. A., Buesseler, K. O., Doney, S. C., Sailley, S. F., Behrenfeld, M. J., and Boyd, P. W.: Global assessment of ocean carbon export by combining satellite observations and foodweb models, Global Biogeochemical Cycles, 28, 181–196, 2014.

Sigman, D. and Boyle, E.: Glacial/interglacial variations in atmospheric carbon dioxide, Nature Reviews, 407, 859–869, 2000.

Sigman, D., Hain, M., and Haug, G.: The polar ocean and glacial cycles in atmospheric CO2 concentration, Nature Reviews, 466, 47–55, 2010.

Sikes, E., Samson, C., Guilderson, T., and Howard, W.: Old radiocarbon ages in the southwest Pacific Ocean during the last glacial period and deglaciation, Nature, 405, 555–559, 2000.

Sikes, E., Cook, M., and Guilderson, T.: Reduced deep ocean ventilation in the Southern Pacific Ocean during the last glaciation persisted into the deglaciation, Earth and Planetary Science Letters, 438, 130–138, 2016.

Skinner, L. and Shackleton, N. J.: Rapid transient changes in northeast Atlantic deep water ventilation age across Termination I, Paleoceanography, 19, PA2005, doi:10.1029/2003PA000 983, 2004.

Skinner, L., Waelbroeck, C., Scrivner, A., and Fallon, S.: Radiocarbon evidence for alternating northern and southern sources of ventilation of the deep Atlantic carbon pool during the last deglaciation, PNAS, 111, 2014.

Skinner, L., McCave, I., Carter, L., Fallon, S., Scrivner, A., and Primeau, F.: Reduced ventilation and enhanced magnitude of the deep Pacific carbon pool during the last glacial period, Earth and Planetary Science Letters, 411, 45–52, 2015.

Skinner, L., Primeau, F., Freeman, E., de la Fuente, M., Goodwin, P. A., Gottschalk, J., Huang, E., McCave, I. N., Noble, T. L., and Scrivner, A. E.: Radiocarbon constraints on the glacial ocean circulation and its impact on atmospheric CO2, Nature Communications, 8, 16 010, doi: 10.1038/ncomms16 010, 2017.

Skinner, L. C., Fallon, S., Waelbroeck, C., Michel, E., and Barker, S.: Ventilation of the Deep Southern Ocean and Deglacial CO2 Rise, Science, 328, 1147–1151, 2010.

Stephens, B. and Keeling, R.: The infuence of Antarctic sea ice on glacial-interglacial CO2 variations, Nature, 404, 171–174, 2000.

Stott, L., Southon, J., Timmermann, A., and Koutavas, A.: Radiocarbon age anomaly at intermediate water depth in the Pacific Ocean during the last deglaciation, Paleoceanography, 24, 2009.

Strutz, T.: Data Fitting and Uncertainty. A practical introduction to weighted least squares and beyond., vol. 2 of *Wiesbaden*, Springer Vieweg, 2016.

Takahashi, T., Sutherland, S., Feely, R., and Cosca, C.: Decadal variation of the surface water PCO2 in the western and central equatorial Pacific, Science, 302, 852–856, 2003.

Talley, L.: Closure of the global overturning circulation through the Indian, Pacific, and Southern Oceans: Schematics and transports, Oceanography, 78, 257–303, 2013.

Tarnocai, C., Canadell, J., Schuur, E., Kuhry, P., Mazhitova, G., and Zimov, S.: Soil organic carbon pools in the northern circumpolar permafrost region, Global Biogeochemical Cycles, 23, GB2023, doi:10.1029/2008GB003 327, 2009.

Toggweiler, J. and Sarmiento, J.: Glacial to interglacial changes in atmospheric carbon dioxide: The critical role of ocean surface water in high latitudes, in The Carbon Cycle and Atmospheric CO2: Natural Variations Archean to Present, Geophysical Monograph Series, American Geophysical Union, 32, 163–184, 1985.

Toggweiler, J. R.: Variation of atmospheric CO2 by ventilation of the ocean's deepest water, Paleoceanography, 14, 571–588, 1999.

Toggweiler, J. R.: Origin of the 100,000-year time scale in Antarctic temperatures and atmospheric CO2, Paleoceanography, 23, PA2211, doi:10.1029/2006PA001 405, 2008.

Treat, C., Kleinen, T., Broothaerts, N., Dalton, A., Dommain, R., Douglas, T., Drexler, J., Finkelstein, S., Grosse, G., Hope, G., Hutchings, J., Jones, M., Kuhry, P., Lacourse, T., Lähteenoja, O., Loisel, J., Notebaert, B., Payne, R., Peteet, D., Sannel, A., Stelling, J., Strauss, J., Swindles, G., Talbot, J., Tarnocai, C., Verstraeten, G., C.J. Williams, Z. X., Yu, Z., Väliranta, M., Hättestrand, M., Alexanderson, H., and Brovkin, V.: Widespread global peatland establishment and persistence over the last 130,000 y, PNAS, 116, 4822–4827, 2019.

van der Sleen, P. et al.: No growth stimulation of tropical trees by 150 years of CO2 fertilization but water-use e ciency increased, Nature Geoscience, 8, 2015.

Vecsei, A. and Berger, W.: Increase of atmospheric CO2 during deglaciation: Constraints on the coral reef hypothesis from patterns of deposition, Global Biogeochemical Cycles, 18, GB1035, doi:10.1029/2003GB002 147, 2004.

Watson, A., Bakker, D. C. E., Ridgwell, A. J., Boyd, P. W., and Law, C.: Effect of iron supply on Southern Ocean CO2 uptake and implications for glacial atmospheric CO2, Nature, 407, 730–733, 2000.

Weeding, B. and Trull, W.: Hourly oxygen and total gas tension measurements at the Southern Ocean time series site reveal winter ventilation and spring net community production, Journal of Geophysical Research: Oceans, 119, 348–358, 2004.

Wolff, E., Barbante, C., Becagli, S., Bigler, M., Boutron, C., Castellano, E., de Angelis, M., Federer, U., Fischer, H., Fundel, F., Hansson, M., Hutterli, M., Jonsell, U., Karlin, T., Kaufmann, P., Lambert, F., Littot, G., Mulvaney, R., Roöthlisberger, R., Ruth, U., Severi, M., Siggaard-Andersen, M., Sime, L., Steffensen, J., Stocker, T., Traversi, R., Twarloh, B., Udisti, R., Wagenbach, D., and Wegner, A.: Changes in environment over the last 800,000 years from chemical analysis of the EPICA Dome C ice core, Quaternary Science Reviews, 29, 285–95, 2010.

Yamamoto, A., Abe-Ouchi, A., Ohgaito, R., Ito, A., and Oka, A.: Glacial CO2 decrease and deep-water deoxygenation by iron fertilization from glaciogenic dust, Climate of the Past, 15, 981–996, 2019.

Yu, J., Broecker, W., Elderfield, H., Jin, Z., McManus, J., and Zhang, F.: Loss of Carbon from the Deep Sea Since the Last Glacial Maximum, Science, 330, 1084–1087, 2010.

Yu, J., Anderson, R., Jin, Z., Rae, J., Opdyke, B., and Eggins, S.: Responses of the deep ocean carbonate system to carbon reorganization during the Last Glacial-interglacial cycle, Quaternary Science Reviews, 76, 39–52, 2013.

Yu, J., Anderson, R., Z.Jin, Menviel, L., Zhang, F., Ryerson, F., and Rohling, E.: Deep South Atlantic carbonate chemistry and increased interocean deep water exchange during last deglaciation, Quaternary Science Reviews, 90, 80–89, 2014a.

Yu, J., Anderson, R. F., and Rohling, E. J.: Deep ocean carbonate chemistry and glacial-interglacial atmospheric CO2 changes, Oceanography, 27, 16–25, 2014b.

Yu, J., Menviel, L., Jin, Z. D., Thornalley, D., Barker, S., Marino, G., Rohling, E. J., Cai, Y., Zhang, F., Wang, X., Dai, Y., Chen, P., and Broecker, W. S.: Sequestration of carbon in the deep Atlantic during the last glaciation, Nature Geoscience, 9, 319–325, 2016.

Yu, J., Menviel, L., Jin, Z., Thornalley, D., Foster, G., Rohling, E., McCave, I., McManus, J., Dai, Y., Ren, H., He, F., Zhang, F., Chen, P., and Roberts, A.: More efficient North Atlantic carbon pump during the Last Glacial Maximum, Nature Communications, 10, https://doi.org/10.1038/s41 467–019–10 028–z, 2019.

Zhao, N., Marchal, O., Keigwin, L., Amrhein, D., and Gebbie, G.: A Synthesis of Deglacial Deep-Sea Radiocarbon Records and Their (In)Consistency With Modern Ocean Ventilation, Paleoceanography and Paleoclimatology, 33, 128–151, 2017.